2015-06-25

Novel Multiple Flame Photometric Detection Methods for Gas Chromatography

Clark, Adrian

UNIVERSITY OF CALGARY

Novel Multiple Flame Photometric Detection Methods for Gas Chromatography

by

Adrian George Clark

A THESIS

SUBMITTED TO THE FACULTY OF GRADUATE STUDIES

IN PARTIAL FULFILMENT OF THE REQUIREMENTS FOR THE

DEGREE OF DOCTOR OF PHILOSOPHY

GRADUATE PROGRAM IN CHEMISTRY

CALGARY, ALBERTA

JUNE, 2015

Abstract

This thesis describes the advancement of a multiple flame photometric detector (mFPD) for gas chromatography (GC). The mFPD modes characterized in this study show great improvements (e.g. up to 20 fold better sensitivity) over its initial prototype, demonstrating similar (and enhanced) performance attributes (e.g. up to 100 fold better quenching resistance) relative to other GC detectors for the selective determination of sulfur and phosphorus compounds.

Through monitoring HSO* emission in the device, a linear sulfur response was found that demonstrated a detection limit of 5.8×10^{-11} gS/s, a selectivity of S/C of 3.5×10^{3}, and fast GC response dynamics. Notably, however, this mode provided enhanced response uniformity and reproducibility (e.g. 1.7% average RSD values and 90% of compounds ± 0.1 of unity response), as well as significant resistance toward interference from hydrocarbon quenching (e.g. signal observed down to 50 ng of analyte).

Next, emission spectra of the mFPD were acquired and examined for the first time. It was found that the mFPD produces sulfur emission as S_2*, but HSO* can also be isolated in the red spectral region. Further, phosphorus emission in the mFPD was found to stem from HPO*, while carbon emission was attributed to CH* and C_2*. Results indicate that a relative reduction of C_2 radical and an increase of oxidized carbon in the mFPD could play a central role in the quenching-resistant behavior of this device.

Finally, a new mFPD design was introduced based upon interconnecting fluidic channels within a planar stainless steel (SS) plate. Relative to the initial mFPD prototype, the SS mFPD provided a 50% reduction in background emission levels, easier operation,

and better signal collection properties. As a result, sulfur response in the device yielded a detection limit of 9×10^{-12} gS/s while also providing large resistance to hydrocarbon response quenching. Furthermore, this SS mFPD design uniquely allows analyte emission monitoring in multiple worker flames for the first time. In all, the new mFPD that has been characterized in this study can serve as a useful alternative method of detection for sulfur and phosphorus applications by providing more versatile monitoring options.

Preface

Portions of Chapter Two and Chapter Three have been published as A.G. Clark, K.B. Thurbide, Properties of a Novel Linear Sulfur Response Mode in a Multiple Flame Photometric Detector. *J. Chromatogr. A* **2014**, 1326, 103-109. Reproduced with permission from Elsevier Science.

Portions of Chapter Two and Chapter Four have been published as A.G. Clark, K.B. Thurbide, Spectral Examination of a Multiple-Flame Photometric Detector for Use in Chromatography. *Can. J. Chem*. **2014**, 92, 629-634. Reproduced with permission from Canadian Science Publishing (NRC Research Press).

Portions of Chapter Two and Chapter Five have been published as A.G. Clark, K.B. Thurbide, An Improved Multiple Flame Photometric Detector for Gas Chromatography. *J. Chromatogr. A* **2015** (*Article In Press*). Reproduced with permission from Elsevier Science.

Acknowledgements

First and foremost I would like to thank my supervisor, Dr. Kevin Thurbide, for his endless guidance, support, and encouragement. Leading by example, his work ethic has been a source of inspiration throughout my research, to which I owe him many thanks. Likewise, I would also like to thank my committee members, Dr. Scott Hinman and Dr. Hans Osthoff, for their continued time, support, and advice during my studies.

Secondly, a special thanks to the wonderful people (past and present) from the Thurbide group with whom I have had the pleasure of working with over the years and who have made each day of graduate school pass by with plenty of laughter.

Thanks also go to my colleagues and the department faculty and staff for making my time at the University of Calgary a great experience. Specifically the people from the Glass, Electronic, and Science Workshops: Mark Toonen, Andy Read, Todd Willis, Mike Siewert, and Ed Cairns, to which none of my work would have been possible without their excellent craftsmanship. As well, I would like to thank Bonnie King and Janice Crawford for all their help and administration assistance.

Finally, I would like to thank my wife, my family, and my friends, for their encouragement, patience, and love. I would especially like to thank my Aunt Vivian whose surprise gift packages always brought a smile to my face.

This work is dedicated to my wife, Teighen, and my parents, Neil and Leslee,

for their continuous love and support.

Table of Contents

List of Tables

List of Figures and Illustrations

List of Symbols, Abbreviations, and Nomenclature

AB	Alberta
~	Approximately
AZ	Arizona
AED	Atomic Emission Detector
×	By
m	Calibration slope
CA	California
cm	Centimetre
R^2	Coefficient of determination
CT	Connecticut
ccFPD	Counter-Current Flame Photometric Detector
°C	Degrees Celsius
°C/min	Degrees Celsius per minute
dFPD	Dual Flame Photometric Detector
et al.	Et alia (and others)
eV	Electron volt
e.g.	Exempli gratia (for example)
FID	Flame Ionization Detector
FPD	Flame Photometric Detector
GC	Gas Chromatography
GA	Georgia

g	Grams
g C/s	Grams of carbon per second
g P/s	Grams of phosphorus per second
g S/s	Grams of sulfur per second
>	Greater-than
≥	Greater-than or equal to
Hz	Hertz
i.e.	Id est (in other words)
I.D.	Inside diameter
INT	Interference
<	Less-than
hν	Light energy
LP	Long pass
MA	Massachusetts
m	Metre
µFPD	Micro-Flame Photometric Detector
µg	Microgram
µg C/s	Micrograms of carbon per second
µL	Microlitre
µm	Micrometre
mg	Milligram
mL	Millilitre
mL/min	Millilitres per minute

mm	Millimetre
ms	Milliseconds
mV	Millivolts
mV/s	Millivolts per second
MDL	Minimum Detectable Limit (or Level)
MDM	Minimum Detectable Mass
MQL	Minimum Quantifiable Limit (or Level)
min	Minute
mFPD	Multiple Flame Photometric Detector
nA	Nanoamperes
ng	Nanogram
nL	Nanolitre
nm	Nanometre
nm/min	Nanometres per minute
NJ	New Jersey
NY	New York
N	Noise
N_{p-p}	Noise peak-to-peak
N_{rms}	Noise root-mean-square
n/a	Not available
n	Number of data points or iterations
OH	Ohio
ON	Ontario

O.D.	Outside diameter
%	Percent
%RSD	Percent relative standard deviation
PMT	Photomultiplier tube
pg	Picogram
pg S/s	Picograms of sulfur per second
±	Plus or minus
α	Proportional to
pFPD	Pulsed Flame Photometric Detector
®	Registered trademark
s	Seconds
S	Signal
S/N	Signal to Noise ratio
S/N_{p-p}	Signal to Noise peak-to-peak ratio
S/N_{rms}	Signal to Noise root-mean-square ratio
S/σ	Signal to sigma ratio (S/N_{rms})
SS	Stainless Steel
σ	Standard deviation or sigma
SCD	Sulfur Chemiluminescence Detector
TCD	Thermal Conductivity Detector
USA	United States of America
ν	Vibrational quantum number
w/v%	Weight per volume percent

CHAPTER ONE: INTRODUCTION

Gas chromatography (GC) is one of the most prolific analytical separation methods in the world today. Commonly explored in the areas of environmental, petroleum, chemical, forensic, and pharmaceutical analysis, it has long been recognized as an excellent method for the resolution of target analytes from complex matrices. Specifically, GC is a chromatographic technique used for the separation, characterization, and determination of volatile and semi-volatile chemical compounds. Despite more than half-a-century in existence, the role of GC and its components have generally remained the same: an inlet for sample introduction, a carrier gas for analyte transportation, a heated column for separation, and a detector to register the presence of target analytes. As such, the detector is employed to simultaneously obtain both qualitative and quantitative information of a sample's composition. It is an essential component in the GC system, playing a critical role in the development of the technique as a whole. Therefore, progress in GC instrumentation strongly depends on the continual development and design of its detectors. For instance, if a sample's complexity increases or more stringent regulations are required, GC detectors must be subject to modification and refinement in order to continue to analyse a sample's composition. In this respect, the research in this study is aimed at developing and improving upon GC detection.

1.1 Classification of Detectors

Gas chromatography is blessed by a number of robust and sensitive detectors based on a number of physical and chemical principles. Of these principles, most GC detectors are founded on detection mechanisms that use gas-phase ionization, bulk property, electrochemical, and optical measurements[1]. Accordingly then, GC detectors are categorized by how they respond to a class of analytes. An analyst can then select a detector by how the analyte is quantified and what type of target analyte it will respond to.

1.1.1 Universal and Selective Methods of Detection

In general, detectors can fall into one of two categories, universal and selective. A universal detector theoretically detects all compounds (or most compounds) that elute from the chromatographic column. Whereas, a selective detector typically only detects compounds with a specific molecular, elemental, or physical property[2]. For example, a conventional universal detector, such as the flame ionization detector (FID) is not very selective and responds uniformly to nearly all organic compounds[1]. In contrast, the flame photometric detector (FPD) is a very selective detector, primarily used for the detection of sulfur and phosphorus-containing compounds[2].

As such, both methods of detection have certain advantages. Universal detectors are important for qualitative screening of new samples whose composition is not fully known; information can therefore be quickly attained on the sample prior to deeper analysis. However, for a comprehensive analysis with a universal detector, higher demands might have to be placed on sample preparation and chromatographic separation[3]. Selective detectors, conversely, can provide enhanced sensitivity for only a

small class of compounds. They can simplify a complex chromatogram, providing trace analysis of a specific compound or element amongst a complex matrix[4]. This research is focused on the performance of such a selective detection method as described later in this Chapter.

1.1.2 Mass-Flow and Concentration Sensitive Detectors

Another important classification of GC detectors is whether a detector is considered mass-flow or concentration sensitive. This classification system distinguishes between how a detector quantifies an analyte. A concentration sensitive detector will generate a response proportional to the concentration (i.e. mass of analyte per unit volume of carrier gas) as it passes through the detector cell[2,4]. As such, the detector cell volume in concentration sensitive detectors is critical to its detectivity. A mass-flow sensitive detector, on the other hand, will produce a signal proportional to the absolute mass of an analyte reaching the detector cell per unit of time[4]. The mass entering the detector is determined solely by the rate of elution from the column and therefore the volume of the detector is less relevant for the signal generation.

To better understand the reason for this detector classification, one can consider the effects of analyte response if the carrier gas flow is completely stopped mid-elution of an analyte in a detector cell. In a concentration sensitive detector, if flow is stopped, the detector cell remains filled with a given concentration of analyte and its response continues to be measured at a constant level. However in a mass-flow sensitive detector, a complete stop in the flow rate will cause the delivery of the analyte response to the detector cell to cease and the signal will quickly drop to baseline; only if flow is then resumed will the signal return.

The issue of flow dependency of each detector type is of great importance when quantitation is based on peak height or peak area measurements. As such, changes in response are observed in each detector when an analyte is introduced at different flow rates. For example, if flow rate is increased in a concentration sensitive detector, peak height will generally remain constant, however peak area and peak width will decrease[5,6]. If flow rate is increased in a mass-flow sensitive detector, peak height will generally increase, peak width will decrease, while peak area will remain constant[5,6]. Therefore comparisons made between concentration and mass-flow sensitive detectors can sometimes be difficult unless concentration and flow rates are specified. As such, for each type of detector, detection limits are often reported in different terms. For example, detection limits of concentration sensitive detectors, like that of a thermal conductivity detector (TCD), are most often stated in concentration terms (e.g., g/mL)[2]. Whereas mass-flow sensitive detectors, like an FPD or FID, detection limits are stated in mass per time (e.g., g X/s, where X is a particular element or compound to which the detector registers a response)[2].

1.1.3 Destructive and Non-Destructive Detectors

One last classification of GC detectors is whether they are considered destructive or non-destructive. This classification is based on the evaluation of changes that take place in the detector cell due to the detection mechanism. Typically, in a non-destructive detector, analytes can pass through the detector without any chemical change[5]. An example of a non-destructive detector would be a TCD. Non-destructive detectors are necessary if the separated analytes are to be reclaimed for further analysis. For instance, another detector can be placed downstream in tandem where analytes may be passed for

additional characterization[2]. Destructive detectors, on the other hand, generally destroy the analyte as part of their process of operation (e.g., by burning in a flame). Examples of destructive detectors would include both the FID and FPD. As such, the focus of this work is directed towards the study of an FPD-based detector.

1.2 Detector Attributes

Like almost every other analytical technique, the success of GC is dependent, to a large extent, upon the efficiency of the detector and its suitability for its intended purpose. Typically, a desirable detector would be one that is economical, rugged, and can sense trace amounts of analyte using simple separation methods and minimal sample preparation. However, when characterizing a detector, specific detector attributes are often reported to gauge the effectiveness of its intended purpose. Such reported attributes would include its sensitivity, detection limits, selectivity, linearity, equimolarity, and reproducibility. To provide a framework for the intentions of this study, these characteristics will be further defined and discussed.

1.2.1 Sensitivity and Detection Limits

In general, the most important characteristic of a detector is the signal (S) it produces[7]. The basis of quantitative analysis relies on this relationship between a signal's magnitude of response in proportion to a known amount of analyte. By definition, sensitivity is a measure of the magnitude of the signal generated by the detector for a given amount of analyte flow per unit time[4]. For example, in mass-flow sensitive detectors, sensitivity refers to the change in detector response as a function of the change in the amount of the analyte[8]. As such, sensitivity is an indication of relative analyte

signal strength. Sensitivity, however, does not allow an unambiguous characterization of the smallest amount of sample still measureable with a given detector[9]. For instance, most analytical detectors produce a background signal even when there is no analyte eluting from the column. Fluctuations of this signal, defined as noise (N), are formally the random perturbations in a signal produced by a detector in the absence of any sample[4]. As a fundamental property of the detecting system, the detectors' noise ultimately determines the detection limits that can be achieved. If possible, the sources contributing to noise should be found and minimized because they restrict the minimum signal that can be detected. Therefore, to assess the actual limit of detectability, the relative magnitude of analyte signal must be evaluated against the inherent background noise associated with the detector. Thus, a numeric measure of the signal-to-noise ratio (S/N) is a much more useful characteristic for describing detector performance[4]. The larger the S/N ratio for a given amount of analyte and set conditions, the better the detection method. As such, noise is conventionally measured over a representative section of baseline signal that is calculated over a span of at least 10 analytical peak widths[10,11]. Consequently, noise can be reported as either peak-to-peak noise, or as a root-mean-square noise[12,13]. Peak-to-peak noise ($N_{p\text{-}p}$) is calculated from the difference between the maximum and minimum deviations of a representative baseline signal[14]. Whereas root-mean-square noise (N_{rms}, also denoted as σ), is the standard deviation calculated from this representative baseline signal[8]. As such, the signal-to-noise ratio ultimately depends on how noise is defined, and therefore it should be indicated how this is calculated when detection limits are reported.

Detection limits are terms used to describe the limits of detection and quantitation. Unlike sensitivity, detection limits are more direct indicators of detector performance, since both detection limits and detector performance are functions of the S/N ratio. Minimum detectability, with respect to the detection step in chromatography, is the minimum mass flux (or concentration) of analyte which gives a detector signal that can be discerned from the noise with reasonable certainty[13]. Minimum detectability is also sometimes used synonymously with the terms minimum detectable level or minimum detectable limit (MDL)[13,15,16]. The most common GC definition of minimum detectability is the analyte quantity in the detector that yields a peak response that is equal to twice the peak-to-peak noise calculated (i.e., $S/N_{p-p} = 2$)[15,17]. As well, minimum detectability can also be defined as the quantity required to produce an analytical signal which is three times greater than the absolute standard deviation of the baseline noise (i.e., $S/\sigma = 3$)[8,18,19]. Thus, to ensure fair performance comparisons between different detectors, specifications should report how the minimum detectability, and hence the noise, is defined.

The quantitation limit however, compared to minimum detectability, is the performance characteristic that marks the ability of a detector to adequately quantify an analyte[20]. For example, when the signal is 3 times greater than the noise, it is detectable and can answer whether an analyte is present or not, but it is still often thought too small for accurate measurements[21]. However, a signal that is 10 times greater than the noise, called the minimum quantifiable level or minimum quantifiable limit (MQL), is considered the smallest amount that can be measured with reasonable accuracy and precision[22,23]. This amount (or concentration) is set higher to the minimum detectability

so that detecting an analyte is not ambiguous and can be confidently quantified. Thus when defining a detectors' detection limits, the minimum detectable limit must be clearly defined to avoid confusion with the quantitation limit and the sensitivity of the detector.

1.2.2 Selectivity

Selective GC detectors, as previously described, can provide enhanced sensitivity for only a small class of compounds. A detector is considered to be selective if its response to a certain type of compound differs markedly from that to another type of compound[24]. An ideal selective detector will elicit a strong response for only the related class of compounds and will disregard any other compounds that may be contained in a sample. However in practice, other compounds contained within a sample, especially in larger amounts, may have some influence on detector performance. Therefore, when comparing selective detectors, an analyst is interested in some measureable ability to detect the compounds of interest while rejecting all others. This ability is normally described as the selectivity of a detector. Selectivity is stated as the ratio of the amount of a non-target interfering compound to the amount of a target compound that generates an equivalent signal[2]. As such, formal selectivity is usually reported as orders of magnitude over a potentially interfering compound in terms of relative molar response or as relative weight response[8]. For instance, FPD detection methods largely describe the response of sulfur-containing compounds to pure hydrocarbon compounds that serve as carbon standards in selectivity ratio measurements[25,26]. For example, if 1 mg of a carbon reference standard (10^{-3} gC) generates the same response as 100 ng of a sulfur-containing reference (10^{-7} gS), then the selectivity ratio of sulfur would therefore be 10^4 (i.e., 10^{-3} gC / 10^{-7} gS = 10^4 gC/gS). In other words, 10,000 times more carbon would be needed to

generate the same signal or the response of a sulfur-containing compound would be ten thousand times larger than that of a potentially interfering hydrocarbon compound present in the same amount. In general then, the larger the difference, the greater the selectivity is for the particular detector.

1.2.3 Linearity, Equimolarity, and Reproducibility

Detector linearity is an important characteristic for any detector that is to be used for quantitative analysis. Ideally, the response of a detector should be consistently linear; whereas the signal is directly proportional to either the concentration of analyte in the carrier gas or to its mass-flow rate. Linearity is a measure of how well data in the calibration graph follows a straight line, showing that response is proportional to the quantity of analyte[21]. Therefore, when analyzing the linear behavior of a detector, it is commonplace to plot the detector response versus the mass-flow rate (or concentration) in a log-log scale, since linearity can extend over several orders of magnitude. In practice, however, a detector is usually only linear over a limited range. This linear range is defined as the range of concentration or mass-flow over which the slope of the calibration plot is constant within a specified variation, commonly ± 5%[16]. However, further deviation from linearity does not necessarily hinder quantitative analysis; sensitivity can still be defined outside this linear range. For example, linearity of most GC detectors can deteriorate at higher concentrations or mass-flow rates[27] but can still provide predictable and reproducible response profiles. Therefore, the term dynamic range is used for the operating range of mass-flow (or concentration) over which there is a measurable response to analyte, even if the response is not linear[21]. This dynamic range extends from the MDL to an upper limit of detection. The upper limit of detection represents a point of

the calibration plot at which the curve levels off and shows no more increase in signal with increasing mass-flow rate (or concentration)[17]. As such, this dynamic range is greater than the linear range and should be clearly stated as to avoid confusion, as both ranges are commonly expressed in orders of magnitude with dimensionless units. For clarification, Figure 1-1 presents a graphical illustration of these aforementioned definitions. In general then, a detector showing good linearity with a large dynamic and linear range is highly desirable.

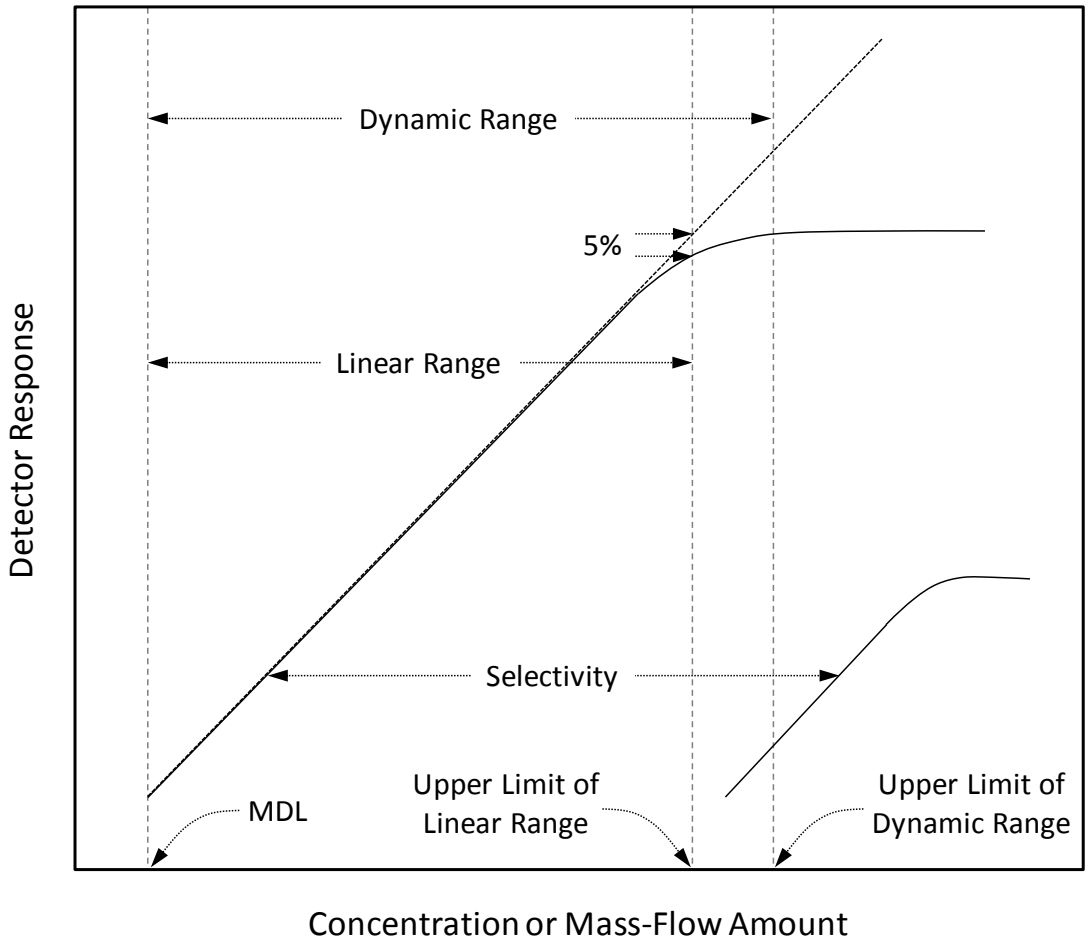

Figure 1-1: Illustration of generic calibration curves of a detector demonstrating selectivity, minimum detectable limit, linear and dynamic ranges.

Equimolarity or equimolar response of a detector refers to the property of the detector that yields equal response to equal amounts of different analytes on a molar basis. The benefit of a detector that provides an equimolar response is that it only requires a single calibration standard to quantify each analyte (including unknowns) present in a sample. This is particularly helpful for estimating concentration levels of components in a sample when identities are unknown and for complex sample analyses which require calibrations for multiple analytes (which can be potentially very time consuming). For instance, an FID is generally acknowledged as an equimolar detector providing a uniform response for most carbon containing analytes independent of compound structure[2]. Whereas, conversely, an FPD does not typically display an equimolar response; as variations in detector response toward sulfur containing compounds of differing molecular structure is quite common[24,28,29]. Therefore in this regard, relative equimolarity calculations are often made in order to show how uniform the detector response is over a range of different compounds of varying molecular structure. As such, detectors that can provide a more uniform response to all compounds are generally preferred.

Having considered the equimolarity of a detector, it is also essential to examine the reproducibility of a detector's response. Consequently, for a GC detector to be widely accepted, it should be reliable and provide reproducible run-to-run and day-to-day response. Therefore, the reproducibility of a detector is qualified by the constancy of the response it provides during its service life[24]. As such, all the parameters which influence the detectors' response should be identified and controlled within satisfactory limits[30]. Ideally, the detector response in a GC instrument should be highly repeatable. Repeatability represents the simplest situation and involves analysis of replicates by the

same analyst, generally one injection after the other[11]. Instrument precision is the reproducibility observed when the same quantity of one sample is repeatedly introduced (≥ 10 times) into an instrument[21]. As such, these replicate analyses performed on a reference sample can yield a standard deviation of the mean response and provide a measure for precision. Often reproducibility is represented by the percent relative standard deviation (%RSD) of these measurements for many compounds owing to variations in the response of the detector over time. The lower the %RSD found for the response of these compounds, the more reproducible the detector response. As a consequence, an analyst will generally choose a detector with high repeatability and reproducibility for routine GC analysis.

1.3 Flame Based GC Detectors

1.3.1 Flame Ionization Detector (FID)

Without question, the flame ionization detector (FID) is one of the most popular and widely used detectors in GC. The FID, as mentioned, is a destructive, mass-flow sensitive detector used for the universal response toward volatile carbon-containing compounds. This serendipitous discovery was first developed (simultaneously and independently) in the late 1950's by McWilliams et al.[31] and Harley et al.[32] when a potential was placed across a hydrogen-air flame and an electrical response was obtained from carbon-containing compounds. As such, the operating principle of the FID has not changed drastically since its original conception. The FID still uses an air-rich hydrogen/air flame to burn carbon-containing compounds as they elute from a

chromatographic column to create electrically charged species[33]. The basic design of an FID is shown in Figure 1-2.

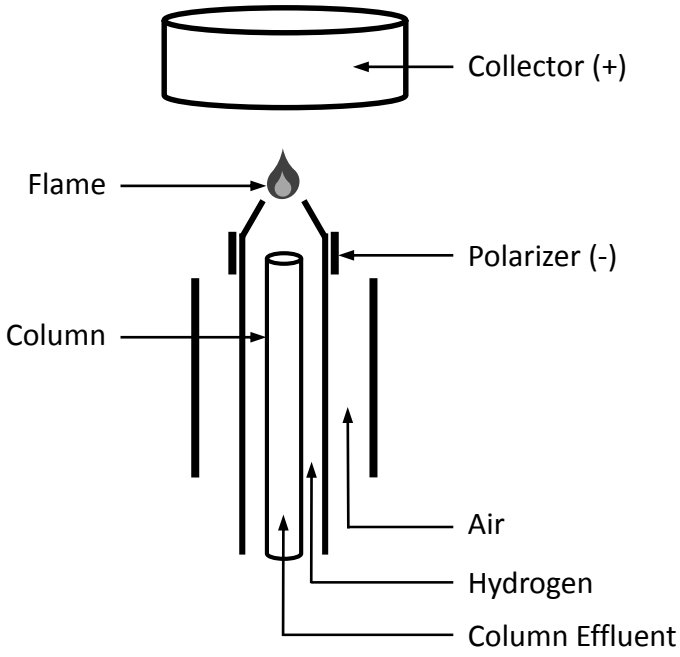

Figure 1-2: Schematic diagram of an FID.

Here, the combustion of these organic compounds gives way to a small number of ions that can be collected with an appropriate electrical field[30]. The positively charged species are attracted to a negatively charged polarizer and the current produced is proportional the number of ions collected. The exact mechanism of ion production is not well characterized, however it is generally accepted that carbon compounds first break down to single carbon species, such as methane[2]. These carbon species then undergo a chemi-ionization reaction forming a charged CHO^+ species and an electron via the following reaction[1,2,30,34,35]:

$CH\cdot + O\cdot \rightarrow CHO^+ + e^-$ **Reaction 1.3-1**

The yield of charged ions produced by the detector, however, is quite small; only about one ion per 10^6 carbon atoms are formed[2]. Despite this, the detector can still produce detection limits in the low picograms of carbon per second (10^{-12} gC/s) range, while providing a large linear range of up to 7 orders of magnitude[2]. This detection mechanism ultimately gives rise to a "unit carbon response" meaning that the FID responds linearly to the mass of carbon flowing through the detector, independent of compound structure[2]. The popularity of the FID can be easily attributed to this reliable and reproducible response, with the added benefit of being very simple, rugged, and easy to maintain[30].

Although the FID is generally thought to respond to all carbon-containing compounds, there are a few exceptions. For example, little to no response is found in the FID for simple non-hydrogenated carbon compounds containing heteroatoms such as CO, CO_2, COS, and CS_2[33]. Consequently, the response of the FID to various analytes ultimately depends on their ability to give CH· free radicals during their combustion[30]. As such, partially oxidized carbon atoms, for instance, have a very low or negligible probability of responding[30,35]. However, such exceptions have been exploited in other forms of chromatography, such as supercritical fluid chromatography; where separations are performed using CO_2 as a mobile phase and FID detection without any complications[36].

1.3.2 Flame Photometric Detector (FPD)

One of the most widely used selective detectors in GC has been the flame photometric detector (FPD). Since its introduction in 1966[37], it has become a very popular detector for the selective monitoring of sulfur and phosphorus containing compounds. Although its primary use has been for compounds containing sulfur and

phosphorus, other elements such as chromium, tin, manganese, and lead, have also generated a selective response in the FPD[18,25,38]. Similar to the FID, the FPD is a flame-based, mass-flow sensitive, destructive detector. However, rather than measuring the current from ions formed, the FPD measures the light emitted from combustion products[2]. As such, the basic principle of an FPD utilizes a hydrogen-rich flame with air (or oxygen) to help promote chemiluminescent emission of these compounds which is then monitored by a photomultiplier tube (PMT). A schematic diagram of an FPD is shown below in Figure 1-3.

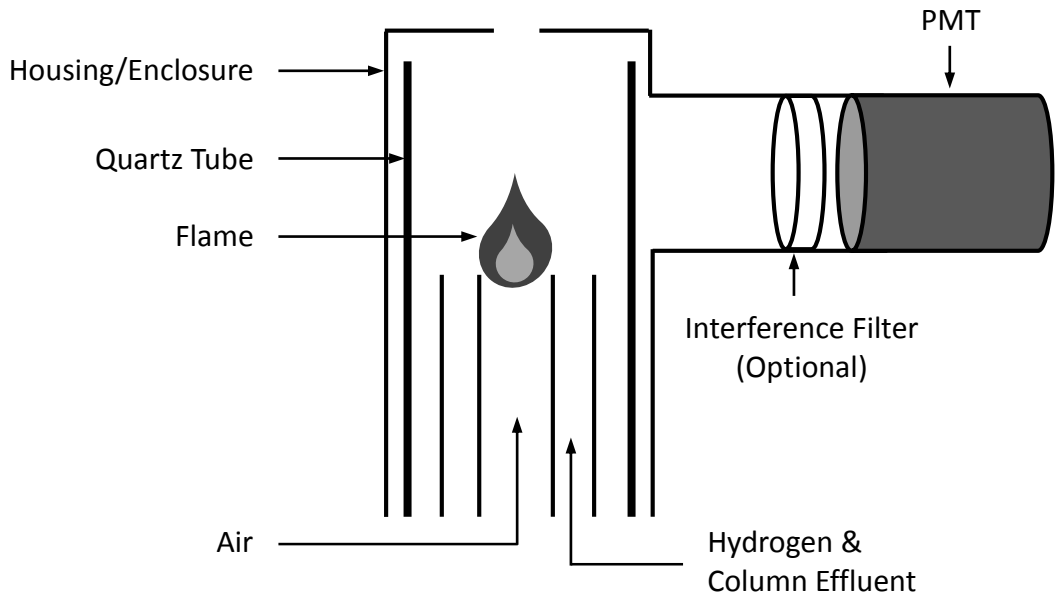

Figure 1-3: Schematic diagram of an FPD.

Here, hydrogen and column effluent are delivered by a tube that concentrically surrounds the air stream to generate a relatively cool (< 1000 °C)[39], hydrogen-rich flame. As such, the hydrogen-rich region around the flame's outer cone is where chemiluminescent emissions are dominant[40]. Depending on the wavelengths emitted by a species,

interference filters can be used to increase analyte selectivity by isolating these emissions and reducing other contributions of flame emission. For instance, sulfur compounds which predominantly emit as S_2* species, have a maximum intensity near 394 nm, while phosphorus compounds emitting as HPO* species, have a maximum intensity near 526 nm[2,24,30]. The advantage of using FPD detection is largely due to its selective and sensitive response to these elements. For example, the detection limits for sulfur are approximately 10^{-11} gS/s with a quadratic response over 3-4 orders of magnitude, while the detection limit for phosphorus is around 10^{-12} gP/s with a response that has a linear range over 5 orders of magnitude[24,33]. As well, the FPD provides selectivity toward sulfur of about 3 to 4 orders of magnitude and toward phosphorus of about 5 orders of magnitude, relative to carbon[24].

The FPD flame, as mentioned, uses a hydrogen/oxygen flame which operates hydrogen (i.e. fuel) rich. This creates varying concentrations of different flame radicals which play important roles in both the sample decomposition chemistry and in chemical reactions that result in light emission. These mechanisms of analyte emission have been widely explored in the FPD[1,41-44]. However, a complete consensus for the emission mechanism of phosphorus and sulfur species in an FPD flame has yet to be established. Still, it has been generally acknowledged that the energy required for chemiluminescence can be provided by the recombination of hydrogen radicals[18,43,45-48].

$H\cdot + H\cdot \rightarrow H_2 + 4.5\ eV$ **Reaction 1.3-2**

As Reaction 1.3-2 shows, a recombination of hydrogen radicals produces 4.5 eV of energy which can be used to excite species in the flame to emit light. For instance, as phosphorus containing compounds elute from the column and enter the flame, the species

HPO can be generated. With the energy provided by the recombination of hydrogen radicals, excitation of the species to HPO* can occur, and upon relaxation it emits this energy as a photon[33,43,48].

$R\text{-}P \rightarrow HPO + 4.5\ eV \rightarrow HPO^*$ **Reaction 1.3-3**

$HPO^* \rightarrow HPO + h\nu$ **Reaction 1.3-4**

Consequently, the response in the FPD is linear, as the amount of HPO* species produced in the flame is proportional to the amount of phosphorus contained within the compound[33,49].

e.g. Response α [P] **Equation 1.3-5**

Conversely, the dominant emitting species in the FPD for sulfur emission is the electronically excited diatomic molecule, S_2*[24,28]. As such, sulfur containing compounds must first undergo a series of degradation reactions in the flame for the required formation of the S_2 dimer. Again, a recombination of hydrogen radicals can produce enough energy to excite the emitting species to S_2*, which upon relaxation can emit this energy as light. Due to the complex nature of the processes occurring in the flame, the exact mechanism of S_2* formation in the FPD is still not completely understood. However, reactions that are presumed to occur when a sulfur compound reaches a hydrogen rich flame are as follows[28,42-44,48-51].

Sulfur Compound $\xrightarrow{\Delta} H_2S$ **Reaction 1.3-6**

$H_2S + H\cdot \rightarrow HS\cdot + H_2$ **Reaction 1.3-7**

$HS\cdot + H\cdot \rightarrow H_2 + S\cdot$ **Reaction 1.3-8**

$HS\cdot + S\cdot \rightarrow S_2 + H\cdot$ **Reaction 1.3-9**

$H\cdot + H\cdot + S_2 \rightarrow S_2^* + H_2$ **Reaction 1.3-10**

$S_2^* \rightarrow S_2 + h\nu$ **Reaction 1.3-11**

Unlike the linear response obtained for phosphorus compounds, the response of the FPD has a less desirable quadratic relationship with mass of sulfur in a given compound, since two atoms of sulfur are required to generate the observed chemiluminescence. As such, the response obtained is theoretically proportional to the square of the amount of sulfur present[1,33,52].

e.g. Response $\alpha\ [S]^n$, where n = 2 **Equation 1.3-12**

However, while the theoretical value for n is 2 (hence S_2), experimentally this number can vary between 1.6 and 2.2 depending on the sulfur compound analyzed[1,24,33,42]. In other words, a non-equimolar response is produced and different sulfur-containing compounds give rise to different emission intensities for the same molar quantity of sulfur. As such, non-optimized flame conditions, compound-dependent decomposition, and competing flame reactions that lead to de-excitation can all contribute to this deviation[1]. Ultimately this variability in FPD response can lead to complications in quantitative analysis. For example, calibration curves (covering the entire analyte concentration range) must be made independently for each specific sulfur compound to quantify the amount of sulfur in a sample. As a result, this calibration process can be rather cumbersome and time consuming.

Another more serious limitation of the FPD is the quenching of analyte chemiluminescence that occurs due to co-eluting hydrocarbons[28,51,53-55]. For instance, chemiluminescent emissions can be virtually eliminated in the presence of even a small amount of hydrocarbon also entering the FPD flame[28,51,55]. Consequently, the response for a given amount of sulfur or phosphorus in a sample can be reduced, and the accuracy

of compound identification and quantification can be compromised[2,44]. This effect can hinder the FPD's detection capabilities particularly when analyzing complex matrices in petroleum products, air pollutants, pesticide residues, and food aromas[53]. In order to employ the FPD in these applications, an analyst may rely heavily on highly resolved separations of analytes and hydrocarbons, often resulting in either complicated separation techniques or long analysis times[56]. Although the exact mechanism for quenching in the FPD is not fully understood, several suggestions have been made[24,44,51,53,54]. The most accepted possibility suggests that hydrocarbons scavenge the hydrogen radicals in the flame, thereby reducing the amount of energy available for chemiluminescence[51,53]. Regardless of the mechanism of quenching, co-eluting hydrocarbons remain a considerable problem and pose a significant complication in FPD analysis.

Despite the issues of linearity, uniformity, and signal quenching due to co-eluting hydrocarbons, the FPD is still one of the most popular detectors for selective monitoring of organosulfur and organophosphorus compounds. The highly selective and sensitive performance of the FPD has been extended in many industrial sectors due to its relative ease of operation, tuning, and maintenance[56]. As well, the detector itself is inexpensive, robust, and does not require a high level of expertise to achieve adequate performance for trace level quantification in most analytical laboratories[56,57].

1.3.3 Dual Flame Photometric Detector (dFPD)

After the invention of the FPD, the dual flame photometric detector (dFPD) was developed by Rupprecht et al.[58], and later improved upon by Patterson et al.[50] as a means to combat the aforementioned complications in FPD analysis. As such, the basic principle

of detection in the dFPD generally remains the same as an FPD with some modifications. A schematic diagram of the dFPD is shown in Figure 1-4.

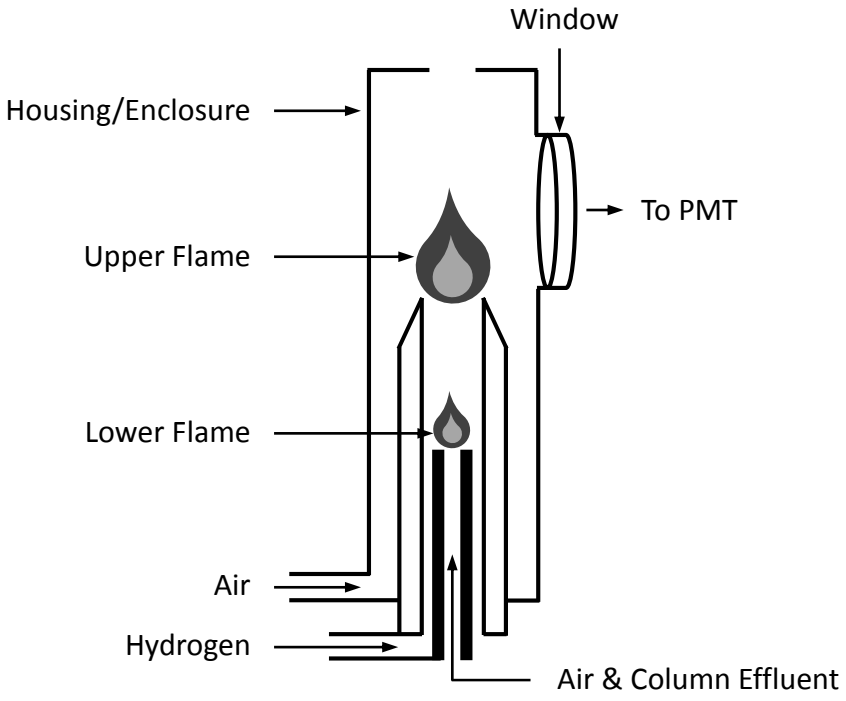

Figure 1-4: Schematic diagram of a dFPD.

Rather than a single-flame, the dFPD operates using two flames in series; one flame to achieve the decomposition of incoming samples, and a second longitudinally separated flame to produce the desired optical emission[50]. Here, the column effluent is mixed with air while hydrogen is added at the base of the detector. The lower (oxygen-rich) flame is responsible for combustion of the sample, while the upper (hydrogen-rich) flame generates the light-emitting excited species that are monitored by the PMT[16].

As previously mentioned, the first main problem of the FPD is the non-uniform response produced toward sulfur-containing compounds. However, in the dFPD design,

the lower flame functions as a matrix-normalization reactor in which all compounds are first partially decomposed before being swept into the upper flame[49]. In other words, the lower flame helps to create a more uniform response toward sulfur by first homogenizing the effluent. As a result, the dFPD provides a more reproducible (quadratic) response which is less dependent on compound structure, thereby following a true square-law dependence on sulfur amount[1,50].

Secondly, it was found that quenching of the chemiluminescence emission of the analyte by co-eluting hydrocarbons was also reduced in the dFPD[58,59]. Again, the lower flame helped to alleviate this problem by first oxidizing hydrocarbons to carbon dioxide. It was concluded that quenching was greatly reduced when carbon is present as carbon dioxide versus a less oxidized hydrocarbon[58]. As a result, samples that contain elevated amounts of co-eluting hydrocarbons would require less sample preparation and less chromatographic resolution with a dFPD.

Detector attributes of the dFPD are often compared to the conventional FPD. For instance, the selectivity of a dFPD generally remains the same. Specifically, selectivity over carbon for sulfur is approximately 10^3 to 10^4, while for phosphorus it is about five orders of magnitude[50,60]. However, the major limitation of the dFPD is its significantly reduced sensitivity. In particular, over a 10-fold loss in response can be found in the dFPD compared to a conventional FPD[60-62]. As a result, the detection limits in a dFPD are higher for both sulfur and phosphorus-containing compounds, which may have contributed to its limited use in chromatography. Despite this, the dFPD has been employed in some applications due to its resistance to analyte emission quenching from co-eluting hydrocarbons[63-67].

1.3.4 Pulsed Flame Photometric Detector (pFPD)

Further significant modifications to the FPD were made by Amirav et al. in the form of a pulsed flame photometric detector (pFPD)[68-70]. Unlike the conventional FPD, the pFPD is based on an ignition source and combustible gas flow rate that cannot sustain continuous flame operation. Instead, the flame propagates through the detector upon ignition and self terminates after the combustible gas is burnt. The combustion products that are created are then removed with the upward flow of fresh combustion gas, and the ignition process begins again; thus establishing a pulsing flame. A basic schematic of the pFPD is shown in Figure 1.5.

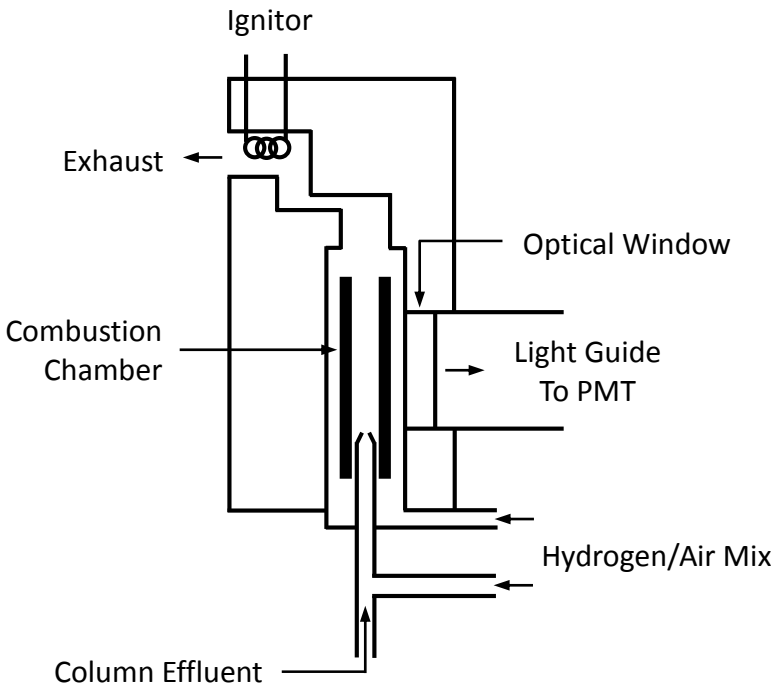

Figure 1-5: Schematic diagram of a pFPD.

Here, a combustible gas mixture of hydrogen and air is continuously fed into the combustion chamber together with the GC column effluent. As well, this combustible gas mixture is also flowing up to a continuously heated ignitor. The ignited flame then propagates back to the gas source through the combustion chamber and is self-terminated within a few milliseconds. As such, the continuous gas flow creates additional ignition in a pulsed periodic fashion at a tunable cycle of 1-10 Hz[69]. The emitted light is then transferred through a light guide and monitored by a PMT.

Unlike the FPD, the pFPD exploits the fact that there is a kinetic aspect to the emission of light; as the emission from excited carbon, phosphorus, and sulfur species happen at slightly different rates after the combustion products are formed[2]. Consequently by electronically gating the analyte emissions, an analyst can choose which part of each pulse to amplify and record as a function of time. For instance, carbon species emit rather instantaneous, usually lasting for approximately 2 ms, while phosphorus emission peaks approximately 5 ms after ignition[2,69,71]. Sulfur emission, on the other hand, happens over a very wide time frame from approximately 5 to 25 ms after ignition[2,69,71]. Therefore, by applying a delayed time gate window for sulfur and phosphorus (after that of carbon), most of the spectral interference from carbon can be eliminated[2]. This also allows the pFPD to selectively and sensitively detect some analytes co-eluting in the presence of others. As a result, the pFPD can produce very good detection limits which have been quoted nearing 10^{-13}g S/s for sulfur and for phosphorus approximately 10^{-14} g P/s[33,60,69]. As well, using a gated integrator, selectivity of sulfur over carbon can reach as high as seven orders of magnitude[60,69,72]. Lastly, the pFPD also

has been quoted to produce a purely quadratic response, as an exponential constant of 2.00 ± 0.03 was reported from a tetrahydrothiophene dilution series[69].

However, the pFPD does have some disadvantages. For instance, the pFPD is still susceptible to quenching by high concentrations of co-eluting hydrocarbons[2,73]. As well, the dynamic range, for sulfur detection is more narrow (~10^3) compared to a conventional FPD[69,72]. Instrumentally, its design is more complicated and often requires specific techniques to obtain optimal results[2,57]. Furthermore, with respect to fast GC applications, the pFPD has not been noted to be particularly well suited for very narrow GC peaks. Fast GC separations often require fast signal transduction (≥ 20 Hz), however the detector pulses occur only a few times each second[2,39,56]. As such, due to these limitations, the range of applications in which a pFPD can be used is narrower than that of the conventional FPD[2].

1.4 Other Sulfur Selective Detectors

Aside from the aforementioned FPD-related devices, other commercial detectors have been made available for sulfur detection. Two of the most well-known of these detectors include the sulfur chemiluminescence detector (SCD) and the atomic emission detector (AED). However, their approach to the selective response of sulfur luminescence is acquired through different methods. Over the years, both GC detectors have received much notoriety for their selective and sensitive response for sulfur-containing compounds[60,74,75], and therefore are particularly worthy of mention in this category.

To begin with, the SCD, first developed by Benner et al., is a mass-sensitive, destructive detector that is based on ozone-induced chemiluminescence[62,76]. The

mechanism of SCD detection generally follows a two-step process[2]. First, sulfur compounds from the GC effluent are directed into a high temperature (~ 1800 °C) reducing hydrogen/oxygen flame to generate the formation of sulfur monoxide[5,76]. As such, a more recent flameless-design of the SCD which employs a ceramic combustion chamber can also be used for this step[77]. Secondly, a vacuum draws the sulfur monoxide into a separate reaction chamber and mixes it with ozone to create excited SO_2* species under a reduced pressure[76]. A schematic representation of the SCD and its operation is shown below in Figure 1-6.

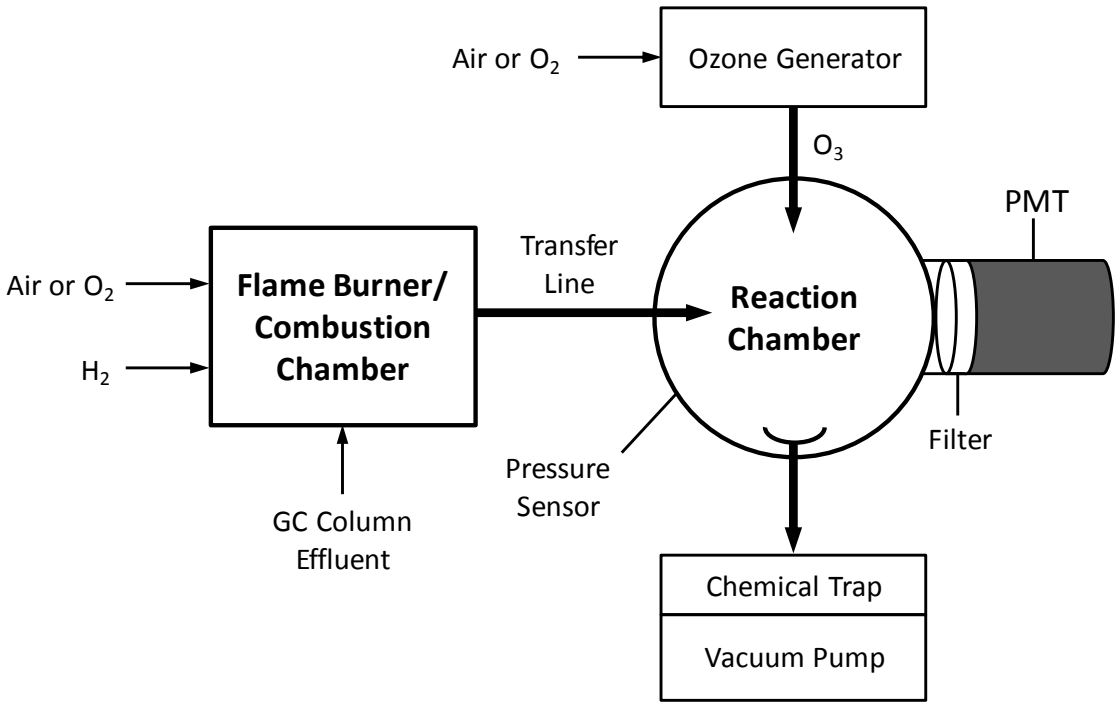

Figure 1-6: Simplified schematic diagram of an SCD.

As such, the general mechanism of SCD detection can be expressed by the following reactions.[2,5,78-81].

Sulfur Compound → SO **Reaction 1.4-1**

$SO + O_3 \rightarrow SO_2^* + O_2$ **Reaction 1.4-2**

$SO_2^* \rightarrow SO_2 + h\nu$ **Reaction 1.4-3**

As shown, upon relaxation of the SO_2^* species, the sulfur dioxide can emit a broad band of light that is centered around 360 nm[2,5,78,79]. The light is then filtered through a wavelength-specific filter and is monitored by a PMT.

Consequently, the SCD can provide detection limits as low as 10^{-13} gS/s, while providing a linear range of 10^4, and a very large selectivity over carbon of about seven orders of magnitude[2,5,82]. The SCD also provides a nearly equimolar response to sulfur containing compounds, as the response is directly proportional to the amount of SO generated in the combustion step[57,77]. As well, unlike the FPD, the SCD does not exhibit significant quenching of response from co-eluting hydrocarbons[57,77]. As a consequence, when operating properly, the SCD is an excellent detector for sulfur-containing compounds.

However, long term stability issues have often plagued the SCD as the sensitivity and performance can degrade with use[2,5,77,79]. For instance, it has been reported that the detector response is highly dependent on the condition and positioning of a ceramic probe that is used to sample the post-flame gases; this often requires re-conditioning to regain detector sensitivity[77]. This diminished sensitivity is most likely from a change in efficiency in the burner (i.e., through deposition of coking products from hydrocarbons)[5]. Coking not only affects the current analysis in progress, but also contaminates the system; often adversely affects the function of the pyrolyzer and hence causes deterioration in SCD sensitivity and stability[79]. Therefore the SCD requires more frequent

calibrations and more attention than most other GC detectors[5]. Additionally, the SCD is a somewhat bulky and moderately complex instrument, compared to more compact and robust detectors like the FID and FPD[79]. Furthermore, compared to other sulfur-selective detectors, the SCD is much more expensive to operate and maintain, as it requires additional components such as an ozone generator and a vacuum pump[83].

The AED, like the SCD, is also a mass sensitive, destructive detector that can be used for the detection of sulfur-containing compounds. However the AED can be classified as both an element-selective and a universal detector[2,84]. This is because the AED is considered a multi-element detector capable of selectively detecting sulfur as well as many other elements simultaneously[74]. A schematic diagram of a conventional AED is shown in Figure 1.7.

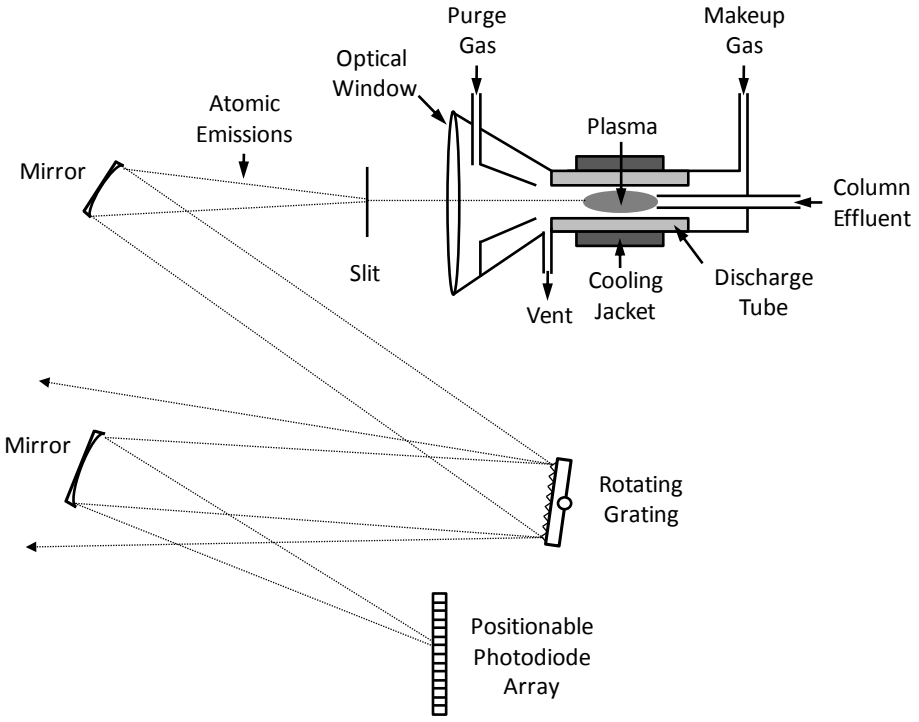

Figure 1-7: Schematic diagram of an AED.

Basically, the AED responds to the light emitted from atoms as they relax to the ground state after having been dissociated and excited in a high-energy (usually helium microwave) plasma[2]. For sulfur detection in GC, column effluent enters the helium microwave plasma where the sulfur components are then atomized. This atomization process leaves the sulfur atoms in an excited state and upon relaxation, the atoms emit light at discrete wavelengths, typically at 181 nm for sulfur emission[2,81,82]. By spectroscopically selecting and monitoring the atomic emission lines, one can selectively detect the sulfur atoms of interest in the eluting compounds[2]. As well, with the incorporation of a photodiode array, simultaneous detection of a number of elements can be enabled[84].

Consequently, the AED can provide detection limits for sulfur around 10^{-12} gS/s, with a selectivity over carbon of about 4 orders of magnitude[2,60,81,82]. As well, the AED provides a linear response with a linear range around 3-4 orders of magnitude[81,82]. Unlike the FPD, the AED also provides an equimolar response for sulfur, as sulfur-containing compounds completely dissociate into their composite atoms in the high-energy plasma[85]. This also contributes to the fact that the sulfur response in the AED does not suffer as greatly from quenching and interferences[77,85]. As such, the AED detector attributes for the detection of sulfur-containing compounds are quite formidable.

While the AED can boast significant improvements over the FPD, it is still afflicted by some fundamental impediments that limit its use in sulfur detection. Ultimately, this can be narrowed down to its cost and complexity. For instance, since a plasma excitation source is incorporated and parallel multi-wavelength optical detection equipment is often included, the AED is one of the most expensive detectors available for

GC[70,77,86]. By comparison, AED instrumentation is typically four times more expensive and requires more laboratory space than SCD instrumentation[74]. Also the AED requires more gases than any other GC detector[2]. Several problems also exist in the AED such as limited selectivity against carbon, discharge tube erosion, high maintenance, high cost, and large operation complexity due to various parameter selections[2,70,86]. Additionally the AED requires a skilled analyst to perform routine maintenance, operate the system, and analyze the data in order to obtain reliable information[77,87].

1.5 Multiple Flame Photometric Detector (mFPD)

One of the most recent additions to the growing arsenal of FPD-related devices is the multiple flame photometric detector (mFPD). Akin to the dFPD, the mFPD employs the use of numerous flames in order to help alleviate issues of non-uniformity and quenching effects that commonly plague the FPD[88]. However, unlike the parallel gas flows for flame production in the dFPD and FPD, the mFPD uses fuel and oxidant gas streams that flow in opposite directions (i.e. stream towards each other) to produce counter-current flames.

Since the 1960's, counter-current or "upside down" flames have been primarily used to study flame characteristics[89,90]. However, it was not until recently that they have been applied in flame-based GC detectors[88,91-96]. For instance, Thurbide et al. developed a counter-current flame as a GC detector that exhibited both an FPD response as well as an FID response[92]. As a result, the counter-current flame photometric detector (ccFPD) was found to produce chemiluminescent emissions and detection limits for sulfur and phosphorus-containing compounds identical to those obtained in the conventional FPD[92].

Efforts by the authors were then directed towards miniaturization of this flame, by employing lower gas flow rates delivered by small capillary tubes[93,94]. It was thought that with such a small flame, it could have the potential to be incorporated as a flame detector in micro-analytical devices and portable GC instrumentation[93,94]. The result was an FPD which utilized a very small flame (30 nL volume) which was deemed the micro counter-current FPD (μFPD)[93,94]. A schematic diagram of the μFPD is shown in Figure 1-8.

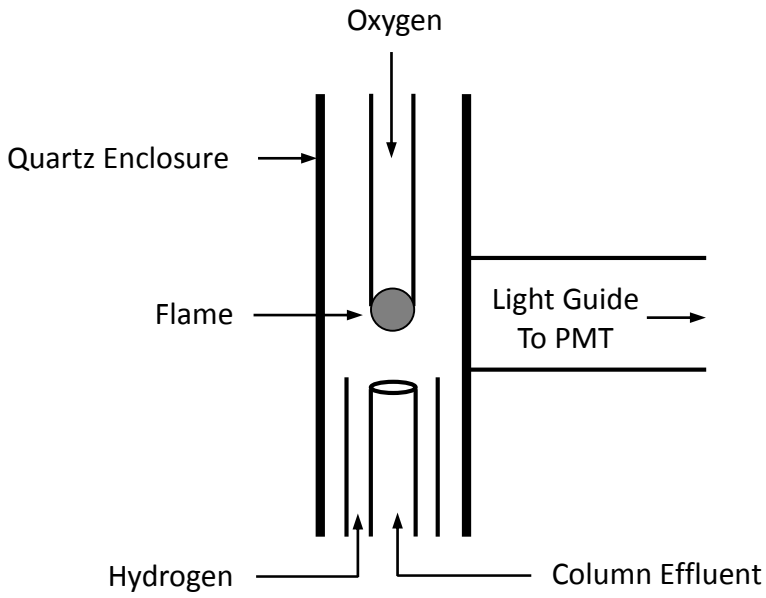

Figure 1-8: Schematic diagram of a μFPD.

Here, hydrogen and column effluent streaming from the base of the GC flows upwards to a downward flow of oxygen to generate a small counter-current flame. Chemiluminescent emissions from the flame are then monitored through a light guide to a PMT. Overall, the performance of the μFPD was comparable to a conventional FPD. Chemiluminescent sulfur response in the μFPD was quadratic over 3.5 orders of magnitude, yielding a detection limit of 3×10^{-11} gS/s, while that of phosphorus is linear over 5 orders of

magnitude down to a minimum detectable limit of 3×10^{-12} gP/s[93]. As well, the µFPD provided a molar selectivity toward sulfur of about 3.5 orders of magnitude and toward phosphorus of 5 orders of magnitude, relative to carbon[93]. Though the results did indicate a potential use in micro-analytical devices and portable GC units, issues of linearity, uniformity, and quenching of analyte chemiluminescence due to co-eluting hydrocarbons, still remained.

While working with the µFPD, the authors soon discovered that additional micro-flames could be added in series prior to the analytical µFPD flame[88]. This revelation gave way to the formation of the mFPD. A basic schematic diagram of the mFPD and its housing is shown in Figure 1.9.

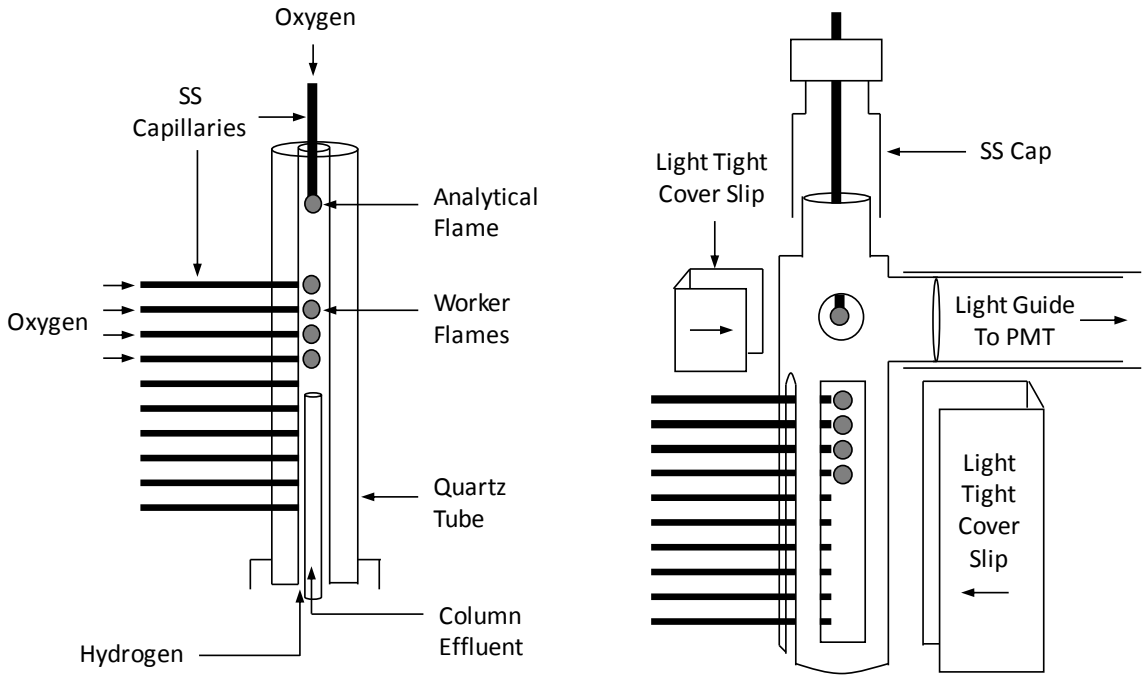

Figure 1-9: Schematic diagram of an mFPD. Left side displays the quartz tube that encloses the flames. Right side displays the housing used for the mFPD.

As shown, the mFPD is comprised of a quartz tube in which small holes are drilled along one side. Through each hole, a stainless steel (SS) capillary is inserted and sealed such that the end of the tube is flush with the inner wall of the quartz cell. Here, oxygen is delivered through these capillaries perpendicular to a stream of hydrogen (and column effluent) delivered up through the quartz tube from the base of the GC. The flames formed at the end of these orthogonal SS capillaries are denoted as "worker" flames. A final counter-current flame is formed by inserting another SS capillary through the top of the quartz tube which is then situated above the top worker flame. This counter-current flame, is denoted as the "analytical flame", and is the location at which chemiluminescent emissions are then monitored through a light guide to a PMT. When operational, the housing of the mFPD can then be slipped over top of the quartz tube and the protruding SS capillaries. Light tight viewport slips for the analytical and worker flames can also slide over the openings as needed. Finally, a SS cap is placed on the housing to provide a light tight conduit for the SS capillary of the analytical flame. Consequently, measurements can be made with or without the housing (while in a dark adapted room), as the sensitivity was found to be identical[88].

The authors then focused on exploiting the advantages of such small flames by situating them in different arrangements for photometric detection. Due to its flexible nature, the mFPD allowed for direct comparison between single, dual, and multiple flame response modes. It was found that the optimized 5-flame arrangement, shown in Figure 1-9, allowed for the most sensitive and uniform response over a range of sulfur and phosphorus analytes[88]. Consequently, this arrangement produced chemiluminescent emissions for both sulfur and phosphorus compounds yielding detection limits of 4 ×

10^{-11} gS/s and 3×10^{-12} gP/s, respectively[88]. As well, these conditions produced a linear range for phosphorus that extended over 5 orders of magnitude and a quadratic response for sulfur over 4 orders of magnitude[88]. Furthermore, the molar selectivity over carbon was found to be nearly 10^5 with respect to phosphorus and around 3.5 orders of magnitude for sulfur[88]. Ultimately, these values agree very well with those that can be obtained from a conventional FPD.

Interestingly, the response equimolarity and reproducibility for sulfur compounds also showed great improvement while operating in the multiple-flame mode of the mFPD. In particular, the 5-flame arrangement produced a more equimolar and reproducible response for compounds of varying molecular structure in comparison to other modes (i.e., single-FPD and dual-FPD)[88]. It is believed, similar to the operation of a dFPD, sulfur compounds (whether aliphatic or aromatic) degrade and homogenize into similar species while passing through the worker flames, prior to entering the analytical flame. Consequently, this implies that multiple flames can facilitate the consistent provision of a homogeneous S_2-containing effluent to the analytical flame, more-so than other modes of operation[88]. However, a spectral examination of mFPD in these modes would be required to corroborate this realization.

More notably, this 5-flame arrangement has also shown to produce excellent resistance to analyte emission quenching. For instance, the mFPD can improve hydrocarbon quenching resistance nearly 20-fold relative to a single-flame (i.e. conventional FPD) mode[88]. As mentioned previously, it has been reported that quenching of analyte response is decreased when hydrocarbons are present as a more oxidized form such as carbon dioxide[58]. Consequently, the same rationalization has been made about the

mFPD; where the bottom worker flames have the ability to convert hydrocarbons to carbon dioxide or to another partially oxidized carbon species[88]. Again, further spectral investigations are required in order to help understand the mechanism of quenching resistance in the mFPD.

Overall then, the mFPD can provide detection limits comparable to those of a conventional FPD, and improved to that of a dFPD[88]. Its response equimolarity and reproducibility are also improved relative to that of single and dual-flame modes. The robust nature, simple inexpensive design, sensitivity, selectivity, and resistance to analyte emission quenching, therefore provides an appealing option for many sulfur and phosphorus specific applications. However, for its optimal performance to be realized, further development of the device and a better understanding of its operating mechanisms and response characteristics are needed.

1.6 Statement of Purpose

The intended purpose of the work described herein is targeted towards the further advancement and development of a multiple flame photometric detector for gas chromatography. This thesis will describe in depth, three major themes that have contributed to its overall progression into a novel mFPD design. In addition, the aims of this project are to further characterize the new mFPD traits, as well as probe its capabilities in new analytical areas and applications. It is the development of this unique detector, and the quest to better understand its operational principles and capabilities, that is the basis of my research.

Given the unique design of the mFPD and its response properties observed thus far, it would be of great interest to further explore the emission characteristics of sulfur analytes in this detector. For example, both the SCD and AED have been shown to provide an equimolar and linear response toward sulfur-containing compounds. As such, increased response equimolarity and linearity can ease calibrations and positively impact reproducibility, while also providing a more uniform response over a broad range of sulfur compounds. Therefore, it would be very useful if such a response for sulfur was also accessible in the mFPD. Thus the first major theme, discussed in Chapter Three, will describe in detail the efforts and investigations made to achieve a linear sulfur response in the mFPD. Consequently, detector properties such as sensitivity, selectivity, equimolarity, reproducibility, and quenching resistance will also be determined in this new mode and compared to the traditional response of a conventional single-flame FPD.

Secondly, while the performance attributes of the mFPD can be established for sulfur response in both the linear and quadratic modes, very little is known about the actual mechanism through which the detector provides such a response. For instance, at the most fundamental level, the identities of the emitting species for sulfur and phosphorus emission in the analytical flame has never been confirmed; such species have only been assumed similar to those present in a conventional FPD flame. Further, any differences between the mFPD and FPD in this regard have also never been established or investigated. Such information is very important, since it can potentially lead to a better understanding of the mFPD and facilitate its continued optimization.

Accordingly, the most effective route to learning more about the composition and dynamics of the analytical flame is to obtain emission spectra of the various species

present in it during operation. Therefore, as a second principal theme, Chapter Four will focus on the characterization and examination of the emission spectra produced in the mFPD for sulfur, phosphorus, and hydrocarbon compounds. These results will then be directly compared to spectra obtained from the same compounds in a conventional single-flame FPD mode. Since this has not yet been done with the mFPD or the counter-current flame that it operates in the analytical position, it can potentially yield valuable information on how the detector functions. For example, a closer examination of how hydrocarbons behave in each could lead to clearer knowledge of how the two differ so dramatically in their resistance to analyte response quenching.

Finally, the results of this analysis will then provide the groundwork for the third principle theme of this research; the construction of a new and improved mFPD design. Although the performance attributes of the current quartz tube mFPD are promising, problems still exist in its basic design. For example, while the quartz tube mFPD prototype allows for easy viewing and monitoring of the flames and their emission, the device is inherently very fragile and requires a bulky housing that is cumbersome to use. Likewise, with respect to optics and the collection of analyte emission, the counter-current analytical flame emission in the quartz tube design is not only localized towards the PMT but emits ubiquitously around itself inside the housing; stray analyte emission can thereby be lost through the quartz tube on the backside of the flame. Most importantly, however, due to the construction of the quartz tube mFPD, high background emissions from flame combustion can be produced that negatively impact its sensitivity and operation. This background emission is caused by an intense glow from the burner tips of the SS capillaries in the quartz tube mFPD, likely due in part to incandescence

from the cement used to hold the burners in place[88]. Therefore, Chapter Five will present the general operating characterizations and design specifications of a new mFPD constructed from stainless steel (SS) that incorporates fluidic channels to primarily direct flame gas flows and analyte emission. The analytical properties and performance characteristics of the new SS mFPD will then be evaluated and compared to that of the original quartz tube prototype to illustrate the improved performance of this new mFPD design. Finally, a promising new multiple-flame monitoring mode in this stainless steel mFPD design, which was not previously possible, will also be presented and discussed.

CHAPTER TWO: EXPERIMENTAL

2.1 Instrumentation

2.1.1 GC Instrumentation

Unless stated otherwise, experiments involving the mFPD were conducted using a Shimadzu model GC-8A gas chromatograph (GC) (Shimadzu Corp., Kyoto, Japan). As such, one of the original FID detectors in the GC instrument was removed and an adapter was fitted to convert the metric fitting to a ¼ inch Swagelock® fitting (Swagelock Company, Solon, OH, USA). This adaptation allowed for the easy attachment of the mFPD device to the GC detector port. Additionally, this adapter allowed hydrogen to be controlled by the GC while blocking the air-port. Injector and detector temperatures were generally maintained at 300 °C, which primarily helped heat the mFPD device preventing water from condensing and extinguishing the flames. When FID analyses were required, the second original FID of the GC instrument was employed. The FID gas flow rates were usually about 400 mL/min of medical-grade air (Praxair, Calgary, AB, Canada) and 40 mL/min of high purity hydrogen (Praxair).

GC separations were typically performed using a DB-5 (5%-phenyl-95%-methylpolysiloxane) megabore column (30 m × 0.53 mm I.D.; 1.0 µm film thickness; Chromatographic Specialties Inc. Brockville, ON, Canada). High purity helium (Praxair) was primarily used as the carrier gas and operated at approximately 11 mL/min. Any variations in the GC operating conditions will be described as required in the text.

2.1.2 Optical Instrumentation and Data Collection

Analyte emissions produced by the mFPD were generally monitored through a quartz light guide (150 mm × 9.21 mm O.D.; made in-house) leading to an R-1104 PMT (spectral response range 185-850 nm; Hamamatsu, Bridgewater, NJ, USA). Typically, an optical filter was situated between the light guide and the PMT to selectively monitor the chemiluminescent emission of the analyte. In general, three modes of operation were investigated in the mFPD, each with a specific optical filter. In the S_2* mode analyte emissions were routinely observed using a 393 nm (12 nm bandpass) interference filter (Oriel Instruments, Stratford, CT, USA). In the linear HSO* mode analyte emissions were typically observed using a 750 nm (40 nm bandpass) interference filter (Thorlabs, Newton, MA, USA). Finally, in the HPO* mode of operation a 527 nm (10 nm bandpass) interference filter (Melles Griot, Rochester, NY, USA) was normally employed. A complete list these and other optical filters examined with the mFPD in this study are shown in Table 2-1.

The PMT was equipped with an external power supply/electrometer constructed in house by the University of Calgary Chemistry Electronics Shop to provide high sensitivity current to voltage conversion with an integrated high voltage power supply. Data acquisition and integration was carried out using PeakSimple® Chromatography Software with a Model 202 Four Channel Data System (SRI Instruments, Torrance, CA, USA) installed on a personal computer. Data acquisition rates typically ranged from 1-50 Hz.

Table 2-1: List of optical filters examined in the mFPD.

Wavelength	Filter Type	Part Number	Vendor
306 nm	10 nm band pass; interference	57030	Oriel Instruments
393 nm	12 nm band pass; interference	39312	Oriel Instruments
527 nm	10 nm band pass; interference	F10-527.0-4-25.0M	Melles Griot
750 nm	40 nm band pass; interference	FB750-40	Thorlabs
435 nm	cut-on; long pass	51282	Oriel Instruments
495 nm	cut-on; long pass	51292	Oriel Instruments
590 nm	cut-on; long pass	51311	Oriel Instruments
610 nm	cut-on; long pass	51312	Oriel Instruments
630 nm	cut-on; long pass	51320	Oriel Instruments
645 nm	cut-on; long pass	51325	Oriel Instruments
665 nm	cut-on; long pass	51330	Oriel Instruments
695 nm	cut-on; long pass	51340	Oriel Instruments
715 nm	cut-on; long pass	51345	Oriel Instruments
725 nm	cut-on; long pass	51315	Oriel Instruments
780 nm	cut-on; long pass	51350	Oriel Instruments
830 nm	cut-on; long pass	51352	Oriel Instruments

2.2 Quartz-based mFPD Design for Linear Sulfur Emission

A schematic diagram of the quartz tube mFPD device designed for linear sulfur emission is shown in Figure 2-1.

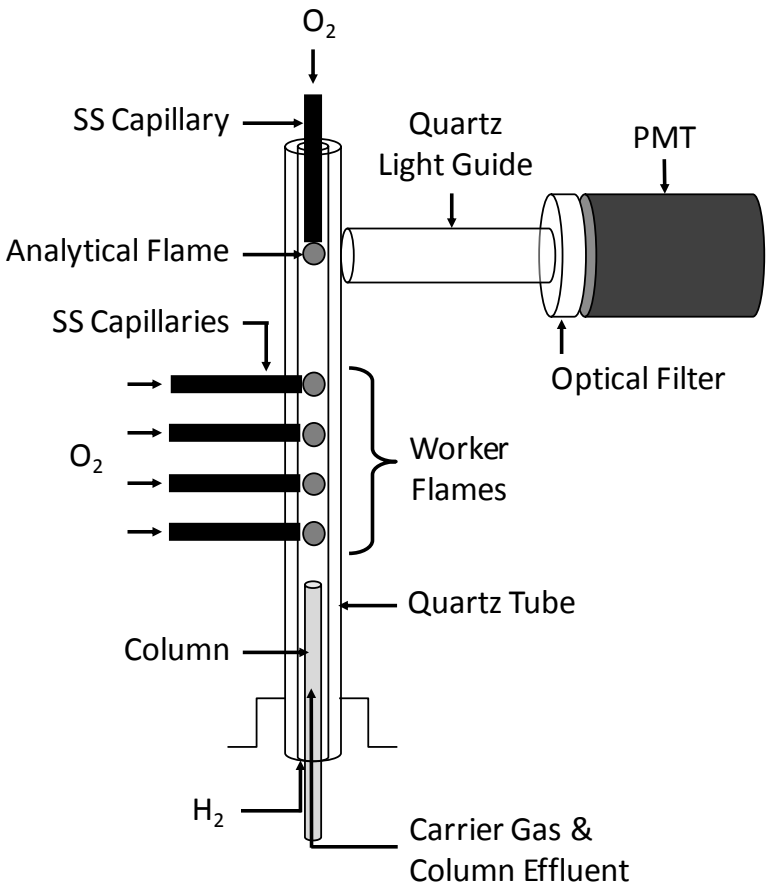

Figure 2-1: Schematic diagram of the quartz tube mFPD assembly.

As shown, the mFPD is comprised of a 125 mm long quartz tube (2 mm I.D. × 6 mm O.D.) that houses several flames along its length for analyte processing and response. This piece is affixed to the detector base of the GC instrument by a ¼ inch Vespel® polyimide ferrule (Chromatographic Specialties Inc.) and SS nut (Swagelock Company). Specifically, in this mFPD design, 4 holes (2 mm I.D.) are spaced 10 mm apart from each

other, starting 45 mm from the bottom of the quartz tube. Into each hole, a 110 mm length of SS capillary tubing (0.838 mm I.D. × 1.27 mm O.D.; McMaster-Carr Supply Company, Atlanta, GA, USA) is sealed with cement (Resbond 940 cement; Cotronics Corp., Brooklyn, NY, USA) into place such that the end of the capillary is protruding 0.4 mm past the inner wall of the tube. High purity oxygen (Praxair) is delivered through these capillaries perpendicular to a hydrogen stream that is delivered up through the quartz tube from the base of the GC. The flames formed at the end of the orthogonal SS capillaries are designated as "worker flames" for processing analytes. A final SS capillary (0.254 mm I.D. × 1.59 mm O.D.; Chromatographic Specialties Inc.) is introduced through the top of the quartz tube and supports a counter-current flame. This is then situated 30 mm above the top worker flame and is used as the "analytical flame". While in a dark-adapted room, chemiluminescent analyte emission is monitored here through the quartz light guide leading to the PMT (R-1104; Hamamatsu).

The worker flames are all ignited from a spark introduced at the top of the quartz tube surface using 50 mL/min of oxygen collectively flowing through the capillaries and 180 mL/min hydrogen flowing up through the quartz tube. Next, the analytical flame capillary (with 7 mL/min of oxygen flowing through it) is inserted into the quartz tube, ignited at the first worker flame, and then positioned across from the light guide. Gas flow rates are subsequently adjusted to 40 mL/min oxygen collectively across the worker flames and 120 mL/min of hydrogen. For the conventional single-flame S_2* mode optimal gas flow rates used were 7 mL/min oxygen and 40 mL/min hydrogen to the lone analytical flame.

Separations were performed on the DB-5 megabore column using helium as the carrier gas. In the linear sulfur mode, chemiluminescence was routinely examined using the 750 nm interference filter (Thorlabs). However, during optimization, the 590, 610, 630, 645, 665, 695, 715, 725, 780, and 830 nm long pass filters (Oriel Instruments) were also each examined. For comparison, the dominant S_2* emission in the conventional quadratic mode was also investigated using a 393 nm interference filter (Oriel Instruments).

2.3 Spectral Measurements

For spectral analyses of the mFPD, a quarter-meter Jarrell-Ash monochromator (Model 82-410, Fisher Scientific Co., Waltham, MA, USA) with a 1180 grooves/mm grating (3.3 nm/mm linear dispersion) blazed for 500 nm, was positioned between the quartz light guide and the PMT (R-1104; Hamamatsu). Entrance and exit slit widths were employed such that they provided either a 6.7 nm or a 0.67 nm bandpass as needed. While in a dark adapted room, spectral measurements were conducted via automatic scanning using a motor speed of 60 nm/min and a data collection rate of 2 Hz. Emission spectra were typically scanned between 250 and 850 nm and all major features observed were reported. In the linear sulfur mode a 495 nm long pass filter (Oriel Instruments) was situated between the monochromator and the PMT and used for order sorting to block out other dominant sulfur emissions in the blue spectral region. Under typical mFPD operation conditions[88], gas flow rates were set to 7 mL/min of oxygen for the analytical flame, 30 mL/min of oxygen collectively across the worker flames, and 100 mL/min of total hydrogen flow. However, in the linear sulfur mode of operation, worker gas flow

rates were adjusted to 40 mL/min of oxygen and hydrogen flow was set to 120 mL/min. For the conventional single-flame mode 7 mL/min oxygen and 40 mL/min of hydrogen were used to support the counter-current analytical flame. A schematic diagram for spectral measurements taken with the mFPD is shown in Figure 2-2.

To obtain spectra, a continuous sample introduction mode was employed to deliver a constant stream of pure analyte headspace into the detector via the carrier gas line. Here, 20 mL of the analyte is sealed in a 125 mL conical flask and placed into the GC oven at a temperature of 25 °C. From the GC injector outlet, a carrier gas transfer line is added through a sealed stopper and placed 0.5 cm above the surface of the liquid. To enable the transfer of the volatiles into the detector, another sealed transfer line (fused silica capillary tubing; 32 cm × 0.53 mm I.D.; Polymicro Technologies, Phoenix, AZ, USA) is added 1.0 cm above the liquid and connected directly to the mFPD. As the carrier gas flows, volatile analytes in the headspace are swept from the sample vessel through the transfer line to the detector. To maintain a constant and measureable response in the detector, flow rates of helium carrier gas were adjusted to 1.5 mL/min for all phosphorus and sulfur-containing compounds and 35 mL/min for the pure hydrocarbon analytes. Further experimental conditions and spectral variations are outlined in Chapter Four.

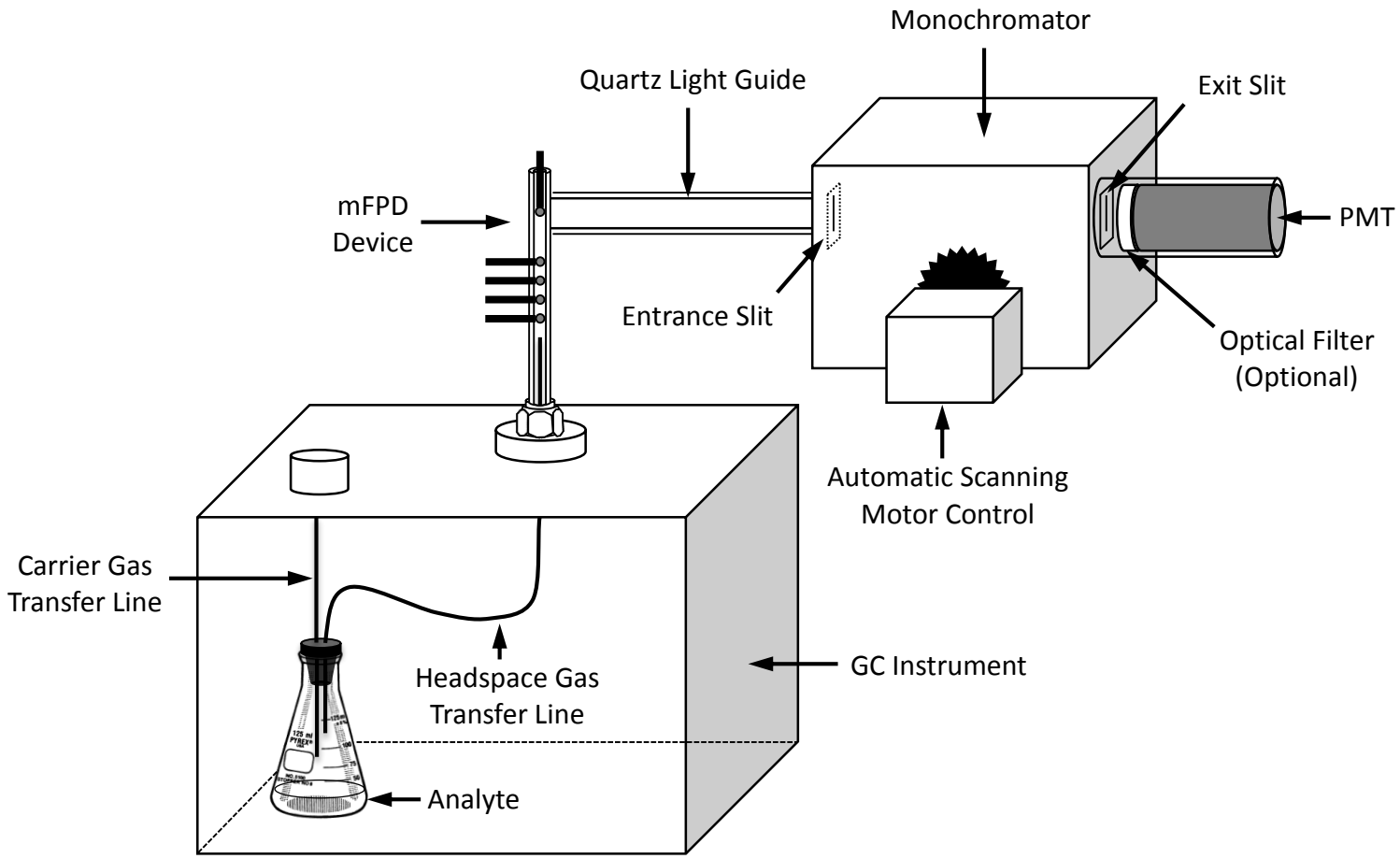

Figure 2-2: Basic schematic diagram for spectral measurements taken with the mFPD.

2.4 Stainless Steel-based mFPD Design

A schematic diagram of the SS mFPD is presented in Figure 2-3.

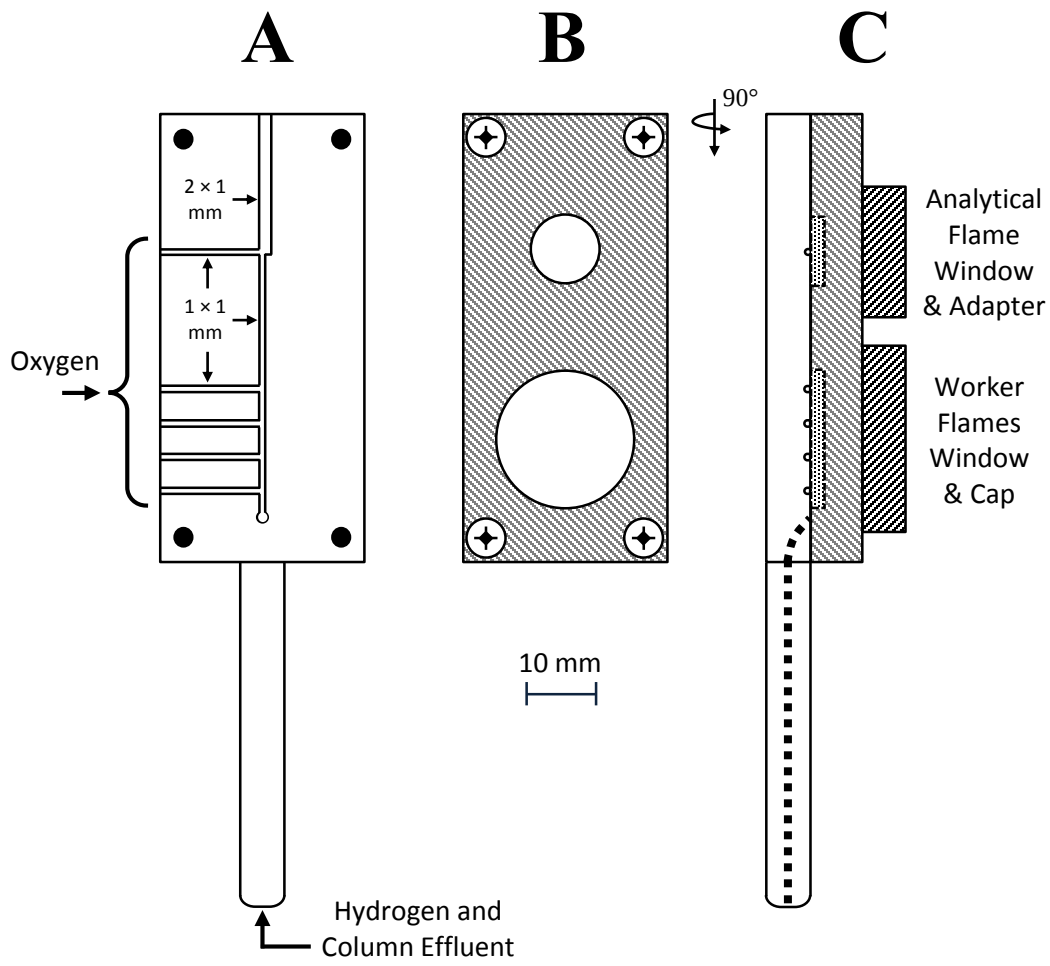

Figure 2-3: Schematic diagram of the SS mFPD displaying (A) the planar channeled face piece, (B) its cover plate, and (C) a side view of the assembled device. The vertical dotted line in (C) depicts the inner bore of the tube connecting to the planar channel. The dashed rectangles in (C) are quartz windows.

As shown, the device is primarily composed of a two piece system, a planar channeled face piece (Figure 2-3A) and a matching cover plate (Figure 2-3B). Both

pieces were machined from 316 grade SS, using a computer numerical controlled mill in the University of Calgary's Science Workshop. As seen in Figure 2-3A, the face piece is comprised of a flat rectangular SS block (6.5 cm × 3.0 cm × 0.635 cm) attached to a SS tube (0.20 cm I.D. × 0.635 cm O.D.; 5.0 cm length). Here, a 2 mm channel was bored through the block to connect with the inner diameter of the SS tube.

On the surface of the block, precision milled U-shaped channels (1 mm wide × 1 mm deep) were used to direct gas flows to the individual flames. These were comprised of a central channel to flow hydrogen and carrier gas laterally through the device, and five branching orthogonal channels to flow oxygen to micro-flames supported at their intersection. Four of these channels (spaced 0.5 cm apart) were added 4.0 cm below the central channel outlet and used to support the "worker flames". The remaining channel was added 2.0 cm below the outlet and used to support an orthogonal "analytical flame". From this position to the outlet, the central channel was also extended to 2 mm wide × 1 mm deep. This is because early design optimization revealed that a 1 mm channel provided the best worker flame performance, while a 2 mm channel produced enhanced analyte emission at the analytical flame (this will be further discussed in Chapter Five). Therefore, this arrangement was deemed optimal for operations going forward.

A SS cover plate was fabricated using similar dimensions (6.5 cm × 3.0 cm × 0.75 cm). As shown in Figure 2-3B, two holes were cut in the cover plate. One hole (1.0 cm diameter) was centered 2.0 cm from the central channel outlet and used to monitor the analytical flame. The other (2.0 cm diameter) was centered 4.75 cm from the outlet and used to monitor the worker flames. A 1.5 mm thick quartz window was snugly fit into each and sealed into place using a high temperature silicon gasket (3.2 mm thick), such

that they were mounted flush with the inner wall of the cover plate. As such, when assembled, the windows rested flat against the channels of the face piece. On the outer wall of the cover plate each hole was threaded (3.0 mm deep) to accommodate a cap for the worker flame window and a light guide adapter for the analytical flame window. In this way, all flames could be easily viewed during operation or covered/monitored as appropriate. The inner side of each piece was polished to a mirrored finish and they were bolted to one another in the corners. To inspect for a gas tight seal, oxygen at a flow rate of 500 mL/min was connected to the device by its SS tube, and it was placed into a container of deionized water. This was done to ensure a gas tight seal around the edges of the device, and to confirm an uninterrupted flow of gas through the channels. Over multiple occasions of disassembling and assembling the device, no leaks were detected and all gas flowed only through the channels.

The SS mFPD is affixed to the detector base of a GC instrument using a ¼ inch SS Swagelock® nut and ferrule set (Swagelock Company). The capillary separation column used was led through the connection and into the SS tube of the mFPD such that it deposited column effluent at the base of the central channel. To supply oxygen to the orthogonal flames, SS capillaries (0.584 mm I.D. × 0.902 mm O.D.; McMaster-Carr Supply Company), were inserted 1.3 cm into each orthogonal channel and sealed into place with a high temperature silicone adhesive (High Temp RTV Red Silicone Gasket Maker; Permatex, Hartford, CT, USA).

Flames were readily ignited at the intersection of each orthogonal channel and the central channel by a spark presented at the central outlet of the mFPD while flowing 50 mL/min of oxygen collectively through the worker channels, 12 mL/min of oxygen

through the analytical channel, and 180 mL/min of hydrogen through the central channel. Gas flow rates were optimized for each mode of operation. The typical flows used for monitoring sulfur in the mFPD were 30 mL/min of oxygen collectively across the worker flames, 12 mL/min of oxygen supplied to the analytical flame, and 100 mL/min of hydrogen.

Separations were generally performed on the DB-5 megabore column with helium as the carrier gas. While in a dark adapted room, analyte emission was monitored at the analytical viewport through the quartz light guide leading to the PMT (R-1104; Hamamatsu). As such, analyte emission was routinely monitored in either the S_2*, linear HSO*, or HPO* operating modes equipped with their respective optical filters. Further details pertaining to these and other modes of operation will be outlined in Chapter Five.

2.5 Chemicals and Reagents

Specifically, high purity hydrogen (99.995%; Praxair) and oxygen (99.99%; Praxair) were used to support the flames of the mFPD. As well, high purity helium (99.99%; Praxair) was used as the carrier gas. Methane (99.0%; Praxair) was also employed for certain quenching experiments involving the mFPD in the linear HSO* mode. All gases, with the exception of methane, were directed through a hydrocarbon trap (C36100; Chromatographic Specialties Inc.) and/or a moisture trap (MT120-2; Agilent Technologies, Santa Clara, CA, USA) to ensure high purity.

Various test analyte compounds used for characterizing the detector modes are described and outlined in the following tables. For calibration experiments, solutions of each test analyte were prepared at concentrations ranges of approximately 0.5 ng - 150 µg

μL^{-1} (weight per volume), stored in glass vials, and refrigerated at ~ 7 °C until used. All reagents were used as received unless otherwise stated.

Table 2-2: Test analytes used for calibration.

Compound	Molecular Formula	Composition and Vendor
Tetrahydrothiophene	C_4H_8S	97%; Fluka Chemika, Oakville, Canada
Diethyl sulfide	$(C_2H_5)_2S$	98%; Sigma-Aldrich, Oakville, Canada
2-Propanethiol	$(CH_3)_2CHSH$	97%; Fluka Chemika
Dimethyl sulfide	$(CH_3)_2S$	99%; Sigma-Aldrich
1-Butanethiol	$CH_3(CH_2)_3SH$	99%; Sigma-Aldrich
1-Methyl-1-propanethiol	$CH_3CH_2CH(SH)CH_3$	98%; Sigma-Aldrich
Methyl disulfide	CH_3SSCH_3	99%; Sigma-Aldrich
Isopropyl disulfide	$[(CH_3)_2CH]_2S_2$	96%; Sigma-Aldrich
Dipropyl sulfide	$(CH_3CH_2CH_2)_2S$	97%; Sigma-Aldrich
Thianaphthene	C_8H_6S	99%; Sigma-Aldrich
Trimethyl phosphite	$P(OCH_3)_3$	99%; Sigma-Aldrich
Dodecane	$CH_3(CH2)_{10}CH_3$	99%; Sigma-Aldrich
Benzene	C_6H_6	99%; EMD Chemicals, Gibbstown, USA

Table 2-3: Test analytes used for spectral measurements.

Compound	Molecular Formula	Composition and Vendor
Carbon disulfide	CS_2	99.9%; Sigma-Aldrich
Trimethyl phosphite	$P(OCH_3)_3$	99%; Sigma-Aldrich
Benzene	C_6H_6	99%; EMD Chemicals
n-Hexanes	$CH_3(CH_2)_4CH_3$	95%; Anachemia, Montréal, Québec

Table 2-4: Solvents used for calibration.

Solvent	Molecular Formula	Composition and Vendor
n-Hexanes	$CH_3(CH_2)_4CH_3$	95%; Anachemia
Acetone	CH_3COCH_3	99%; Sigma-Aldrich

Table 2-5: Petroleum/Hydrocarbon samples used.

Label	Contents	Vendor
Diesel Sample A	Diesel Fuel	Local Gas Station
Diesel Sample B	Diesel Fuel	Local Gas Station

CHAPTER THREE: CHARACTERIZING A NOVEL LINEAR SULFUR RESPONSE MODE IN THE MULTIPLE FLAME PHOTOMETRIC DETECTOR

3.1 Introduction

To date, chemiluminescent emissions of sulfur compounds obtained in the mFPD have only been examined under conventional quadratic S_2* conditions. This is primarily due to the dominance of S_2* emission that is prevalent in the flames, (similar to that of an FPD), which inherently produces a quadratic response. However, a small number of attempts have been made in both the FPD and other FPD-related devices to obtain a linear sulfur response[25,69,92,94,97-99]. As mentioned, a linear response may facilitate calibrations and positively impact reproducibility, particularly if it provides a more uniform response over a broad range of sulfur compounds. Given the unique design of the mFPD and its response properties observed thus far, it would be interesting to further explore if a linear sulfur response is attainable in this detector, and if so, examine its characteristics.

In the past, one early attempt at a linear sulfur response in an FPD used a high sulfur background[97]. That is, a steady stream of sulfur (e.g. CS_2) was introduced into the flame during analysis. As a sulfur containing compound would enter the flame, the response for the analyte was obtained in addition to the sulfur background. The authors found that this could linearize the response over a limited range. Although this method allowed for a linear sulfur response to be attained, the response spanned only a couple orders of magnitude over a small mass range (1-100 ng)[97]. As well, the detection limits were found to be higher than those obtained under non-doped conditions, as the noise also increased with the high sulfur background[97]. Additionally this method relied upon

the assumption that the FPD response was not dependent on structural differences of other sulfur-containing compounds, and that a purely quadratic response is obtained for both the dopant and analyte[97].

In other attempts, this assumption has also been made by some GC manufacturers by incorporating a pure quadratic correction circuit in their FPD detector electronics so that the sulfur response appears linear[2]. As mentioned in Section 1.3.1 (Equation 1.3-12), the response exponent n does not always perfectly equal 2. Since deviations from this expected n value are known to occur, electronically linearizing the sulfur response by taking the square root of the signal can often lead to significant errors, and therefore is considered impractical[28,100]. Thus, the use of a square root linearization function can only be used when the FPD response is known to be purely quadratic for all sulfur compounds analyzed[49].

The most direct and useful solution to this problem was found years later by monitoring a different sulfur emitting species, HSO*, in the flame, which resulted in a linear sulfur response and improved sulfur equivalency among sulfur compounds compared to S_2* emission[25,69,92,94,98,99]. Spectrally, it has been shown that this HSO* emission spans across the range of approximately 550-850 nm, with the most intense bands around 590, 700, and 750 nm[25,101]. Typically, this emitter was optimally produced under hydrogen-rich conditions and monitored with the use of specific optical filters. Optical filters were necessary for selective observation of this linear emitter since the emission of S_2* still dominated in the flame. That is, the red HSO* chemiluminescence can only be monitored by suppressing the blue S_2* bands through the use of long pass and/or interference filters[92]. For instance, investigations done with an FPD and a pFPD

required the use of a 600 nm and 590 nm long pass filter, respectively[25,69]. In both cases the detection limit for this operating mode was reported as 2×10^{-11} gS/s ($S/N_{p\text{-}p} = 2$)[25,69]. As well, a linear sulfur response of HSO* has been demonstrated in the µFPD using a 750 nm (40 nm bandpass) interference filter exhibiting an MDL of approximately 2×10^{-10} gS/s ($S/N_{p\text{-}p} = 2$)[94]. Moreover, the response found in the FPD was linear over 4 orders of magnitude with a selectivity over carbon of at least three orders of magnitude[25]. In addition to this, the HSO* emission produced in the FPD flame was directly proportional to the amount of sulfur contained within the test compound and largely independent of molecular structure[25].

While this alternative emitter provides a linear response toward sulfur analytes and yields relatively good sensitivity and selectivity, very little is known about the actual mechanism of HSO* formation. As mentioned, there is no consensus in the literature even of the mechanism of quadratic S_2 response, let alone a more recently discovered HSO* emitter with far fewer reported studies. Nonetheless, the linear sulfur response obtained in the FPD and FPD-related devices from HSO* was demonstrated to be quite useful[25,69,94].

Prior to this work, HSO^* emission has not been reported in the mFPD. However, considering the potential benefits of this detector (e.g. high resistance to hydrocarbon quenching), it could possibly be very useful if such a linear response mode was also accessible in the mFPD. Further, if a linear response is attainable, it would be interesting to closely examine its properties such as sensitivity, selectivity, reproducibility, equimolarity, and hydrocarbon quenching resistance (if any), and determine how they compare to the conventional single-flame FPD S_2^* response mode. This is most

convenient in the mFPD since it readily toggles between a single and multiple flame operating mode, both of which can be optimized for S_2* response. Further, the counter-current flame operated in the single-flame FPD mode has been previously shown to produce response characteristics that are very similar to a conventional FPD in direct comparisons[92,94]. Therefore the S_2* single-flame mode of the mFPD provides a useful and suitable *in-situ* comparator of conventional FPD operation.

This Chapter presents the first observations of a linear sulfur response mode in the mFPD. The primary parameters for isolating and optimizing this mode are described in Section 3.2. Further, its analytical performance characteristics are examined in Sections 3.3-3.5. As well, the hydrocarbon quenching behavior of this linear response mode is explored and discussed in Section 3.6. Finally, comparisons of commercially available sulfur selective detectors to the mFPD operated in the linear HSO* mode will be discussed in Section 3.7. Comparisons with sulfur response from the conventional single-flame FPD S_2^* operating mode are additionally drawn where possible in order to illustrate the potential utility of this new mFPD response mode.

3.2 Optimization of Analyte Sensitivity

As stated previously, the chemiluminescence of sulfur-containing compounds in the mFPD flames is particularly dominated by strong blue S_2* emission. To illustrate this, Figure 3-1 shows an image of the mFPD with and without sulfur present under typical operating conditions. As seen in this figure, four worker flames are lit beneath the analytical flame.

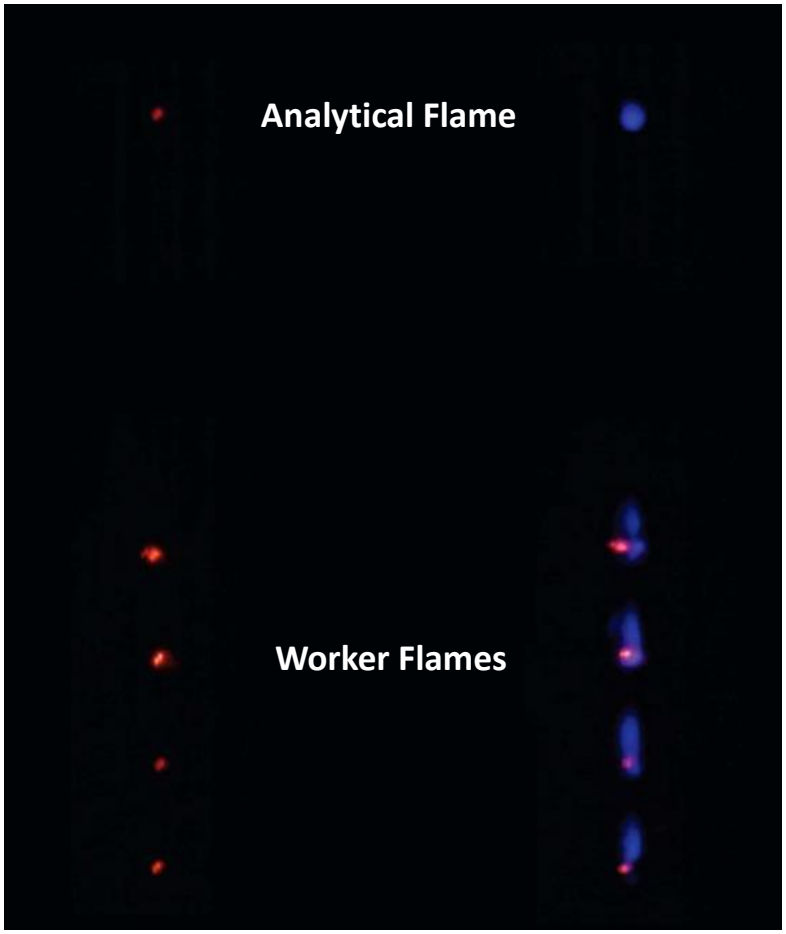

Figure 3-1: An image displaying the mFPD under normal operating conditions with (right) and without (left) sulfur present.

Without sulfur present, as shown on the left, there is an orange glow at the burner tips of the worker flame SS capillaries, while a dim background emission is also seen at the analytical flame. When sulfur is present, as shown on the right side of the photo, the analytical and worker flames display the notable S_2* chemiluminescence, similar to that of a conventional FPD[24]. Thus, analyte degradation and excitation is occurring within each flame enroute to the final analytical flame where analyte emission is monitored[88]. However, many other species[28] such as HSO* can also co-exist and normally require a

carefully chosen optical filter to isolate their emission from that of S_2*[25,69,92,94,98]. Therefore several optical filters were first explored for their ability to isolate HSO* emission in the mFPD design as described in Section 2.2.

As mentioned, unlike conventional blue S_2* emission situated around 400 nm[2,24,28], it has been shown that HSO* emission primarily exists in the red region from about 550-850 nm[25,101]. Therefore, while monitoring emission at the analytical flame, long pass (LP) optical filters with cut-on values ranging from 590-830 nm were examined. As well, a 750 nm interference (INT) filter was also explored separately and in combination with the above filters. Using standard sulfur analytes to examine each, it was found that all optical filters (and combinations thereof) readily shifted the resulting response calibrations from a quadratic to a clearly linear proportionality, indicating that HSO* emission was being isolated from S_2* in the mFPD.

Initially, these optical filters were examined under typical operating S_2* conditions (i.e. 100 mL/min hydrogen, 30 mL/min collective oxygen to workers, and 7 mL/min oxygen to analytical)[88] using a broad series of sulfur-containing compounds of varying chemical structure. Table 3-1 displays the typical results obtained with signal-to-noise ratios (S/N_{p-p}) of six sulfur compounds (~1 µg injected mass of each) analyzed using eleven different optical filters in the 590-830 nm wavelength range. In general it was found that while some LP filters could improve HSO* response, this was also accompanied by larger background noise. As well, it was found that both signal and noise generally decreased as the optical filter transmittance moved toward the near-infrared.

Table 3-1: Signal-to-noise ratios for 6 sulfur analytes (~1 µg injected mass of each) measured in the mFPD with different optical filters.

	S/N_{p-p} Ratio of Sulfur Compound										
Compound	590 nm LP	610 nm LP	630 nm LP	645 nm LP	665 nm LP	695 nm LP	715 nm LP	725 nm LP	780 nm LP	830 nm LP	750 nm INT
Dimethyl Sulfide	154	96	143	209	162	127	133	76	45	25	282
2-Propanethiol	140	80	114	176	151	108	106	65	36	20	237
1-Methyl-1-propanethiol	170	96	168	124	196	152	139	96	50	38	360
Ethyl Sulfide	151	95	138	271	185	128	134	82	45	29	299
1-Butanethiol	101	94	112	208	160	105	116	68	38	23	244
Methyl disulfide	168	97	153	255	208	141	146	97	49	37	337

However, the 750 nm interference filter gave the best results of a strong HSO* response and low background that provided the highest signal-to-noise ratio of all the optical filters tested. Additionally, combinations of optical filters with this 750 nm interference filter were further examined, since this was previously explored in one study[98], however no significant advantages were realized. Given its initial performance in the mFPD and its demonstrated benefits in other FPD experiments exploring HSO*[25,94], the lone 750 nm interference filter was used for further optimization.

After optically isolating the linear HSO* emitter, optimization of the flame-gas flows of this signal was undertaken using sulfur test analytes. Initially, it was wondered if the optimal flame-gas flow rates for S_2* emission in the mFPD (i.e. 100 mL/min hydrogen, 30 mL/min collective oxygen to workers, and 7 mL/min oxygen to analytical)[88] would give an equally strong signal for HSO* emission. However, under these conditions it was found that HSO* response was quite weak relative to that of S_2* emission. It has been suggested that if a precursor such as SO is required to react with a hydrogen radical in order to form the excited species, then an oxygenating environment should facilitate the formation of HSO*[92]. For instance, both the ccFPD and µFPD required a pre-mixture of hydrogen and oxygen/air to help promote HSO* formation on its way to the analytical flame[92,94]. Still, it is interesting to note that in the conventional FPD, the optimum conditions for HSO* required a very hydrogen-rich flame stoichiometry by comparison[25].

Considering its design, the mFPD could potentially allow for easy tunability of this, where the worker flames could be adjusted so that there are more oxygen-bearing flames upstream to process sulfur towards HSO*. Therefore various combinations of

hydrogen flow (100-180 mL/min), oxygen flow for the analytical flame (7-90 mL/min), and oxygen flow collectively across the worker flames (20-70 mL/min) were explored. It was found that if larger hydrogen and oxygen gas flow rates were used for the worker flames, a very large background emission would occur. Consequently, this large background at the worker flame location hindered the detection of HSO* emission at the analytical flame. This is because the quartz tube could ultimately act as a light guide where emission from the worker flames can produce an internal reflection to the location of the analytical flame where the light sensitive PMT monitors emission. As shown in Figure 3-2, when increasing the oxygen flow to the worker flames the background emission does become more intense as the flames become larger within the quartz tube.

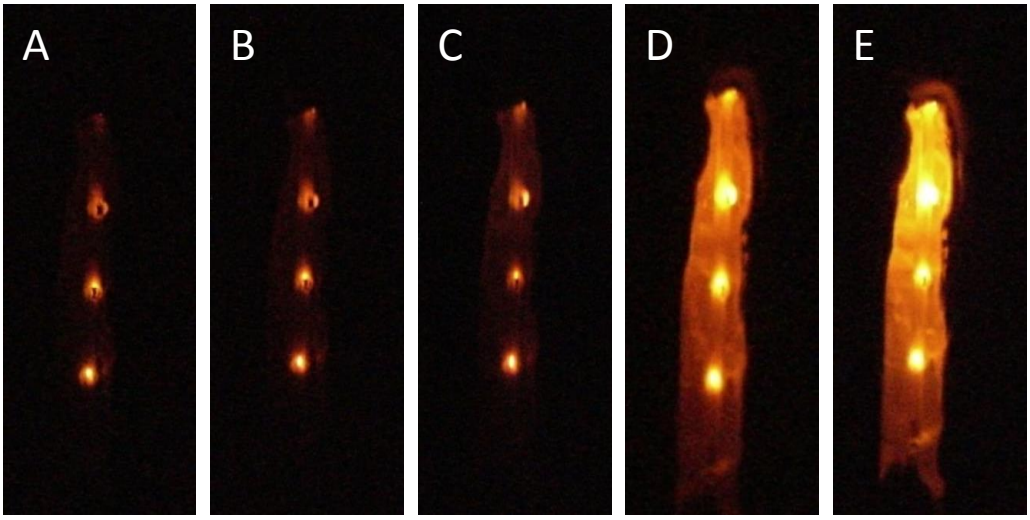

Figure 3-2: Images of worker flames when A) 30, B) 40, C) 50, D) 60, and E) 70 mL/min of oxygen is spread over the four worker flames supplied by 180 mL/min of hydrogen.

It was thought that a larger flame in the quartz tube could allow for more efficient analyte processing towards HSO*. However, the high background emission of the worker flames made this impractical to pursue further.

Through exploring different fuel/oxidant ratios using various combinations of hydrogen and oxygen flow to the detector flames the greatest signal-to-noise ratio obtained was ultimately found for 120 mL/min of hydrogen, 40 mL/min of oxygen collectively across the worker flames and 7 mL/min of oxygen to the analytical flame. These conditions improved the HSO* response by roughly 2 orders of magnitude compared to using the optimal S_2* gas flows. Interestingly, both conditions share the same residual hydrogen/oxygen ratio at the analytical flame (i.e. 40 mL/min to 7 mL/min) and differ only in the extra 10 mL/min of oxygen and 20 mL/min of hydrogen supplied to the worker flames in the HSO* mode. Thus, this indicates that these optimal conditions arise more likely from increasing HSO* production in the worker flames with the extra oxygen, rather than solely further promoting HSO* chemiluminescence at the analytical flame. Even so, as also noted in previous FPD work[94], it should be stated here that under these conditions the blue S_2* emission was still visibly prevalent and no red HSO* emission could be detected with the naked eye.

The most promising optical filters that provided the greatest S/N response ratios were then re-evaluated and compared under these optimal gas-flow conditions to be sure the choice was still optimal with the new flows. For instance, Figure 3-3 shows a calibration curve of dimethyl sulfide (approximately 1 ng - 10 µg mass injections) using the 590 nm, 645 nm, and 665 nm LP optical filters as well as the 750 nm INT filter. Here, lines are shown depicting a quadratic (m = 2) and linear (m = 1) trend line. As

shown in this figure, on the whole, the calibration curves measured with these optical filters tend to respond in a linear fashion.

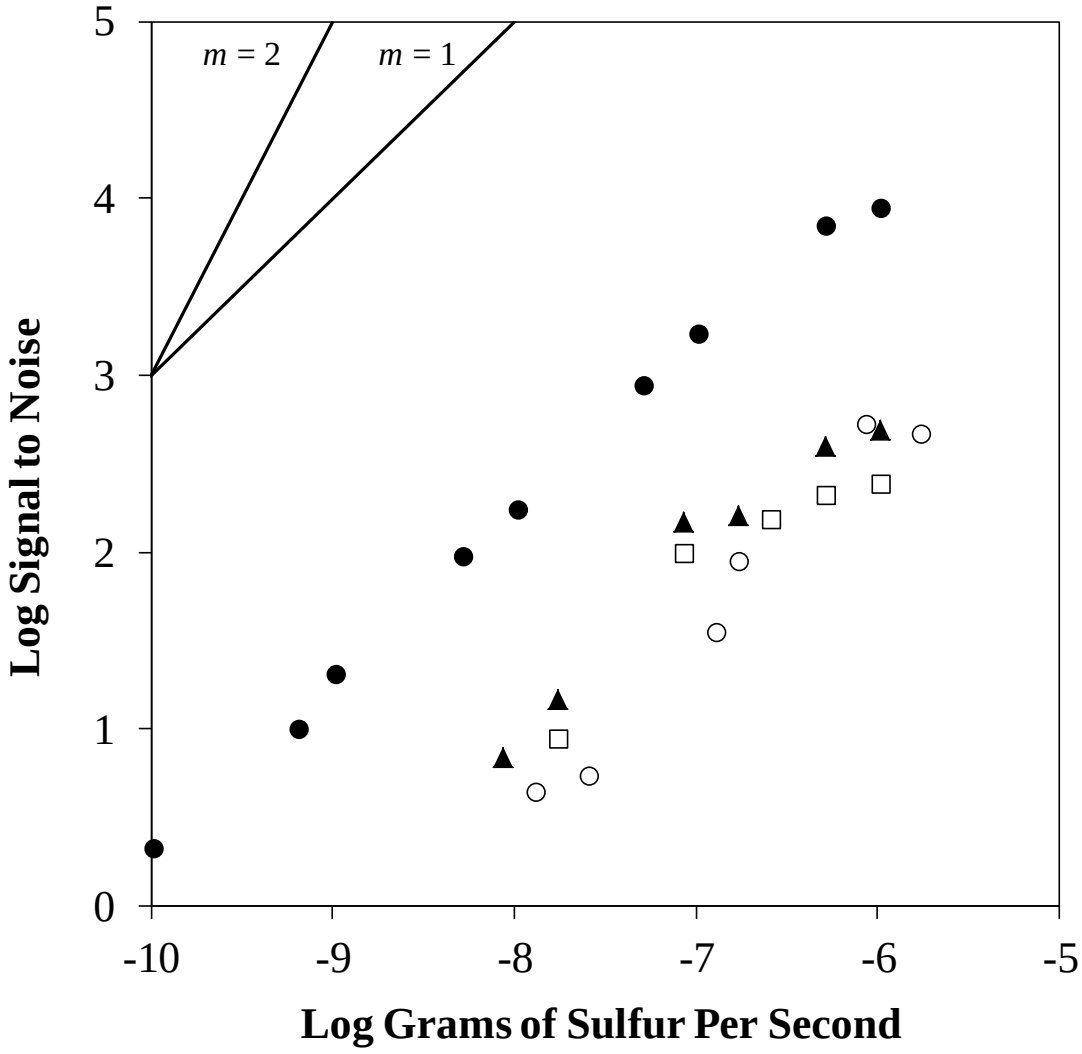

Figure 3-3: mFPD calibration curves for dimethyl sulfide under optimal HSO* gas flows using a 750 nm INT (●), 665 nm LP (○), 645 nm LP (▲), and 590 nm LP (□) optical filter. Also shown are lines depicting a quadratic (*m* = 2) and linear (*m* = 1) trend line. Column temperature is 30 °C.

Overall, the 750 nm interference filter clearly emerged as the best response for HSO* emission, as well as the most consistently linear of the optical filters used in this calibration. Authors of earlier linear sulfur emission work using a conventional FPD have shown spectra of the HSO* emission to have a prominent band feature at 750 nm[25]. As well Schurath et al. noted a prominent HSO* band that is well defined near 750 nm[101]. Similarly then, this band feature is likely responsible for the strong response and linearity in the mFPD; however spectral studies are required in order to confirm this (which is examined further in Chapter Four). Subsequently, using the 750 nm interference filter with the optimal flame gas flows determined above, proved to provide the best conditions for producing and monitoring a strong HSO* response in the mFPD.

3.3 Sensitivity and Detection Limits

After achieving optimal HSO* conditions in the mFPD, studies were focused towards exploring the analytical performance of this response mode. Figure 3-4 shows the change in mFPD response for varying masses of ten sulfur containing compounds in the linear HSO* mode. As such, these compounds were chosen to represent a good variety of sulfur species, which can vary widely in their behavior in the FPD[28,42]. As well, a single calibration of tetrahydrothiophene in the quadratic S_2* mFPD mode and reference lines depicting both a purely quadratic (slope of 2) and linear (slope of 1) trend for comparison are also included. As seen, compared to the decidedly quadratic trend established in the S_2* mode, the HSO* mode can provide a linear response toward all of the sulfur compounds examined.

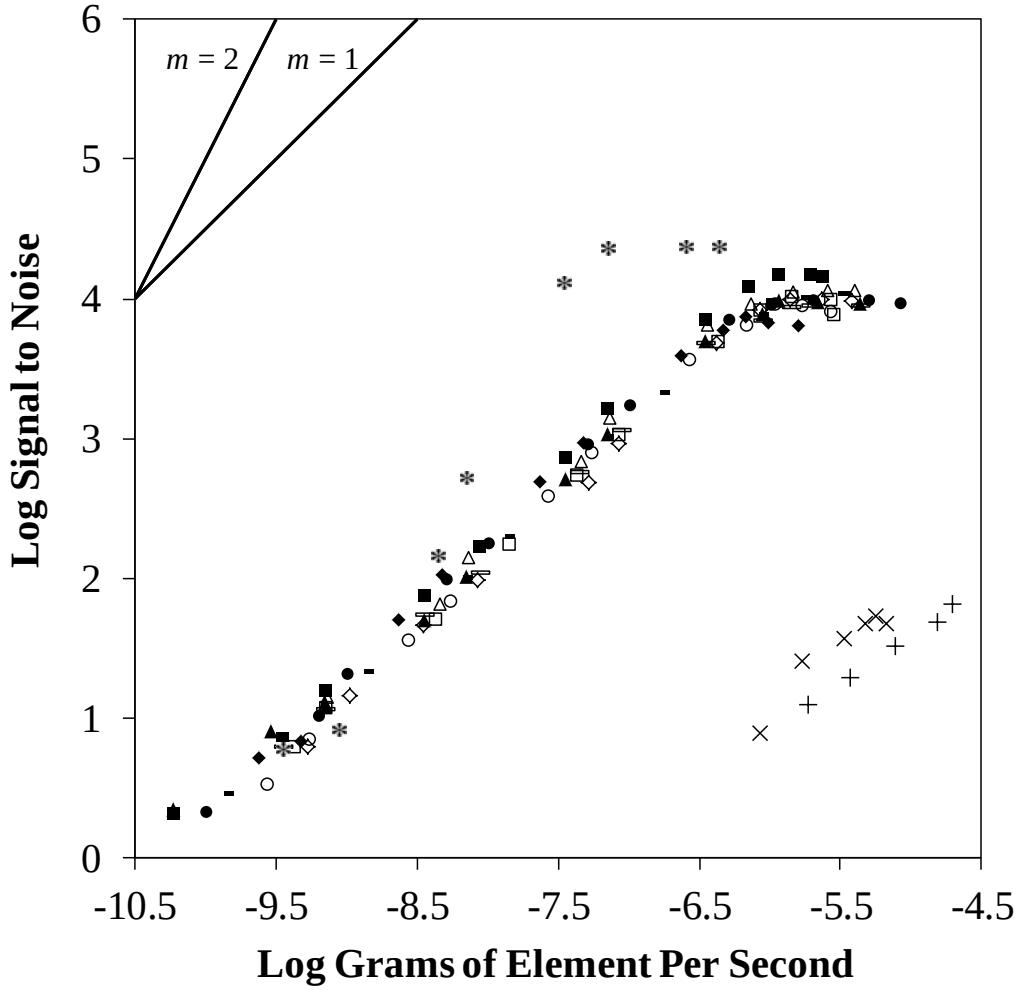

Figure 3-4: Calibrations under linear HSO* mFPD conditions for diethyl sulfide (■), 2-propanethiol (◊), dimethyl sulfide (●), 1-butanethiol (▲), 1-methyl-1-propanethiol (▭), methyl disulfide (▬), tetrahydrothiophene (Δ), isopropyl disulfide (□), dipropyl sulfide (○), thianaphthene (♦), dodecane (×), and benzene (+). That of tetrahydrothiophene (✻) under quadratic S_2* conditions, and reference lines depicting a quadratic (*m* = 2) and a linear (*m* = 1) trend are also shown for comparison. Column temperatures for sulfur analytes are described in Table 3-2, column temperatures for benzene and dodecane were set at 50 °C and 200 °C respectively.

Consequently this response spans a linear range of nearly 4 orders of magnitude and yields an MDL of approximately 5.8×10^{-11} gS/s ($S/N_{p\text{-}p} = 2$). As well, a simple linear regression analysis was done to determine the coefficient of determination (R^2) values and the slope of the calibration curves within the respective linear range of each sulfur compound. These results are tabulated for each sulfur analyte in Table 3-2. Data in this table shows that linearity is satisfactory in all cases, with coefficients of determination ranging from 0.994 to 0.999, and slopes ranging from 0.896 to 0.987. Additionally, in more direct terms of detectability, the individual minimum detectable masses (MDM) for each of these compounds are also given in Table 3-2. As can be seen they range from 0.4 to 3.6 ng for peak half-widths of 4.0 to 6.0 seconds. Overall, these values agree very well with those reported for the mFPD quadratic S_2* mode as well as those obtained for linear HSO* modes operated in conventional FPD and pulsed FPD platforms[25,69].

3.3.1 Response Dynamics of the mFPD

With respect to response dynamics, the speed of this linear HSO* detection mode was also examined in the mFPD. Since both conventional and counter current FPD designs have been successfully used previously to monitor S_2* in rapid GC applications[56,96], no particular issues were anticipated in this regard. However, this was still necessary to probe given the alternative detector and sulfur flame species being employed. To survey this, the hydrogen flow (120 mL/min) was re-routed into the mFPD as the carrier gas through a short 2 m length of DB-5 megabore column, and the sudden response of highly volatile carbon disulfide headspace injections (to simulate a step function response) were monitored with the fastest data acquisition rate available to us (50 Hz).

Table 3-2: Linear correlation data and minimum detectable masses (MDM) for the 10 sulfur compounds in the HSO* linear mode of Figure 3-4.

Analyte	Molecular Formula	Column Temperature (°C)	R^2	Slope (*m*)	Intercept	Data Points (*n*)	MDM (ng; $S/N_{p-p} = 2$)	Peak Half Width (s)
Diethyl sulfide	$(C_2H_5)_2S$	30	0.999	0.987	10.202	8	1.1	6.0
2-Propanethiol	$(CH_3)_2CHSH$	30	0.999	0.966	9.795	8	0.8	4.0
Dimethyl sulfide	$(CH_3)_2S$	30	0.999	0.966	9.961	8	0.7	5.0
1-Butanethiol	$CH_3(CH_2)_3SH$	50	0.994	0.896	9.387	8	0.6	6.0
1-Methyl-1-propanethiol	$CH_3CH_2CH(SH)CH_3$	50	0.999	0.957	9.811	7	1.3	5.0
Methyl disulfide	CH_3SSCH_3	50	0.999	0.922	9.544	9	0.4	5.0
Tetrahydrothiophene	C_4H_8S	90	0.997	0.967	9.997	8	2.2	5.0
Dipropyl sulfide	$(CH_3CH_2CH_2)_2S$	100	0.997	0.966	9.831	8	2.3	5.0
Isopropyl disulfide	$[(CH_3)_2CH]_2S_2$	150	0.999	0.951	9.728	9	2.6	5.0
Thianaphthene	C_8H_6S	200	0.998	0.939	9.795	7	3.6	5.0

Using this arrangement and following standard protocol (i.e., the time taken from the creation of an input signal until 63.2% of the signal is realized)[102], the detector time constant of HSO* emission in the mFPD was estimated to be on the order of about 90 ms. This indicates that the mFPD linear sulfur mode should be applicable for separations in the range between formal 'fast' and 'very fast' GC designations[103-105]. Figure 3-5 illustrates this with a tetrahydrothiophene peak eluted under these conditions in the linear HSO* mode of the mFPD.

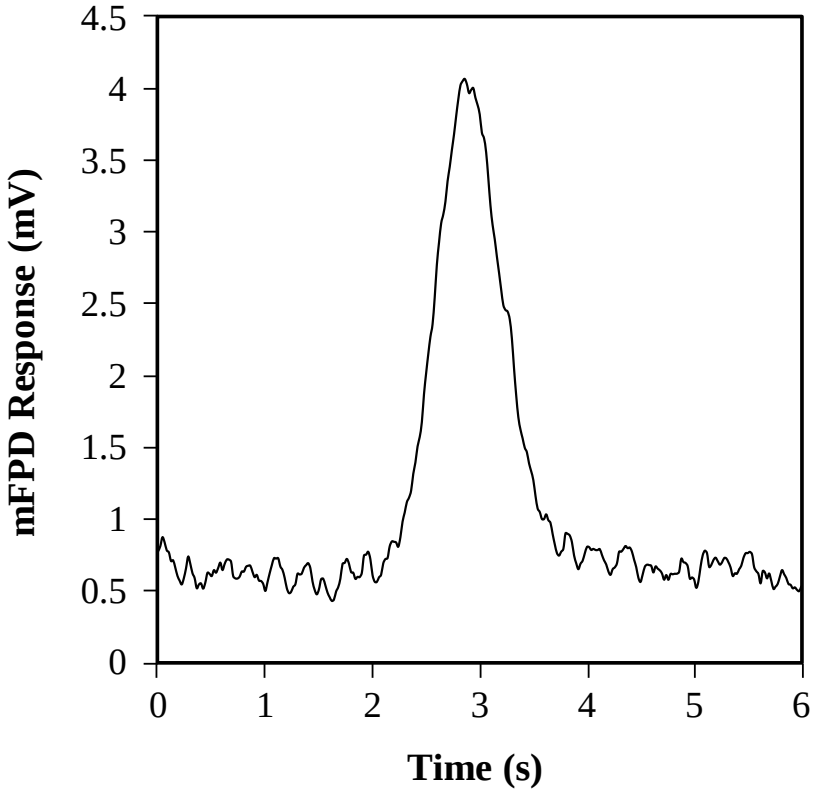

Figure 3-5: A fast peak for 540 pg of tetrahydrothiophene in the linear HSO* mode of the mFPD using hydrogen as the flame and carrier gas (120 mL/min) and employing a DB-5 column (2 m × 0.53 mm I.D.; 1.0 µm film thickness) for separation. Column temperature is 25 °C.

As seen, a good response profile is obtained, which displays a peak width at half-height of about 700 ms. While this is in the range between 'fast' to 'very fast' GC application, it still appears to be outside of that fully required for 'very fast' to 'ultra fast' modes[103,104]. Incidentally, due to this much narrower peak width, the MDM for tetrahydrothiophene is measured to be 153 pg. At present, it is unclear if even faster time constants and peaks can be realized in this mFPD response mode by using, for example, faster acquisition rates, superior electronics, and equipment formally suited for 'ultra fast' GC operation. However, when such measures were invoked with other conventional and counter current FPD formats, narrower peaks were successfully monitored[56,96]. Therefore, further refinements in this regard should be beneficial.

3.4 Selectivity

Also included in the calibration curves of Figure 3-4 is the response toward carbon test analytes (both aliphatic and aromatic) measured under the linear HSO* conditions. As can be seen, both dodecane and benzene produce a very limited response range spanning roughly an order of magnitude. Compared to the sulfur response obtained, this corresponds to a formal selectivity of sulfur over carbon of about 3.5×10^3, which also agrees very well with that found for the HSO* mode operated in a conventional FPD system[25]. In practical terms, this translates into fairly large hydrocarbon quantities being required to obtain a measurable signal in the HSO* mode of the mFPD. For example, little to no response was attainable for injected amounts below about 5 µg. Further, for quantities nearing about 50 µg, the analytical flame began to saturate and its response leveled off. Therefore, considering the sizable injected amounts typically required to

respond, no major interferences are anticipated in the ability to selectively monitor sulfur containing compounds in this HSO* mode. Consequently, this linear HSO* mode in the mFPD could be useful in analyzing complex matrices. An illustration of this is provided in Section 3.6.

3.5 Reproducibility and Equimolarity

As mentioned in Section 1.3.2, due to the quadratic nature of the conventional S_2* emission, reproducibility of sulfur response is an important issue in the FPD and related devices. As well, the intensity of this S_2* emission, with respect to equimolarity, can differ greatly over a broad range of sulfur compounds yielding a relatively non-uniform response factor[29,42]. To probe the relative reproducibility of this linear sulfur response and the extent to which it varied with molecular structure, a range of analytes were examined in both the conventional single-flame S_2* mode and the multiple-flame HSO* mode of the mFPD. Specifically, the response in each of these modes was measured for replicate injections (n = 10; ~500 ng each) of ten different sulfur-containing compounds. Results for each respective mode are presented in Tables 3-3 and 3-4.

Reproducibility of sulfur response in each mode was determined by measuring the individual analyte peak areas over the ten consecutive trials and then calculating the %RSD of the average value. As seen in Table 3-3, the conventional single-flame S_2* mode of the mFPD displays RSD values ranging from 3.2 to 16.8%, with an average of 6.7% over all the analytes. These values agree well those previously established for the single-flame S_2* modes of the mFPD and a conventional FPD[88,94].

Table 3-3: Reproducibility and equimolarity of response in the conventional single-flame S_2* mode of the mFPD (*n* = 10; ~500 ng of each analyte). Chromatographic conditions as described in Table 3-2.

Compound	Injected Mass (ng)	Average Peak Area (mV · s)	% RSD of Area	Normalized Equimolarity of Response (per mole S)
Diethyl sulfide	522	4727	4.8	1.4
2-Propanethiol	514	3771	5.0	0.9
Dimethyl sulfide	549	8094	6.3	1.6
1-Butanethiol	529	4621	4.8	1.3
1-Methyl-1-propanethiol	539	2650	3.8	0.8
Methyl disulfide	538	9546	3.2	1.4
Tetrahydrothiophene	540	3546	4.2	1.0
Dipropyl sulfide	533	3791	10.4	0.9
Isopropyl disulfide	518	3117	7.4	1.2
Thianaphthene	521	282.8	16.8	0.1

Table 3-4: Reproducibility and equimolarity of response in the multiple-flame HSO* mode of the mFPD (*n* = 10; ~500 ng of each analyte). Chromatographic conditions as described in Table 3-2.

Compound	Injected Mass (ng)	Average Peak Area (mV·s)	% RSD of Area	Normalized Equimolarity of Response (per mole S)
Diethyl sulfide	522	285.6	0.9	0.9
2-Propanethiol	514	282.2	1.1	0.8
Dimethyl sulfide	549	413.4	1.2	0.9
1-Butanethiol	529	318.4	1.4	1.0
1-Methyl-1-propanethiol	539	319.8	1.7	1.0
Methyl disulfide	538	567.1	1.9	0.9
Tetrahydrothiophene	540	348.4	1.1	1.1
Dipropyl sulfide	533	411.9	2.6	1.0
Isopropyl disulfide	518	241.7	1.2	1.1
Thianaphthene	521	240.2	3.4	1.1

By comparison, response reproducibility for the same analytes in the multiple-flame HSO* mode, shown in Table 3-4, yielded a much narrower range of RSD values spanning from 0.9 to 3.4%, with an average value of 1.7%. Figure 3-6 demonstrates this with a chromatogram of 16 consecutive manual injections of diethyl sulfide in this multiple-flame HSO* mode. As seen in this figure, peak response for this test analyte is very repeatable indicating good detector precision.

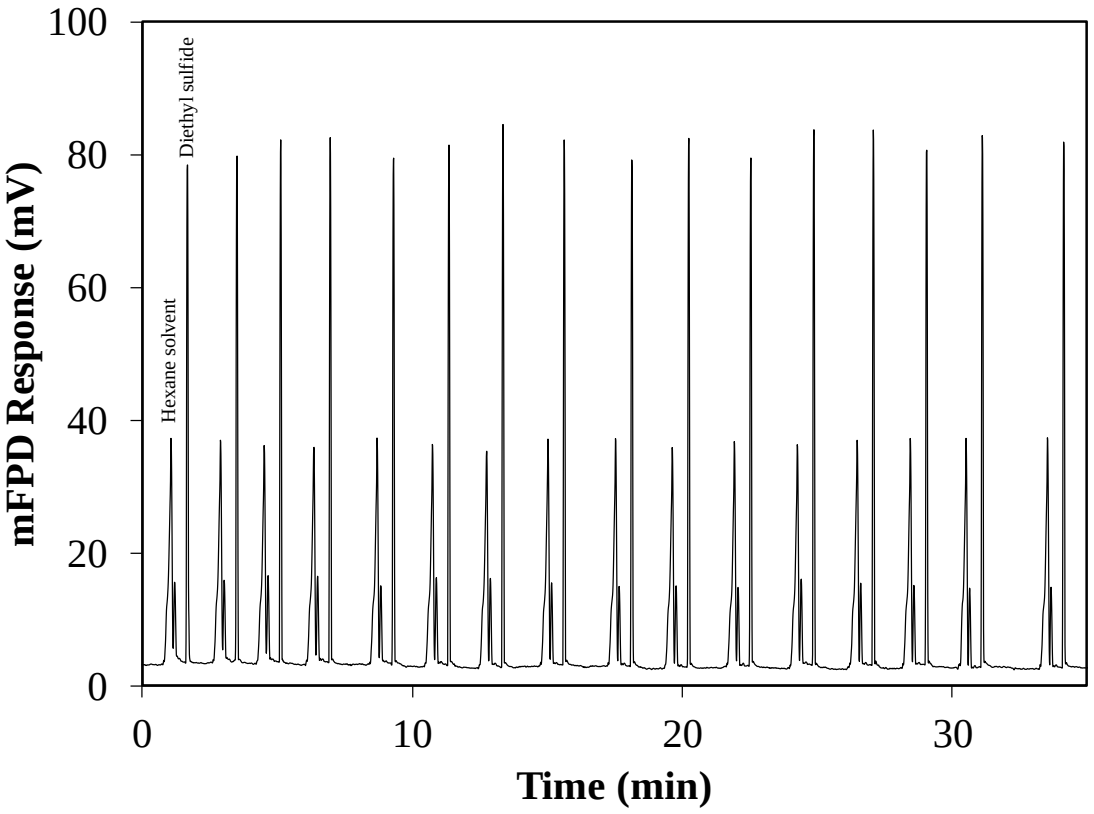

Figure 3-6: Repeated peaks produced in the HSO* linear mode of the mFPD using 16 × 1.0 µL injections of 522 ng/µL of diethyl sulfide in hexane solution spaced approximately every 2 min. Order of elution is hexane (solvent peak) then diethyl sulfide.

To investigate the relative equimolarity of response in each mode, the average peak area for each analyte was converted to a value of response per mole of sulfur injected. The set of values resulting from this was then normalized for comparison by using the median value as unity. As seen from the findings in Table 3-3, equimolarity data from the single-flame S_2* mode produced values ranging from 0.1 to 1.6 over the ten sulfur analytes. Further, of these, only half are within ± 0.2 of unity, and just 3 of 10 are within ± 0.1 of unity. This large variability is consistent with the relatively non-uniform response factor that has been observed previously with conventional single-flame S_2* FPD modes[24,29,42,94]. By comparison, for the same analytes in the multiple-flame HSO* mode, shown in Table 3-4, response equimolarity is greatly improved. As seen, this linear response mode yields values ranging from 0.8 to 1.1, where all reside within ± 0.2 of unity, and 9 out of 10 are within ± 0.1 of unity.

In general then, these findings of the multiple-flame HSO* mode represent a notable improvement in the reproducibility and equimolarity of sulfur response over the conventional single-flame S_2* mode. This can be attributed to the respective linear and quadratic natures of the species being monitored as well as the homogenizing effect of the multiple flames processing analyte ahead of the analytical flame. As such, it appears that this linear mode of the mFPD can facilitate the delivery of a sulfur-containing effluent to the analytical flame that is more consistent in its composition and hence stable in the response that it provides. While it would also be interesting to further examine the formation of excited species in this multiple-flame array, more detailed spectroscopic investigations are required to better understand this.

3.6 Hydrocarbon Response Quenching Behavior

The relative response quenching characteristics of the multiple-flame HSO* and single-flame S_2* modes of the mFPD were next examined using methane as a model hydrocarbon source. To do this, different flows of methane were introduced at the detector base of the GC and combined with the hydrogen and column effluent prior to reaching the detector. Under each condition, the response toward a sulfur test analyte was measured and compared against its equivalent response in the absence of methane (i.e. 'unquenched') to quantify the relative quenching effects observed.

Figure 3-7 displays this for a tetrahydrothiophene test analyte in both the conventional single-flame S_2* mode and the multiple-flame HSO* mode of the mFPD. Here, response is given as a percentage of its original unquenched value and plotted as a function of methane flow (displayed as µg C/s). As shown, in the conventional single-flame S_2* mode, the sulfur response was reduced to 50% of its original value for methane flows that presented about 2-3 µg C/s into the detector, which is very similar to experiments previously performed with a conventional FPD in the S_2* mode[53]. Further, as the amount of methane increased to levels of about 27 µg C/s, the response eroded to 0.07% of its original value. By comparison, over this same range of hydrocarbon introduction, linear HSO* response in the mFPD maintained nearly 100% of its original unquenched value up to the higher methane level where it decreased to about 75%. Considering this difference in quenching behavior, these findings suggest that the new linear mFPD response mode could potentially offer beneficial performance for the analysis of sulfur compounds in complex hydrocarbon matrices.

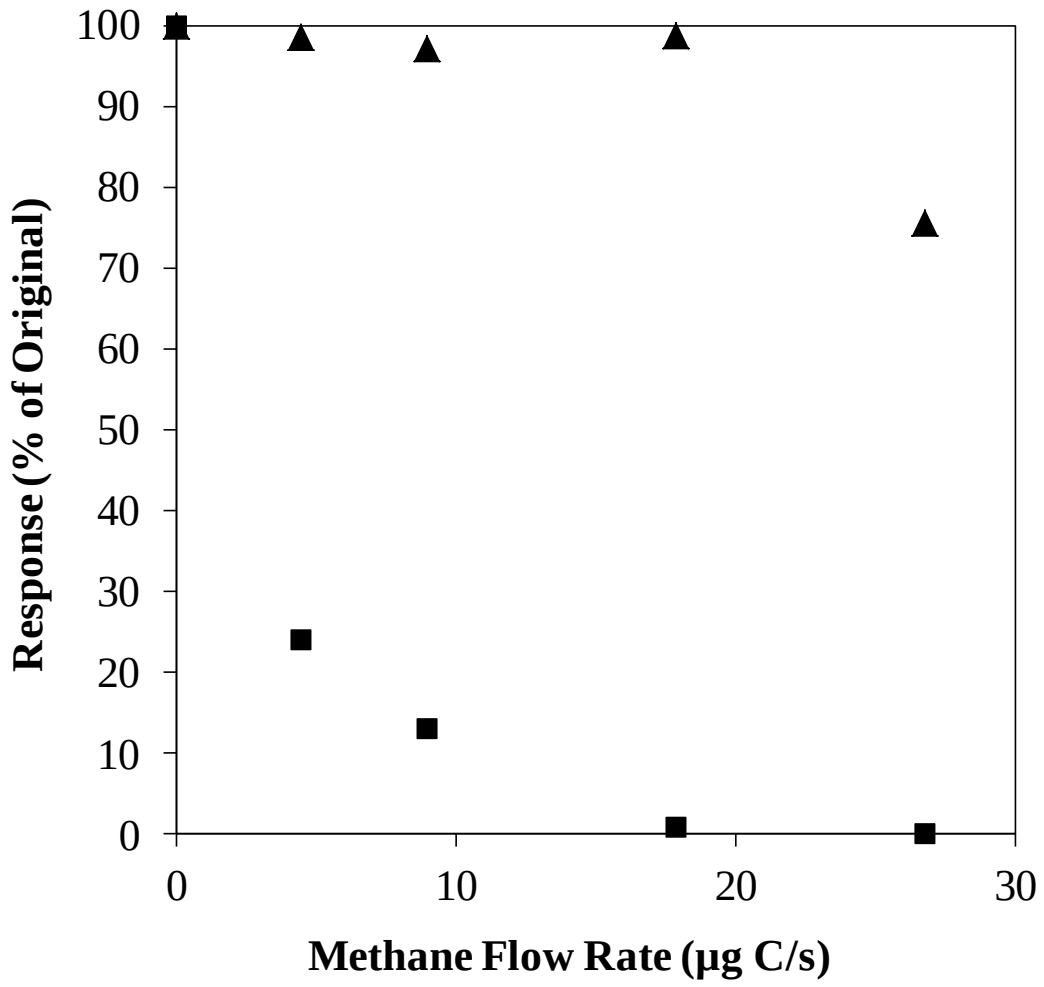

Figure 3-7: mFPD response toward tetrahydrothiophene (1 µg) as a function of methane flow in the conventional single-flame S_2* mode (■) and the multiple-flame HSO* mode (▲). Column temperature is 90 °C.

To investigate this further, commercial diesel fuel (Diesel Sample A) was spiked with various amounts of a thianaphthene standard and analyzed using these two detection modes to compare the sulfur response obtained amongst the numerous species of co-eluting hydrocarbons present. To create conditions conducive to severe response

quenching for this experiment, the diesel fuel was injected directly as a neat, undiluted 1 µL sample onto the DB-5 megabore column used for separation. It was found that significant differences in response existed for these detection modes, which became particularly apparent for injected masses of thianaphthene near the 50 ng level. An illustration of this is shown in Figure 3-8.

As seen, the upper trace (Figure 3-8A) shows a standard FID response towards this sample, which reveals a very large number of unresolved hydrocarbon components continuously eluting during the hour long separation. Figure 3-8B shows the same sample analyzed in the multiple-flame HSO* mode of the mFPD. As seen, even though the amount of hydrocarbon simultaneously proceeding through the mFPD flame is quite large, minimal interference is noted from the sample matrix, and a clear peak arising from thianaphthene is identified with a retention time near 12 min. In contrast to this, the conventional single-flame S_2* mode (Figure 3-8C) failed to produce a thianaphthene peak under the same conditions. Incidentally, when a range of thianaphthene masses were similarly examined here in diesel fuel, as demonstrated in Figure 3-9, a linear sulfur response could also still be observed down to this 50 ng level in the multiple-flame HSO* mode. Thus this new HSO* mode can provide a linear sulfur response even under heavy quenching conditions which could be potentially very useful in various sulfur monitoring applications.

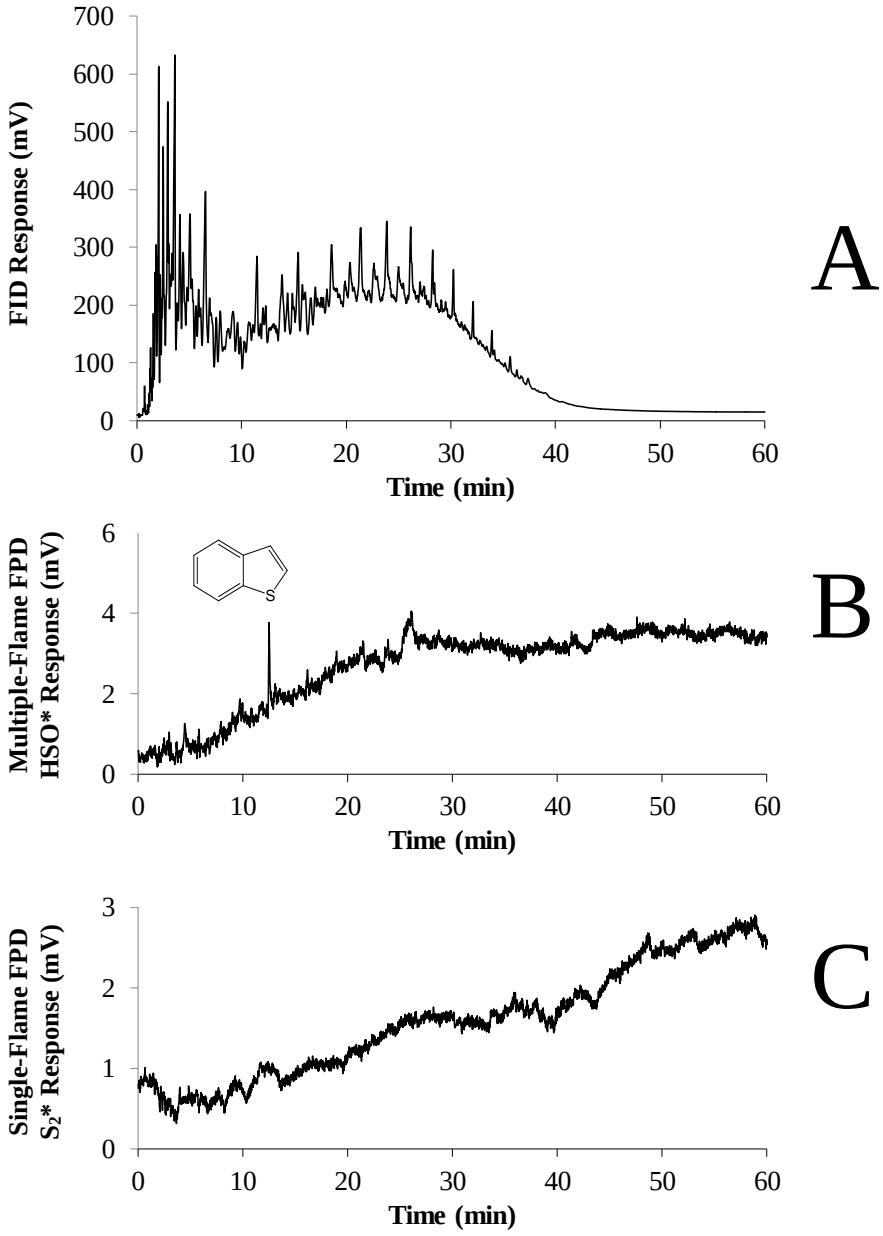

Figure 3-8: Chromatograms resulting from a 1 µL injection of pure commercial diesel fuel (Diesel Sample A) containing 50 ng of thianaphthene using three modes of detection: FID mode (A), multiple-flame HSO* mode (B), and conventional single-flame S_2* mode (C). The temperature program used was 70 °C initial for 5 min, then increasing to 280 °C at 5 °C/min.

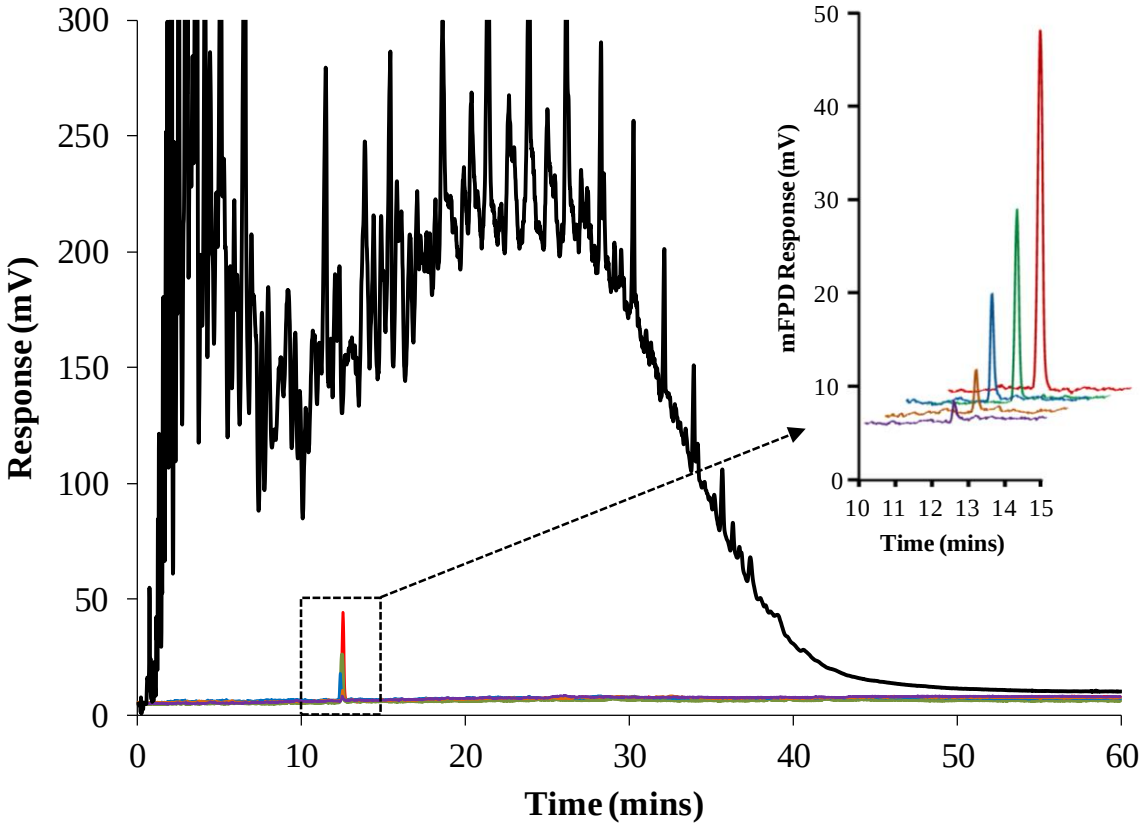

Figure 3-9: Chromatograms resulting from a 1 µL injection of pure commercial diesel fuel (Diesel Sample A) containing 50 - 1000 ng of thianaphthene. Here response is shown using the FID mode (black trace), while mass injections of 1000 ng (red trace), 500 ng (green trace), 250 ng (blue trace), 100 ng (orange trace), and 50 ng (purple trace) of thianaphthene are shown in the multiple-flame HSO* mode. Top right inset is an enlarged view of the thianaphthene peaks as represented by the dashed outline. The temperature program used was 70 °C initial for 5 min, then increasing to 280 °C at 5 °C/min.

3.7 General Comparisons

Over the past few decades a number of highly selective GC detectors have been developed for trace-level detection of sulfur-containing analytes. Table 3-5 lists some basic characteristics for several popular sulfur selective detectors that are conventionally employed. Included in this table are figures of merit for the mFPD's linear HSO* mode of operation described from this work for comparison.

As shown in Table 3-5, the performance of the mFPD is reasonable compared to these other detectors. For instance, the detection limit of the mFPD in the linear HSO* mode is near 10^{-11} gS/s, similar to the values found in both the FPD and pFPD HSO* modes. Also, the HSO* mode of the mFPD shows a near 10 fold improvement over the dFPD[60], and aligns well with the S_2* response of most modern FPDs[81,82]. However, it should be mentioned that a few studies have reported improved FPD S_2* detection limits in the low pg S/s range[56,106,107]. The pFPD S_2* response mode, on the other hand, is notably more sensitive, as are the SCD and AED as well[2,60,82].

Also shown in this table is the selectivity of sulfur response over carbon response for each detector. As seen, selectivity in the HSO* mode of the mFPD is between 3 to 4 orders of magnitude. This aligns well with the selectivity values also reported for the dFPD[60], some FPD reports (in both the HSO* and S_2* modes)[25,60,82], and the AED[82]. However, selectivity found in the SCD, the pFPD, and certain FPD modes are notably much greater, as they have been reported nearing about six to seven orders of magnitude[2,60,106].

Table 3-5: Basic characteristics of gas chromatographic sulfur selective detectors.

Detection Method	Monitored Emission	Detection Limit (gS/s)	Selectivity (S/C)	Response Range (decades)	Response Slope	References
Flame Photometric Detection (FPD)						
Multiple Flame (mFPD)	HSO*	5.8×10^{-11}	3.5×10^{3}	4	linear	Current Work
	S_2*	10^{-11}	10^{3} - 10^{4}	4	quadratic	[88]
Single Flame (FPD)	S_2*	10^{-11} - 10^{-12}	10^{3} - 10^{6}	3-4	quadratic	[81,82,106,107]
	HSO*	2×10^{-11}	10^{3}	4	linear	[25,60]
Pulsed Flame (pFPD)	S_2*	10^{-13}	$>10^{7}$	3	quadratic	[2,60,69]
	HSO*	2×10^{-11}	n/a	n/a	linear	[69]
Dual Flame (dFPD)	S_2*	10^{-10}	10^{3} - 10^{4}	3	quadratic	[60]
Sulfur Chemiluminescence Detection (SCD)	SO_2*	10^{-13}	10^{6} - 10^{7}	3-4	linear	[2,60,82]
Atomic Emission Detection (AED)	S	10^{-12}	10^{4}	3-4	linear	[2,60,82]

Additionally, the HSO* mode of the mFPD demonstrates a linear response range of about four decades, which is consistent with the other values presented for the other methods. More specifically, this agrees well with the HSO* mode of the FPD[25], and the linear ranges found in both the SCD and the AED[2,60,82]. Moreover, this response range also aligns with the response range of the S_2* mode in the FPD[25,82], and is improved relative to that of the S_2* modes of the dFPD and the pFPD[60]. Therefore, this is useful since the response found in the HSO* mode of the mFPD is linear.

While other detectors such as the pFPD, SCD, and AED are generally more sensitive and selective towards sulfur compounds than the mFPD, they are, however, not without their limitations. For example, where quenching due to co-eluting hydrocarbons often plagues the quadratic response of the FPD and pFPD[2,73], the mFPD in the HSO* mode provides a more desirable linear response and greatly reduced quenching effects. Furthermore, with respect to fast GC applications, the pFPD is not compatible with very narrow GC peaks[2,39,56], whereas the mFPD shows capacity for fast GC studies. While both SCD and AED provide a linear response towards sulfur compounds over a response range of 3-4 decades, similar to the mFPD, they are much more expensive and complex in their designs[2]. The SCD requires more maintenance, is more complicated to run, and is far more costly than the FPD[2,39]. As well the AED's complexity, high maintenance, size, and tremendous cost due to its variety of parameter selections as a multi-element detector[2,70,74], can be a deterrent for many analysts. Overall then, the robust nature, very low relative cost, small size, and linear response of the mFPD could provide an appealing option for many sulfur specific applications.

3.8 Conclusions

A new linear sulfur response mode was established in the mFPD. Through monitoring HSO* emission at 750 nm, linearity over about 4 orders of magnitude was observed with a detection limit of 5.8×10^{-11} gS/s that compared well to that of the S_2* mode of the mFPD[88]. Further, HSO* emission in the mFPD provided very good reproducibility and equimolarity over a broad range of sulfur compounds. As well, consistent with previous studies[88], the linear mFPD response also exhibited significant resistance toward interference from hydrocarbon quenching. Therefore, these results suggest that this new linear mFPD response mode could be a potentially useful alternative tool for the analysis of sulfur-containing compounds in conventional or fast GC applications.

CHAPTER FOUR: SPECTRAL EXAMINATION OF THE MULTIPLE FLAME PHOTOMETIC DETECTOR

4.1 Introduction

While the performance attributes of the mFPD have been established for both sulfur and phosphorus response[88,108], very little is known about the actual mechanism through which the detector provides such response. For instance, at the most fundamental level, the identities of the emitting species in the analytical flame have never been confirmed, and have only been assumed to be similar to those present in a conventional FPD flame[2,25,109]. Further, any differences between the two devices in this regard have also never been established or investigated. Such information is very important, since it can lead to a better understanding of the mFPD and facilitate its continued optimization and development. For instance, a closer examination of how hydrocarbons behave in each device could lead to clearer knowledge of how the two differ so dramatically in their resistance to analyte response quenching.

The most effective route to learning more about the composition and dynamics of the analytical flame is to obtain emission spectra of the various species present in it during operation. Since this has not yet been done with the mFPD or the counter-current flame that it operates in the analytical position, it can yield very valuable information on how it functions. Further, since the mFPD has been shown to provide a direct means of comparing multiple flame performance to that of a conventional single-flame[88,108], this device can also be used to obtain comparative spectra from both modes of operation under otherwise identical conditions.

This Chapter presents the first spectral examination of the mFPD. As such, Section 4.2 examines the background emission spectra obtained under both typical mFPD and single-flame FPD operating conditions. Similarly, Sections 4.3 and 4.4 examine the mFPD emission spectra of sulfur, phosphorus, and hydrocarbon analytes and then directly compare those produced from identical runs performed in a conventional single-flame FPD mode. The primary species present are identified and several key differences are observed. Finally, some potential mechanistic implications from these results are presented and discussed in Section 4.5.

4.2 Background Emission Spectra

Background emission spectra were first monitored in the mFPD under typical single-flame (i.e. 7 mL/min oxygen and 40 mL/min of hydrogen) and multiple-flame (i.e. 100 mL/min hydrogen, 30 mL/min collective oxygen to workers, and 7 mL/min oxygen to analytical) operating conditions. To gain a clearer understanding of the background emission located within the PMT's spectral response range, a representative wavelength section of 250-850 nm was initially examined. Figure 4-1 shows the background spectrum obtained at the analytical flame for both the multiple- and single-flame operating modes. As shown, a background examination of both modes reveals similar emission profiles; each producing features located near 281, 306, 562, 586, and 612 nm respectively. The most prominent feature of both modes, however, is the band located near 306 nm. This feature, as well as the minor band located near 281 nm, is believed to be that of OH emission[48,110], as these features are typically produced in a hydrogen/oxygen flame during combustion[48,110].

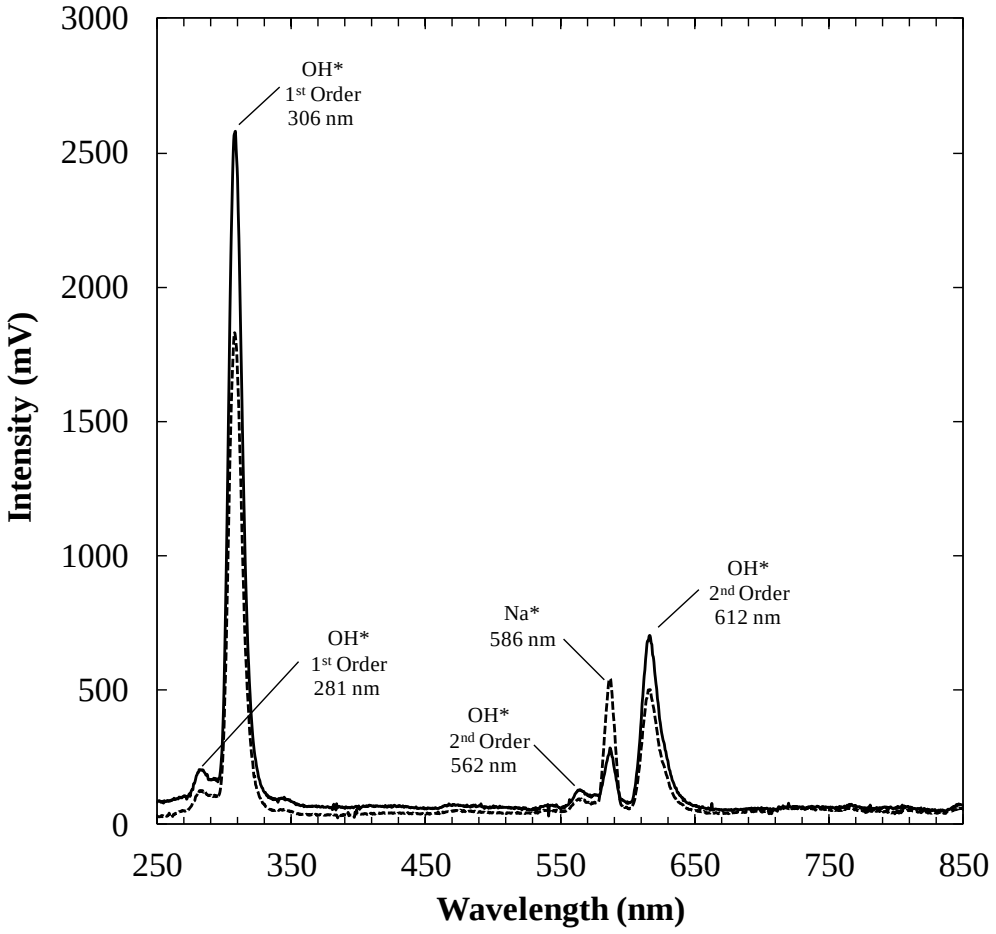

Figure 4-1: Background emission spectrum taken in the conventional single-flame (solid line) and multiple-flame (broken line) modes. Monochromator bandpass is 6.7 nm.

Similarly, this presence of OH emission can be found in the flames of the FPD[92,111], the pFPD[69,70,112], and many other hydrogen/oxygen flames[48,110,113-120], and it therefore is a reasonable finding in the mFPD.

Additionally, the bands located at 562 and 612 nm are also considered to be 2nd-order features of OH emission resulting from the transmission of second-order diffraction in the monochromator. As such, these emission bands appear at twice the original

emission wavelength[121]. As seen, the lower intensity OH features at 562 nm and 612 nm match exactly twice the wavelength location of the bands produced at 281 nm and 306 nm. Similarly, such second order OH emissions are also commonly noted in other FPD detectors[68-70]. As a result, order-sorting optical filters are often used to confirm this and block off any extraneous light derived from the monochromator's grating[25]. For instance, Figure 4-2 demonstrates the same background spectrum in the multiple-flame mode using a 435 nm long pass optical filter. As shown, the band features from OH emission at 281 and 306 nm are removed, as well as their second-order emissions at 562 and 612 nm. This was also found in the single-flame mode under the same conditions. However, as shown in Figure 4-2, a feature near 586 nm still remained.

This mysterious band emission was presumed due to sodium emission, which was further supported when the tip of the analytical SS capillary was dipped into a solution of 5.36 w/v% NaCl in deionized water, dried, and re-evaluated without an order-sorting filter. As shown in Figure 4-2, using the sodium chloride dipped SS capillary, a very strong emission band appears at 586 nm, along with the OH emission features previously identified. Consequently this indicated that the unknown feature was likely due from sodium emission in the hydrogen/oxygen flame[89]. This sodium emission feature has been previously identified in FPD work[109,122] and is likely due to handing the SS capillary during construction and initial detector setup. Therefore before examining any subsequent analyte emission spectra, a new clean analytical SS capillary was employed, and the detector was thoroughly cleaned to minimize any sodium emission.

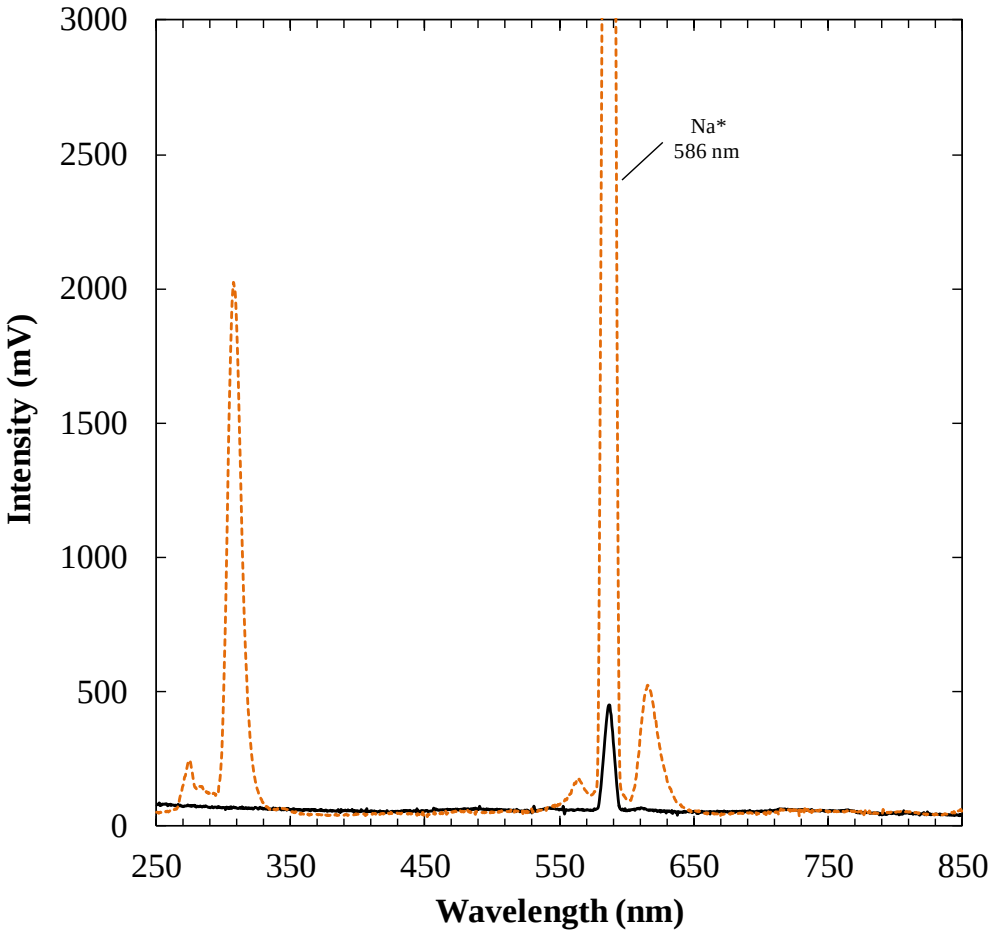

Figure 4-2: Background emission spectrum of the mFPD in the multiple-flame mode using a 435 cut-on filter (solid line) and without an optical filter using a NaCl coated SS analytical capillary (broken line). Monochromator bandpass is 6.7 nm.

4.3 Analyte Emission Spectra

Since previous mFPD studies have focused on both sulfur and phosphorus-containing analytes[88,108] they were examined next in both the multiple- and single-flame modes to gain a clearer understanding of their emission properties. Again, emission spectra were typically scanned between 250 and 850 nm and all major features observed

were reported. As such, representative sections demonstrating the prominent features of the analyte spectra are shown below.

4.3.1 Phosphorus Emission

Figure 4-3 shows the emission spectra for phosphorus as trimethyl phosphite in both the multiple- and single-flame FPD response modes.

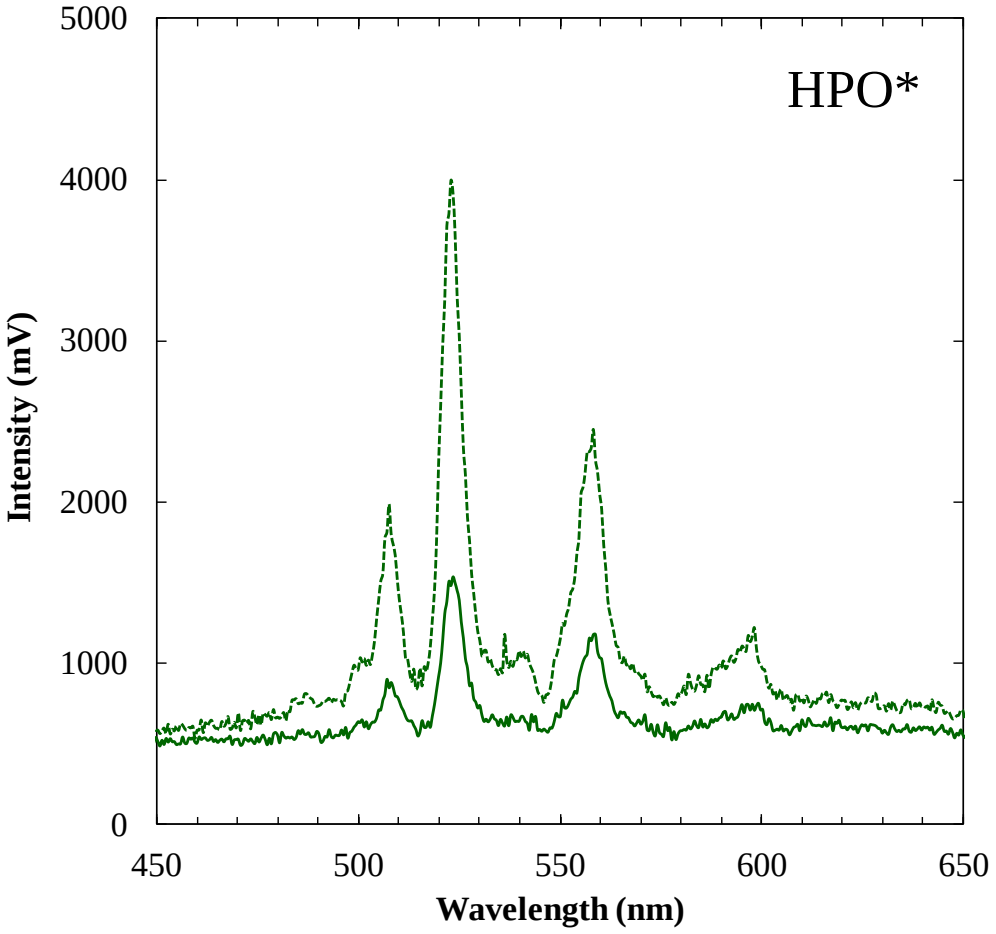

Figure 4-3: Emission spectrum of phosphorus as trimethyl phosphite in the conventional single-flame (solid line) and multiple-flame (broken line) modes. Monochromator bandpass is 0.67 nm.

As can be seen, both spectra yield very strong bands in the green region of the spectrum at identical wavelengths of 507, 523, 558, and 596 nm. This series of emission bands and their respective intensities matches very well with that assigned to HPO* in hydrogen flame systems[110], and is consistent with the emission properties of phosphorus found previously in conventional FPD[43,109] and pFPD[68,69] experiments. Therefore, since no other significant bands were observed, it appears that phosphorus response in the mFPD stems from HPO* emission. Table 4-1 further demonstrates the relative intensities of these HPO* emission features found in the multiple- and single-flame modes. As seen in this table, the HPO* spectrum of the multiple-flame mode also reveals that all the emission bands are nearly three times more intense than that of the single-flame mode.

Table 4-1: Relative intensities of the phosphorus emission bands of the multiple- and single-flame modes in the mFPD shown in Figure 4-3.

Band Feature (nm)	Band Feature Identity	Band Head Vibrational Transition Assignment[110] $(v_1\ v_2\ v_3)'$, $(v_1\ v_2\ v_3)''$	Single-Flame Intensity (mV)	Multiple-Flame Intensity (mV)
507	HPO*	(0 1 2), (0 0 0)	411	1417
523	HPO*	(0 1 0), (0 0 0)	1046	3425
558	HPO*	(0 0 0), (0 0 0)	686	1879
596	HPO*	(0 0 0), (0 1 0)	255	648

4.3.2 Sulfur Emission

Similarly, Figure 4-4 presents the emission spectra for sulfur as carbon disulfide in both the multiple- and single-flame FPD formats.

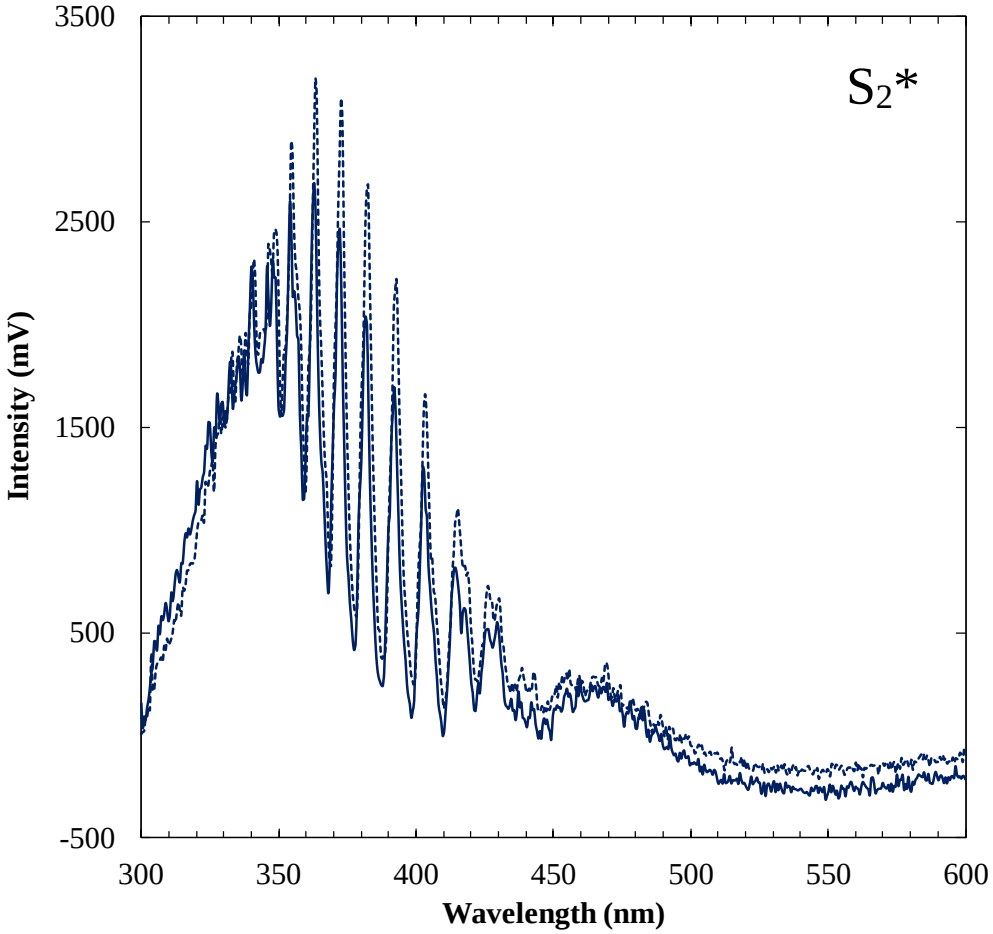

Figure 4-4: Emission spectrum of sulfur as carbon disulfide in the conventional single-flame (solid line) and multiple-flame (broken line) nonlinear response modes. Monochromator bandpass is 0.67 nm.

As seen, each spectrum produces a rich display of fluted bands at the exact same wavelengths within the blue region of the visible spectrum. This spectrum matches exactly with that of S_2* emission[110] and is widely recognized as the primary source of

sulfur emission in conventional FPD[2,5,24,25,42] and pFPD[68,69,112] platforms. Therefore, S_2* also appears to be primarily responsible for the chemiluminescence of sulfur in the mFPD. Table 4-2 further demonstrates the relative intensities of the major S_2* emission band features found in the multiple- and single-flame modes. As seen in this table, the S_2* spectrum of the multiple-flame mode also reveals that the emission bands are on average about 25% more intense than that of the single-flame mode.

It should be mentioned that all the emission spectra shown here were also found to be very reproducible. For instance, Figure 4-5 illustrates this with the sulfur emission spectrum taken over three separate trials in the multiple-flame mode. As seen, very similar profiles are obtained, demonstrating 0.2 to 5.4 %RSD intensity values over the band features found between 350 to 415 nm.

Table 4-2: Relative intensities of the sulfur emission bands of the multiple- and single-flame modes in the mFPD shown in Figure 4-4.

Band Feature (nm)	Band Feature Identity	Band Head Vibrational Transition Assignment[110] (v', v'')	Single-Flame Intensity (mV)	Multiple-Flame Intensity (mV)
354	S_2*	(0, 5)	2598	2889
363	S_2*	(0, 6)	2690	3198
372	S_2*	(0, 7)	2461	3101
382	S_2*	(0, 8)	2040	2680
393	S_2*	(0, 9)	1697	2217
403	S_2*	(0, 10)	1307	1662
414	S_2*	(0, 11)	816	1068

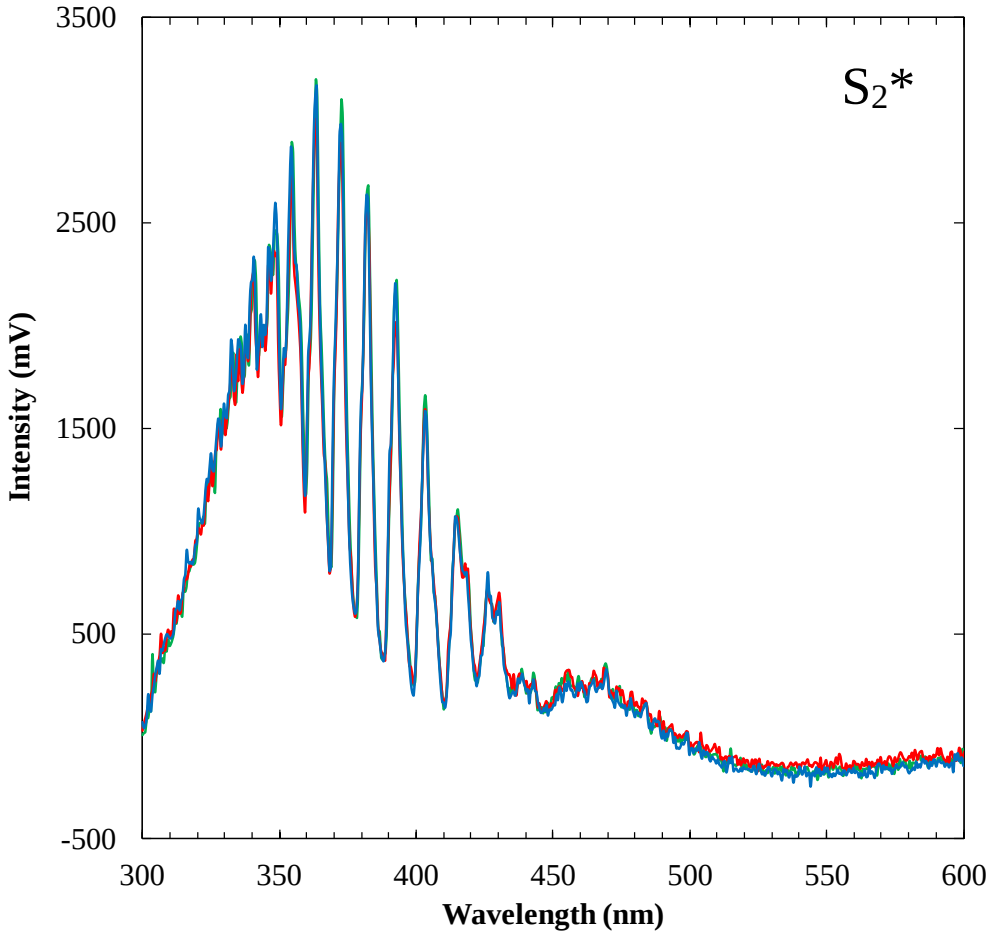

Figure 4-5: Emission spectrum of sulfur as carbon disulfide in multiple-flame nonlinear response mode over three separate trials (indicated by the red, blue, and green solid lines). Monochromator bandpass is 0.67 nm.

Since an alternate linear sulfur response was also earlier isolated and demonstrated as a useful emission source in the mFPD (see Chapter Three), it was necessary and beneficial to also examine its spectral properties here as well. Figure 4-6 presents the emission spectra of sulfur in both the multiple- and single-flame FPD formats, where the conditions have been optimized to produce a linear sulfur response. This involved altering the detector gas flows slightly in the multiple-flame mode (i.e. 120

mL/min hydrogen, 40 mL/min collective oxygen to workers, and 7 mL/min oxygen to analytical), and inserting a 495 nm cut-on filter into the optical train in order to eliminate the dominant blue S_2* emission from the background in order to observe the other species present.

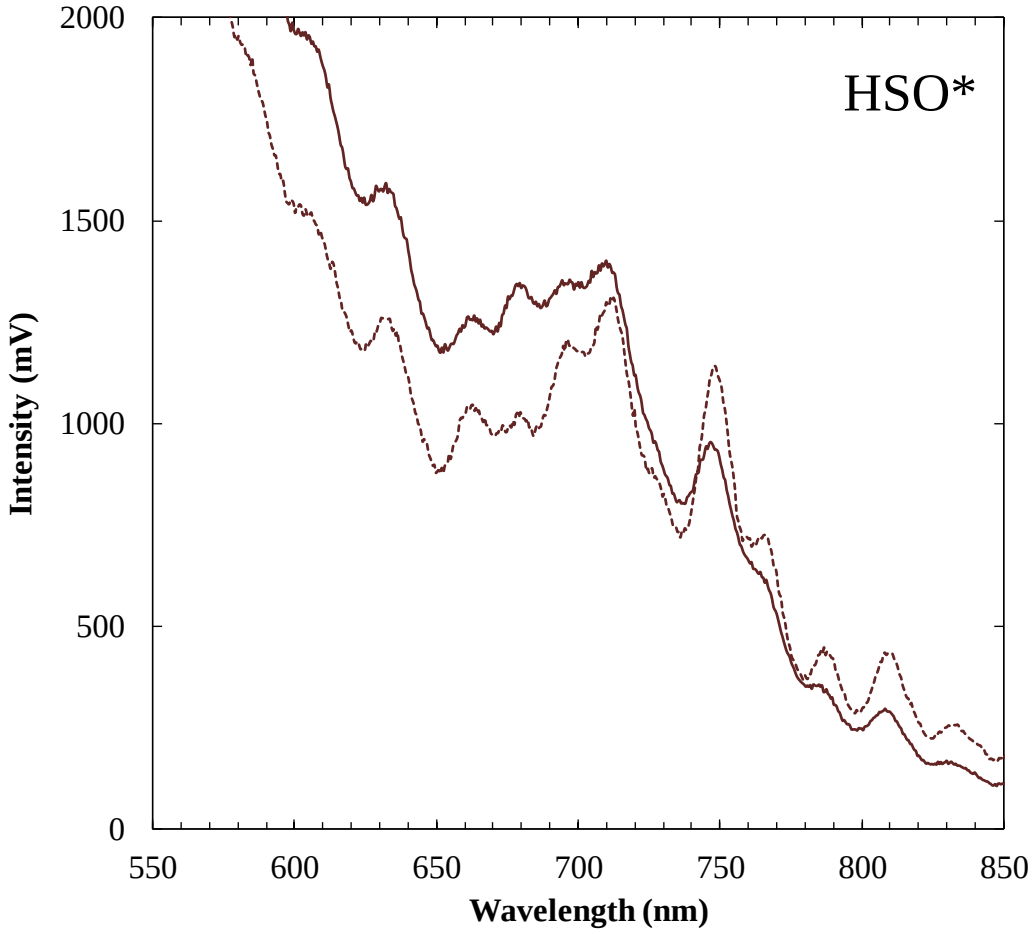

Figure 4-6: Emission spectrum of sulfur as carbon disulfide in the conventional single-flame (solid line) and multiple-flame (broken line) linear response modes. A 495 nm cut-on filter was employed to suppress second-order sulfur emission. Monochromator bandpass is 6.7 nm.

As seen, both spectra produce a similar profile in the red-region of the spectrum with prominent bands appearing near 713, 748, 766, 786, 810, and 833 nm. These wavelengths correspond very well to those previously assigned to HSO*, which has also been identified as the source of linear sulfur emission in a conventional FPD[25,101] and a pFPD[69]. Therefore, this indicates that HSO* emission is responsible for linear sulfur response in the mFPD as well. Table 4-3 further demonstrates the relative intensities of some of the HSO* emission features found in the multiple- and single-flame modes. As seen in this table, with the exception of the band at 713 nm, this HSO* spectrum of the multiple-flame mode reveals that the emission bands are on average about 30% more intense than that of the single-flame mode.

Table 4-3: Relative intensities of the sulfur emission bands of the multiple- and single-flame linear response modes in the mFPD shown in Figure 4-6.

Band Feature (nm)	Band Feature Identity	Band Head Vibrational Transition Assignment[101] (v', v'')	Single-Flame Intensity (mV)	Multiple-Flame Intensity (mV)
713	HSO*	(1, 1)	1366	1255
748	HSO*	(0, 1)	935	1148
766	HSO*	(1, 2)	614	723
786	HSO*	(2, 3)	354	448
810	HSO*	(0, 2)	286	433
833	HSO*	(1, 3)	161	257

Interestingly, the two HSO* spectra do not otherwise overlay as closely as the other spectra do. While the reason for this is not entirely clear, previous studies have shown that the addition of water vapor to the system can significantly depress the HSO* emission features at lower wavelengths[101]. Hence, since additional water vapor from the worker flames of the mFPD mode was also travelling into the analytical flame with the analyte, it seems likely that this could contribute to the difference observed. Nonetheless, the emission bands normally monitored (i.e., near 750 nm or more) are clearly stronger in the mFPD.

Consequently then, these results reveal that the primary species that yield chemiluminescence for phosphorus and sulfur in the analytical flame of the mFPD appear to be the same as those of a conventional single-flame FPD. This is quite reasonable and is consistent with the fact that the typical optical filters used to isolate emissions[25,53] and the visual appearances of analyte chemiluminescence in the flame are practically identical between the two devices. However, as can be seen from the figures, one very interesting difference that can be noted in these experiments concerns the intensity of these bands rather than their wavelength. In particular, the spectral bands of the species produced in the mFPD are consistently much more intense than those of the conventional single-flame FPD mode.

In considering this further, it can be seen that the spectra shown were acquired under identical conditions using a constant analytical flame stoichiometry, where the only existing difference was the creation or elimination of the four worker flames below. For example, the background spectra obtained here from the single- and multiple-flame modes (Figure 4-1) both displayed the same prominent band near 306 nm attributed to

OH* species[110,123]. Therefore, the species presented in the analytical flame itself do not appear to be greatly altered between the two modes. As such, the increased mFPD intensity observed could be attributed to the worker flames processing analytes ahead of the analytical flame. For instance, all flames in the mFPD emit the same color during analyte chemiluminescence[88,108]. As well, the mFPD provides a more reproducible and uniform response toward a broad range of compounds with varying molecular structures than does a single-flame FPD[88,108]. Therefore, taken together, these things indicate that the mFPD likely processes and converts more analyte into the necessary emitting species prior to entering the analytical flame for measurement. This, in turn, can promote better sensitivity in the mFPD than in a conventional FPD, which must first decompose analytes into the same emitting species and then promote excitation/emission all within a single flame region.

4.4 Hydrocarbon Emission Spectra

Since a fundamental difference between the mFPD and a conventional FPD concerns how they behave in the presence of hydrocarbons[88,108], it was of further interest to examine hydrocarbon emission spectra in each of these modes. Figure 4-7 shows the emission spectra for aliphatic carbon (as hexane) in both the multiple- and single-flame FPD response modes, while Figure 4-8 shows the same for aromatic carbon (as benzene). As seen, the same features are produced in each. Of note, a minor band near 387 nm and a major band near 430 nm appear as a result of CH* emission[68,110]. As well, prominent bands near 469, 516, and 558 nm also appear due to C_2* emission from the well-studied Swan band system[110].

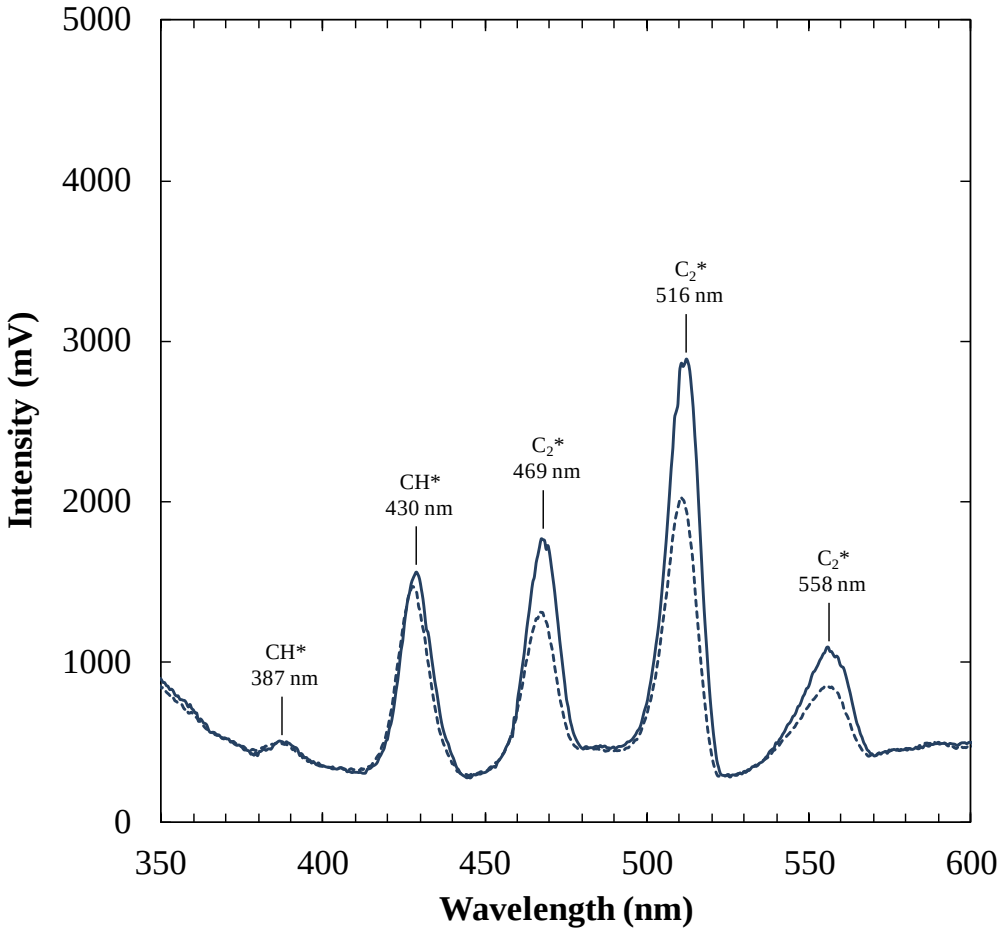

Figure 4-7: Emission spectrum of carbon as *n*-hexane in the conventional single-flame (solid line) and multiple-flame (broken line) modes. Monochromator bandpass is 6.7 nm.

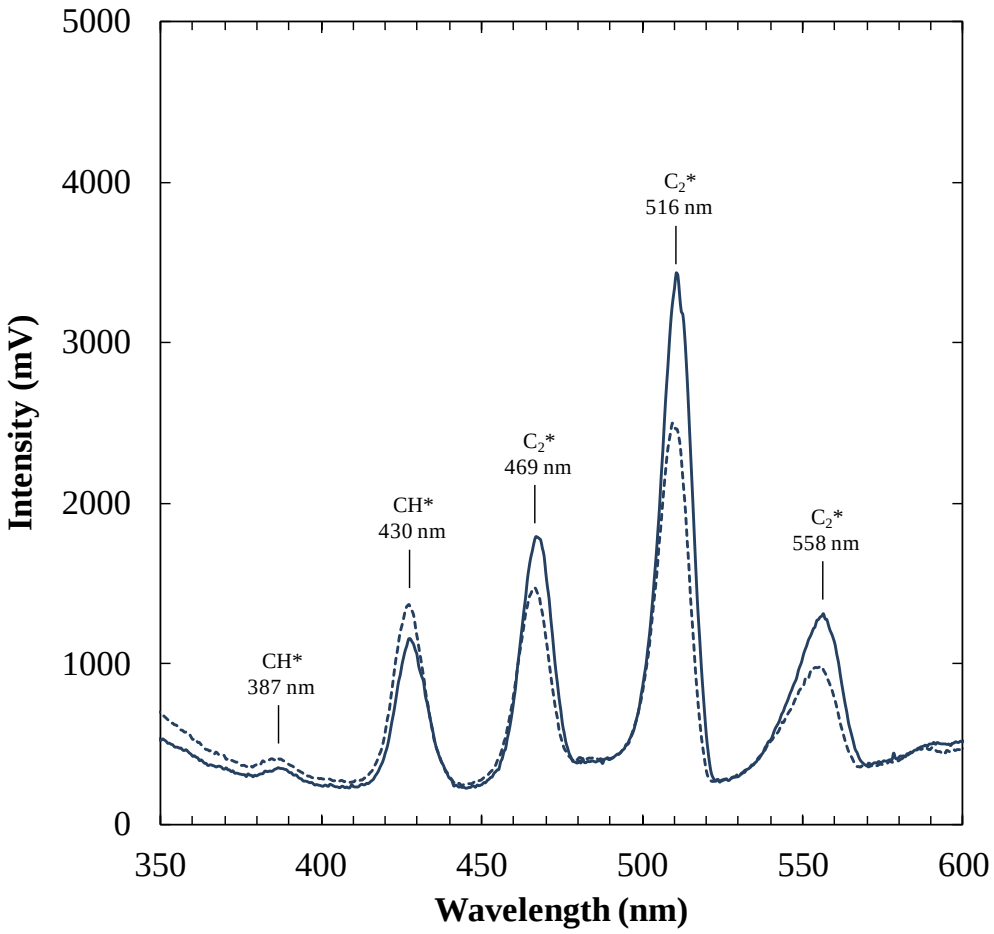

Figure 4-8: Emission spectrum of carbon as benzene in the conventional single-flame (solid line) and multiple-flame (broken line) modes. Monochromator bandpass is 6.7 nm.

These species are commonly observed in conventional FPD[2,18,123,124] hydrocarbon spectra and the results indicate that the mFPD does not qualitatively differ in this regard either. Again, however, several interesting quantitative features arise in the figures when the relative intensities of these bands are considered. For instance, in the single-flame spectra, aromatic carbon produces greater proportions of C_2* to CH* than does aliphatic carbon. Such spectral discrimination between these hydrocarbon forms is known for the conventional FPD, which often responds more strongly towards aromatic compounds[18]. Comparatively, however, the relative production of C_2* and CH* is much more consistent in the mFPD mode. Table 4-4 demonstrates this with the ratio of emission band intensities for aromatic and aliphatic hydrocarbon sources in the multiple- and single-flame modes.

Table 4-4: Response ratio of carbon emission for aromatic and aliphatic analytes. Aromatic and aliphatic hydrocarbons are introduced as benzene and hexane from data in Figure 4-7 and 4-8.

	Band Wavelength (nm)				
	387	430	469	516	558
Aromatic to Aliphatic Ratio Single-Flame FPD	0.8	0.7	1.0	1.1	1.2
Aromatic to Aliphatic Ratio Multiple-Flame FPD	1.0	0.7	1.0	1.0	1.0

For this, band peak heights (in mV) were measured for all of the features present in Figures 4-7 and 4-8, the intensity ratio at each wavelength was calculated, and the results were normalized using the median value as unity. As seen in this table, the single-flame FPD mode presents values ranging from 0.7 to 1.2, indicating that widely different amounts of each species are produced in the flame for aliphatic and aromatic hydrocarbons. By contrast, the multiple-flame data show that almost all of the species are produced in equal amounts regardless of the hydrocarbon source. Therefore, the mFPD appears to better homogenize hydrocarbons into the same ultimate form inside the analytical flame. This also agrees with earlier calibration data that showed a more uniform response for aromatics and aliphatics in the mFPD relative to a single-flame mode[88,108].

Most interestingly, however, in contrast with the enhanced mFPD analyte spectra observed earlier, the hydrocarbon spectra in Figures 4-7 and 4-8 show that emission intensity in the mFPD mode is clearly reduced compared to the conventional single-flame FPD mode. Specifically, all of the C_2* bands are notably smaller. By comparison, the CH* bands at 387 and 430 nm are less conclusive, since Figures 4-7 and 4-8 show a respective slight reduction and increase in their intensities. Therefore, for aliphatic and aromatic hydrocarbons, the amount of C_2* produced in the analytical flame appears to be significantly lowered in the mFPD.

4.5 Hydrocarbon Quenching Resistance Discussion

This hydrocarbon emission spectra found in the multiple- and single-flame modes provide some potentially interesting and revealing mechanistic implications for mFPD operation. For example, hydrogen radical recombination (as mentioned in Section 1.3.2, Reaction 1.3-2) is believed to provide a prominent source of excitation energy for analyte chemiluminescence in the FPD[24,26,125]. One route for producing this species involves the hydroxide radical through propagation steps[89,125] such as that shown in Reaction 4.5-1.

$OH\cdot + H_2 \rightarrow H_2O + H\cdot$ **Reaction 4.5-1**

In relation to this, the flame species $C_2\cdot$ is also known to play a major role in various reaction pathways of hydrogen/oxygen flames containing hydrocarbons[126]. For instance, $C_2\cdot$ is known to be centrally involved in Reaction 4.5-2, which is only one of several routes known to create CH* in such flames[123,125,126].

$C_2\cdot + OH\cdot \rightarrow CH^* + CO$ **Reaction 4.5-2**

Thus, Reaction 4.5-2 above suggests that the removal of $OH\cdot$ by $C_2\cdot$ could readily impede Reaction 4.5-1 and the production of hydrogen radicals that are critical to analyte response. In this way, $C_2\cdot$ may in fact play a central role in the mechanism of the hydrocarbon response quenching that has long been observed in the conventional FPD. Accordingly, then, if a relatively reduced amount of $C_2\cdot$ were created in the mFPD (based on observations of reduced C_2^* emission in Figures 4-7 and 4-8), this could potentially explain the unique quenching-resistant behavior of this device over a single-flame FPD[88,108], since relatively more $OH\cdot$ would be available for hydrogen radical production (i.e., Reaction 4.5-1) when hydrocarbons are present. In this regard, it is interesting to note that further experiments here monitored OH* emission through a 306 nm

interference filter in both the mFPD and conventional single-flame FPD mode while injecting hydrocarbons. It was found that the single-flame mode consistently produced a notable negative dip following the hydrocarbon elution, indicating that OH* (and by extension OH·) was being removed from the flame as a result. In contrast with this, the mFPD trace produced no such negative dip. Figure 4-9 demonstrates this effect using mass injections of 661 µg of hexane and 877 µg of benzene in both the multiple- and single-flame modes.

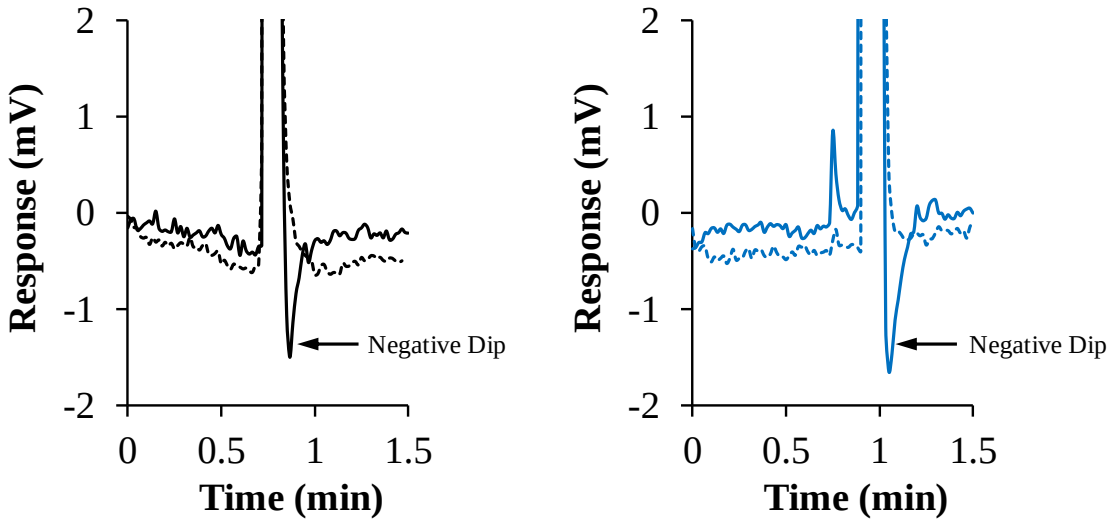

Figure 4-9: Enlarged chromatograms representing mass injections of 661 µg of hexane (black trace) and 877 µg of benzene (blue trace) in the single-flame (solid line) and multiple-flame (broken line) modes using a 306 nm (10 nm bandpass) interference filter. Column temperature is 80 °C.

This notion of hydrocarbons quenching exciting flame species in the FPD rather than excited analytes directly has been proposed in the past[53], although the hydrocarbon species involved in such a process has not been fully established. Still, similar

observations regarding the direct involvement of $C_2\cdot$ have been made with another quenching-resistant photometric device that operates on a hydrogen/oxygen combustion mechanism that is very different from that of a conventional FPD[125]. While other hydrocarbon species and (or) quenching mechanisms could also certainly be involved[24,28,51], the above scenario does agree well with the existing observations made in the FPD and mFPD.

Finally, since a considerable reduction of C_2* emission is observed in the mFPD, it is worth examining what indeed may happen to such hydrocarbons if they are not being transformed into C_2*. For example, spectrally there is no clear indication that they are largely being converted into more CH*, since no consistent and significant changes were noted in the bands monitored for this species. As well, there is no evidence within the broad range scanned (i.e., 250 to 850 nm) of any new emission features present in the mFPD mode that might suggest an alternate carbon emitter being formed. However, some interesting results were noted when the detector was modified to acquire a flame ionization signal at the analytical flame.

Here, high voltage polarization was supplied through the SS analytical capillary, and the collection of analyte signal was taken using the first SS worker capillary nearest to the analytical flame. While keeping the analytical flame stoichiometry constant, FID response from hydrocarbon analytes were taken using the conventional single-flame mode as well as the multiple-flame mode with 1, 2, 3, or 4 worker flames ignited. Consequently, it was found that the FID response generally decreased as a function of the number of worker flames ignited. For example, Table 4-5 shows the FID response for hexane and benzene generated using the conventional single-flame and multiple-flame

(i.e. four worker flames) mode. As shown in this table, the single-flame mode yielded a sizable ionization response for both hydrocarbon injections. However, when the four worker flames are ignited below this analytical flame (i.e. the conventional multiple-flame mode), the ionization signal was greatly reduced. By comparison, this corresponds to a 67% and 73% loss of the hexane and benzene signal respectfully while in this multiple-flame mode.

Table 4-5: FID response of hydrocarbon analytes in the single- and multiple-flame modes of the mFPD.

Analyte	Injected Mass (µg)	Single-Flame FID Response (mV)	Multiple-Flame FID Response (mV)
n-Hexane	661	692	230
Benzene	877	600	162

This is significant, since the flame ionization detector is known to be nonresponsive to oxidized carbon[35,127,128]. Therefore, this indicates that a significant portion of the hydrocarbon that travels through the mFPD is very likely converted into a non-emissive, oxidized carbon species (e.g., CO_2) that otherwise does not interfere with the excitation energy of the analytical flame. In this regard, it is worth noting that chromatography using CO_2 as the mobile phase has been found to be quite compatible with the FPD[129], whereas only a small percentage of CH_4 present in a mobile phase can destroy the photometric signal[53].

4.6 Conclusions

Emission spectra of the mFPD have been acquired and examined for the first time in both the multiple- and single-flame modes. Through monitoring a broad spectral range from 250 to 850 nm, it was found that the mFPD produces sulfur emission predominantly as S_2*, but HSO* can also be isolated in the red spectral region. Further, phosphorus emission in the mFPD was found to stem from HPO*, while carbon emission was attributed to CH* and C_2*. Finally, background emission in the mFPD was determined to be from OH*. Qualitatively, these findings agree very well with the species found in a conventional single-flame FPD. However, quantitatively, the mFPD spectra in the multiple-flame mode consistently produced analyte emission bands that were relatively more intense. In contrast with this, hydrocarbon spectra in the mFPD yielded significantly reduced relative intensities, owing to decreased C_2* emission. As well, aromatic and aliphatic hydrocarbons produced much more similar distributions of CH* and C_2* emission in the mFPD than in the conventional single-flame FPD mode. Mechanistically, the findings suggest that a relative deficiency in C_2 radical and a greater abundance of oxidized carbon in the mFPD could possibly play a central role in the detector's quenching-resistant behavior.

CHAPTER FIVE: AN IMPROVED MULTIPLE FLAME PHOTOMETRIC DETECTOR FOR GAS CHROMATOGRAPHY

5.1 Introduction

The properties of the mFPD, as far as investigated, have demonstrated similar spectral response characteristics and performance attributes to a traditional FPD. It's simple and inexpensive design offers the analytical sensitivity and selectivity that is reasonable relative to a conventional FPD[88] and improved over a dFPD[50]. Additionally, it was found that a useful linear sulfur response mode can also be readily established in this device[108,130]. Most notably, however, the mFPD has also demonstrated high resistance to hydrocarbon quenching and an enhanced response uniformity and reproducibility[88,108].

Despite its promising attributes, in working with the mFPD a number of difficulties in its basic design were encountered that hinder its current performance. For example, the simple quartz tube burner used in the initial mFPD prototype allows for easy monitoring of the flames, but is inherently very fragile and requires a bulky cumbersome detector housing[88]. Further, the counter-current analytical flame emission in the quartz tube design is not only localized towards the PMT but emits ubiquitously around itself inside the housing; stray analyte emission can thereby be lost through the quartz walls on the backside of the flame. Even more important, though, the current mFPD design suffers from high background emission from the worker flames. This arises because the cement used to fix the stainless steel capillary burners into the quartz tube wall produces an intense glow when contacting the flames[88]. In all, these features can very negatively impact the sensitivity of the mFPD and make it difficult to operate.

Therefore, an improved mFPD design that can bypass these issues is needed in order to promote wider implementation and development of the device.

This Chapter presents the properties and operating characteristics of an improved mFPD device. As demonstrated in Section 2.4, the design of the SS mFPD is based upon a novel use of fluidic channels machined into a planar SS surface to primarily direct flame gas flows and analyte emission. As such, the general operating characteristics of this new SS mFPD design are discussed in Section 5.2 while its analytical flame characteristics are examined in Section 5.3. As well, the analytical performance attributes of this SS mFPD are presented and discussed in Section 5.4. Further, the hydrocarbon quenching behavior of this SS mFPD is explored in Section 5.5. Additionally, where possible, these findings are evaluated relative to that of the original quartz tube prototype in order to help illustrate its advantages. Finally, a promising new multiple flame monitoring mode of this mFPD, which was previously impossible to access in the initial quartz device, is presented in Section 5.6.

5.2 General Operating Characteristics

As mentioned, the previous generation quartz tube mFPD arrangement used four orthogonal worker flames and a lone counter-current analytical flame situated on an inserted SS tube delivering a counter flow of oxygen[88,108,130]. This counter-current arrangement allowed for great flexibility in situating and operating the analytical flame in various positions and conditions within the detector. Once the position was optimized, it was normally fastened in place. Consequently then, when it came to manufacturing the new SS mFPD here, much time and consideration was made with respect to flame

positioning and its measurements. Optimized distances and channel dimensions found in the quartz tube mFPD were then translated carefully to the new SS mFPD design. As such, these channels were precision cut into bulk SS material; which, unlike the quartz tube mFPD, were no longer constructed using thin-walled SS tubes cemented into place.

In operating the SS mFPD, one of the first aspects noted was that it was comparatively much more robust and sturdy due to its SS design. For example, the original quartz tube mFPD had holes drilled along its side into which SS worker flame capillaries were cemented. In working with it over time it was found that not only were these awkward to cover in a detector housing, but they were also inherently fragile and a frequent point of breakage in the device if it was not handled carefully. By comparison, the worker flame channels milled directly into the monolithic housing of the SS mFPD make for a much stronger device that is able to withstand routine aggressive handling without problems. Of note, no breakage has occurred in regular operation of the SS mFPD for over a year, whereas the quartz tube prototype normally required replacement every few weeks.

Another feature noted in operating the SS mFPD concerned ignition of the flames. Specifically, the fixed channels in the device appeared to allow for very easy ignition of all flames at once by simply presenting a spark at the central channel outlet. Alternatively, any sequence of individual flames could also be lit on demand as desired by simply controlling the oxygen source of each. This is in contrast to the quartz tube prototype, which often required a capillary pilot flame to be inserted through the outlet to ignite each of the flames in their respective positions prior to operation[88,108]. Therefore,

given its relative durability and easier operation, the emission attributes of the SS mFPD were next investigated.

5.3 Orthogonal vs. Counter-Current Analytical Flame

As mentioned above, the original quartz tube mFPD prototype used a counter-current analytical flame. This flame was situated on an oxygen-bearing SS capillary inserted into the tube outlet from the top and was operated in a counter-flowing stream of hydrogen and column effluent coming from the detector base below[88,108,130]. As well, this flame was normally fixed at an optimal distance above the four orthogonal worker flames. Since this position was well characterized[88,108,130], it was interesting to see if an orthogonal channel placed at the same location in the SS mFPD could also be used for the analytical flame. This is because such an advent could further simplify mFPD operation and it was not possible to explore in the quartz tube mFPD due to the large background emission associated with the orthogonal SS capillary burners[88]. Therefore as shown in Figure 2-3, a new orthogonal analytical flame channel was also fabricated in the SS mFPD and compared here with the normal counter-current analytical flame operating mode.

Figure 5-1 demonstrates the results with the response of a tetrahydrothiophene test analyte in the SS mFPD in each analytical flame mode using the same gas flows (i.e. 100 mL/min hydrogen, 30 mL/min collective oxygen to workers, and 7 mL/min oxygen to analytical). Each mode is also illustrated to clarify the difference between the two. Figure 5-1A displays the analyte response obtained in the normal arrangement using a

counter-current analytical flame on a SS capillary inserted through the top of the device. As seen, a modest analyte peak eluting near 1.5 minutes is produced.

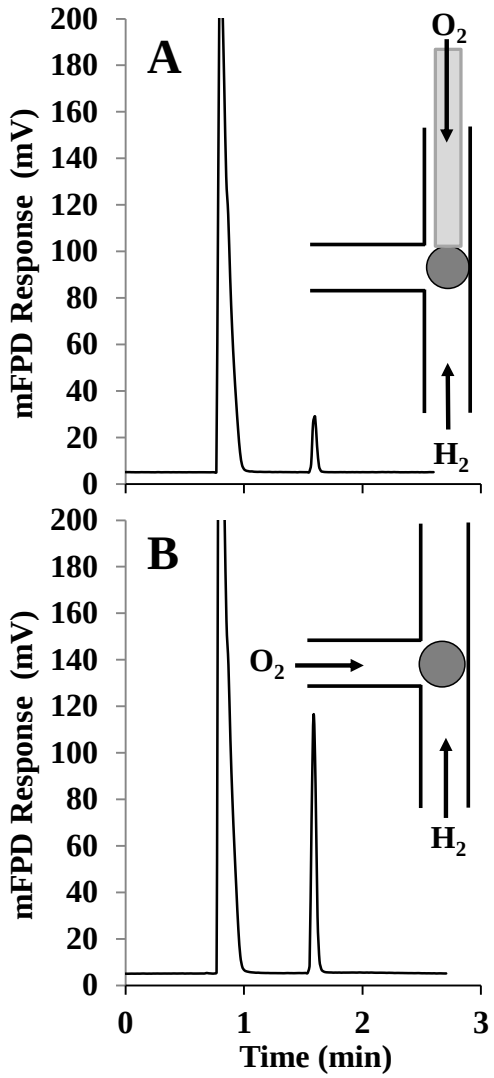

Figure 5-1: Chromatograms showing the typical SS mFPD S_2* response obtained in (A) the conventional counter-current and (B) the new orthogonal channel analytical flame operating modes under otherwise identical conditions. Each flame arrangement is illustrated. The elution order is hexane (solvent) and tetrahydrothiophene (50 ng). An oven temperature of 90 °C was used.

By comparison, Figure 5-1B demonstrates the same experiment when the analytical flame is operated at the junction of the new orthogonal and central SS mFPD channels (i.e. without a SS capillary). As shown, under the exact same conditions and flow rates, analyte response increases over 4 times relative to the conventional counter-current flame. Further, as anticipated, no flame stability issues were found in this new mode either.

Therefore, the perpendicular flame gas flow of the orthogonal channel does not appear to present any problems relative to the opposing flow of the conventional counter-current mode in operating the analytical flame of the mFPD. Moreover, this channel is even found to notably enhance the signal. While the reason for this is not certain, it may involve analyte emission occurring behind the stainless steel capillary in the conventional mode. This can block the emission from being viewed by the PMT and decrease the observed signal. If so, the new orthogonal channel (i.e. without the SS capillary) should direct more emission to the PMT. Nonetheless, since this latter mode was preferable it was employed in further studies.

Next, to ensure the best possible S_2* signal in this new operating mode, the SS mFPD flame gas flows for the orthogonal channel were fully optimized. Through exploring various hydrogen and oxygen ratios, the best detector performance at the analytical channel for sulfur was realized using 100 mL/min of hydrogen, 30 mL/min of oxygen distributed equally across the worker flames, and 12 mL/min of oxygen supplied to the analytical flame. Note that this leaves about 40 mL/min of optimal hydrogen flow to the final analytical flame after travel through (and consumption by) the worker flames. These values are identical to those used previously in the mFPD[88] with the exception of

the 12 mL/min analytical flame oxygen flow, which is larger than the typical 7 mL/min used earlier in the quartz tube prototype[88,108,130], and was found to provide improved S/N ratios here for sulfur test analytes. Conversely, such a flow increase was not possible with the previous quartz tube design since it resulted in a large background emission at the counter-current flame and worse response. As well, it was found that when the central channel was extended from 1 to 2 mm wide × 1 mm deep, further improvements in response were obtained as shown in Figure 5-2.

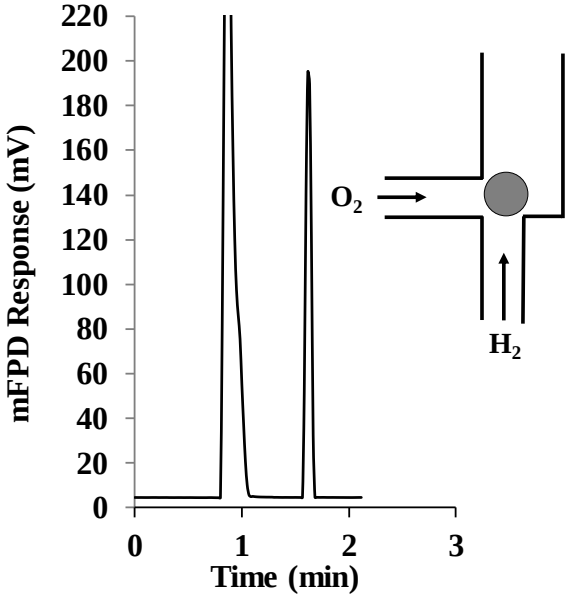

Figure 5-2: Chromatogram showing the typical SS mFPD S_2* response obtained in the new orthogonal channel analytical flame using 12 mL/min of oxygen supplied to the analytical flame. The flame arrangement (demonstrating the 2mm central channel extension) is illustrated. The elution order is hexane (solvent) and tetrahydrothiophene (50 ng). An oven temperature of 90 °C was used.

It can be seen that the increased oxygen flow rate and the extended central channel at the analytical flame proved beneficial, since the signal observed nearly doubled compared to the lower oxygen flow rates used in the similar experiments of Figure 5-1. Thus, this new channel can provide greater flexibility for optimization.

5.3.1 Background Emission Properties

To better understand the background emission characteristics of the new SS mFPD device relative to the quartz tube mFPD prototype, the properties of each were investigated under the same multiple-flame conditions. For this, measurements of background emission intensity were performed with both devices under their respective optimal conditions for measuring S_2* response. Specifically, background measurements of each mFPD device were taken at the analytical flame location with and without the flames ignited to measure the relative background contribution of the flames. As such, the measured background current contributed by the flames were about 0.209 nA in the quartz tube mFPD and 0.129 nA in the SS mFPD. This translates into approximately 50% lower contribution of the flame's background emission in the SS mFPD compared to the quartz tube device. Visually this could also be readily affirmed.

For instance, Figure 5-3 illustrates this difference with typical images of both devices with and without sulfur emission present under normal operating conditions. As seen in Figure 5-3A, the quartz tube mFPD exhibits a notable orange glow at the burner tips of the SS capillaries, while a dim background emission is also seen at the analytical flame. Figure 5-3B then demonstrates the same during sulfur analyte emission.

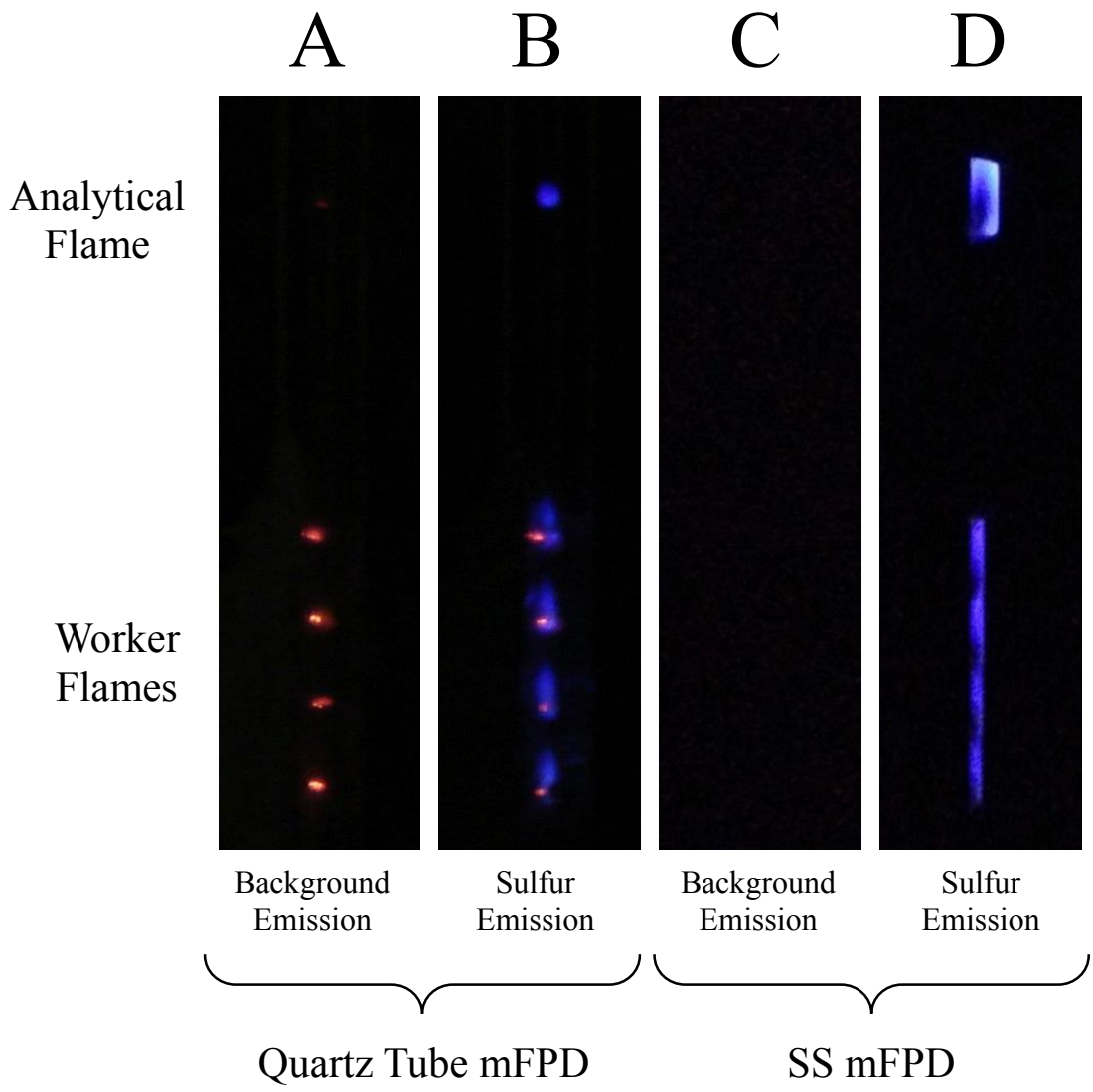

Figure 5-3: Images of the quartz tube mFPD (A, B) and the SS mFPD (C, D) during operation both without (A, C) and with (B, D) S_2* sulfur emission present.

Here again, even though blue S_2* chemiluminescence can be clearly seen, the dominant orange background emission persists. As noted above, this results from incandescent glowing of the cement used to hold the flame burners in place[88]. However, the respective images taken in the SS mFPD (Figure 5-3C and D) are very different by comparison. For example, no background emission can be visually detected at either the

analytical or worker flame positions with or without sulfur present. As a result, the strong S_2* emission generated (Figure 5-3D) occurs on a much darker background, which should improve detector performance. Also interesting is that the analytical flame profile (Figure 5-3D) assumes the channel shape, and appears rectangular relative to the typical spherical flame seen in the counter-current mode (Figure 5-3B). This is presumably because the gas flow (and hence emission) can more freely flow upward and fill the central channel without the opposing flow of the conventional counter-current flame mode. Thus, the SS mFPD can significantly reduce background emission and interference relative to the original quartz tube mFPD.

Consequently a spectral examination of the worker flames was done to further understand this background emission difference between the two mFPD devices. Here, a large quartz light guide (150 mm × 18 mm O.D.) was placed in view of the worker flames location and emission spectra was taken over a wavelength range of 250-850 nm for each mFPD device (as similarly described in Section 4.2). Figure 5-4 shows the background emission spectrum obtained at the worker flames for both the quartz tube and SS mFPD. As shown, an examination reveals similar background OH emission features in each device, with a notable band located near 306 nm.

However, beyond this wavelength section, the quartz tube mFPD produced an intense emission continuum spanning from 350 to 850 nm, whereas the SS mFPD only reveals a minor OH emission band due to second-order diffraction. Again, this intense continuum in the quartz tube mFPD is due to incandescent glowing of the cement used to hold the flame burners in place[88]. Accordingly, such a continuum can interfere with essentially all key analytical wavelengths for FPD measurement. As such, the resulting

background emission and baseline noise observed in the quartz tube prototype can serve to inhibit the overall performance of the detector.

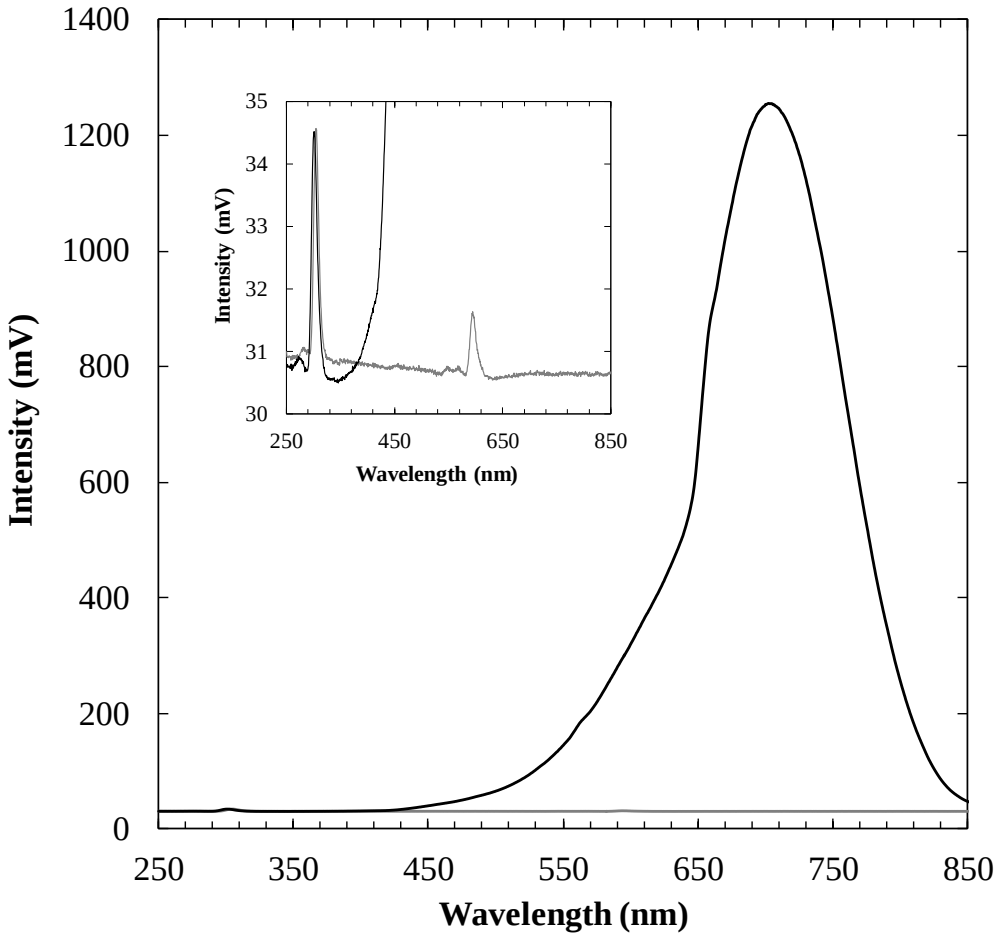

Figure 5-4: Background emission spectrum taken from the worker flames in the quartz tube mFPD (black line) and in the SS mFPD (grey line). Top inset is an enlarged view of these emission spectra near their respective baselines. Monochromator bandpass is 6.7 nm.

5.4 Analytical Figures of Merit

5.4.1 Sensitivity and Detection Limits

With the SS mFPD optimized, its analytical performance attributes were characterized. Figure 5-5 illustrates the typical results with a calibration plot for tetrahydrothiophene response as a function of analyte quantity in the S_2* operating mode. As seen, sulfur response in the SS mFPD increases over about 4 orders of magnitude. Further, the slope of this response is nearly quadratic (slope = 1.7) for higher analyte amounts (10^{-9} to 10^{-7} range) and reduces (slope = 1.0) at lower concentrations (below 10^{-9}), which is commonly observed for S_2* emission in a conventional FPD[24]. At the lower end, this provides a MDL for sulfur in the SS mFPD of about 9×10^{-12} gS/s, as determined at an S/N ratio of 3, where noise is measured as the standard deviation of the baseline fluctuations over at least 10 analyte peak base widths.

As demonstrated previously in Table 3-5, Section 3.7, these features generally compare quite well with those expected of a conventional FPD[24]. In particular, the MDL for sulfur in the SS mFPD is improved over twice of the earlier quartz tube mFPD prototype[88], and agrees very well with current commercial FPD models[106,107](e.g. within a few pg S/s). Conversely, the MDLs reported for the SCD and pFPD are lower (e.g. 10^{-13} gS/s)[60,69,74,77]. Overall, this improved performance of the SS mFPD relative to the quartz tube mFPD can be largely attributed to its lower background emission and better light collection. For instance, since the channel was well polished it helped reflect more analyte emission back towards the PMT that would normally have been lost through the quartz walls of the previous mFPD burner.

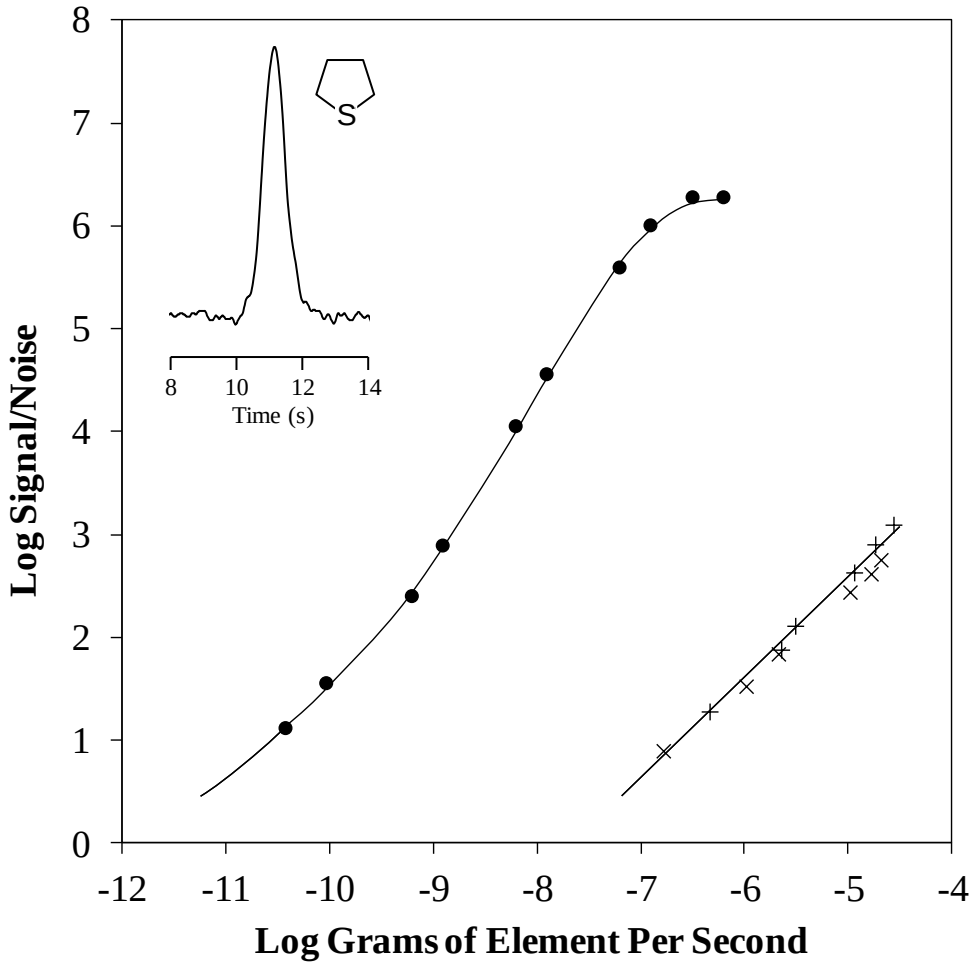

Figure 5-5: Plot showing SS mFPD response as a function of analyte amount in the S_2* operating mode for tetrahydrothiophene (●), dodecane (×), and benzene (+). The oven temperatures used were 90 °C for tetrahydrothiophene, 50 °C for benzene and 200 °C for dodecane. Also shown inset is the typical profile of a fast 500 pg tetrahydrothiophene peak.

Regarding response dynamics, the quartz tube mFPD has previously been shown to be compatible with fast GC separations[108]. Thus, no differences in this respect were

anticipated or observed here for the SS mFPD. For example, Figure 5-5 additionally illustrates the typical SS mFPD response obtained for a fast tetrahydrothiophene peak approaching the detection limit. Here, performed similarly as in Section 3.3.1, hydrogen flow was re-routed into the SS mFPD as the carrier gas through a short 2 m length of DB-5 megabore column and analyte injections were monitored at a data acquisition rate of 50 Hz. As seen, a good profile is obtained for this narrow peak possessing a half-width near 700 milliseconds, which aligns well with formal designations of 'fast' GC[103,104]. Although even narrower peaks are produced in techniques of 'very fast' and 'ultra fast' GC, these were not further probed here and would require more appropriate conditions of faster detector electronics to properly examine[103,104]. It is also unknown if peak tailing may arise when using such very fast FPD response in a mode such as GC×GC operation. Still, given that other FPD methods are compatible with such high-speed GC separations[96], it seems reasonable to anticipate that the SS mFPD should be as well.

5.4.2 Selectivity

Also included in Figure 5-5 is the SS mFPD response toward aliphatic and aromatic hydrocarbon test analytes measured under the same S_2* conditions. As seen, both dodecane and benzene each produce a very similar modest response in the SS mFPD. This is reasonable since spectral studies of the mFPD have shown that both aliphatic and aromatic hydrocarbons degrade into similar species in the worker flames prior to entering the analytical flame (see Chapter Four). Overall then, this response translates into a formal selectivity of sulfur over carbon in the SS mFPD of about 4 orders of magnitude. This value correlates well with that obtained from the quartz tube mFPD[88,108,130], most conventional FPD devices[2,24,82,106], and the AED[74]. Conversely, it is

lower than that of the SCD[77] and the pFPD[69,131]. Practically, however, this SS mFPD selectivity still corresponds to fairly large hydrocarbon quantities being required for a measurable signal. For example, no hydrocarbon response could be observed here for amounts below 1 µg of compound introduced to the analytical flame. Therefore, major hydrocarbon interference should not normally be anticipated during sulfur monitoring in the SS mFPD. This is examined more closely in Section 5.5.

5.5 Hydrocarbon Response Quenching Behavior

A primary feature observed in the quartz tube mFPD prototype is its resistance toward hydrocarbon quenching of analyte emission, which is achieved through the presence of the worker flames[88,108,130]. Since the SS mFPD does not differ in this aspect of its core design, such quenching-resistant behavior should also be anticipated in its operation. However, since the SS mFPD has also shown decreased background emission and improved signal characteristics here compared to the quartz tube prototype, this property was still necessary and interesting to further investigate. To better gauge this, experiments were performed under severe quenching conditions with the SS mFPD.

For this, commercial diesel fuel (Diesel Sample B) was spiked with a thianaphthene standard and analyzed in an FID mode, the SS mFPD mode, and also in the conventional single- and multiple-flame mFPD modes using the quartz burner for comparison[88,92,94,108,130]. Further, to induce demanding hydrocarbon quenching conditions as much as possible, the diesel fuel was injected without splitting as a neat, undiluted 1 µL sample onto the column. The results for these modes are presented in Figure 5-6.

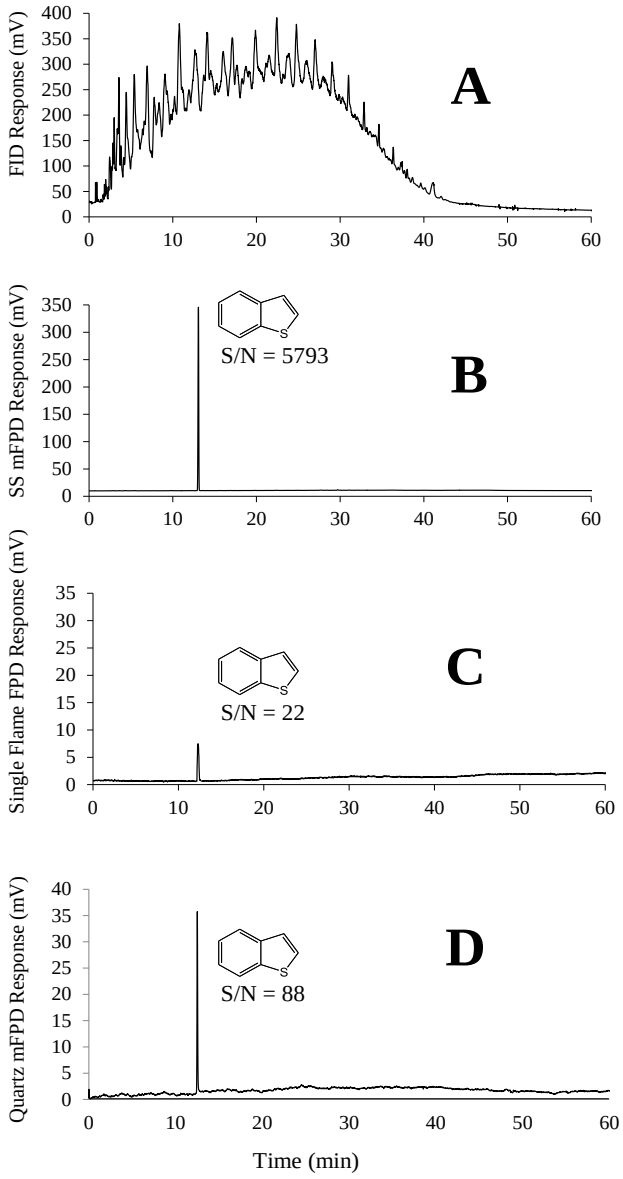

Figure 5-6: Chromatograms from a neat 1 µL injection of diesel fuel (Diesel Sample B) containing 250 ng of thianaphthene as monitored in the FID mode (A), SS mFPD S_2* sulfur mode (B), conventional single flame FPD S_2* sulfur mode (C), and quartz tube mFPD S_2* sulfur mode (D). For (C) the flame used 7 mL/min oxygen and 40 mL/min hydrogen. The temperature program was 70 °C for 5 minutes, then increasing to 280 °C at 5 °C/min.

Figure 5-6A shows the FID response for the separation, which reveals a very large number of unresolved hydrocarbon compounds eluting in the first 40 minutes or so. By comparison, Figure 5-6B displays the diesel sample as monitored in the SS mFPD sulfur mode. As seen, the thianaphthene peak elutes after about 13 minutes amongst the bulk of the fuel components. In diesel this comprises mainly saturated and aromatic hydrocarbons, and from the 1 µL volume injected, this represents nearly 1 mg of fuel flowing through the column. However, despite co-eluting with a very large amount of hydrocarbons, the analyte produces a strong response with an S/N value near 5800. Incidentally, experiments using the same amount of analyte standard without diesel present (i.e. unquenched) indicated that 50% of the original SS mFPD signal is still preserved in this highly complex hydrocarbon matrix. Conversely, Figure 5-6C demonstrates the same using a conventional single-flame FPD operating mode. Here, thianaphthene response is relatively much weaker with an S/N value near 20 owing to the clear effects of severe hydrocarbon signal quenching. In fact, lower quantities of analyte failed to produce a signal in this mode.

Finally, similar experiments performed with the quartz tube mFPD prototype yielded an S/N value near 100 (Figure 5-6D). Therefore, since all of the peaks have a similar profile (i.e. retention near 13 minutes and base width of 15-18 seconds) these results indicate that the SS mFPD provides a resistance to hydrocarbon response quenching that is over 2 orders of magnitude larger than a conventional single-flame FPD operating mode, and over an order of magnitude larger than that obtained in the quartz tube mFPD. This is a direct result of the mFPD worker flames in the former case, and the improved signal characteristics of the SS mFPD in the latter. It should be noted that

geometry and design can significantly differ among conventional FPD manufacturers and so some variation in this comparison may be anticipated depending on the model used. Therefore, the SS mFPD could help facilitate monitoring sulfur species in complex matrices with minimal sample interference.

5.6 Worker Flame Response Characteristics

A final set of experiments here involved a closer examination of the SS mFPD worker flames and the intense chemiluminescence that was routinely observed in them during operation. Figure 5-7 demonstrates this with the bright blue sulfur and green phosphorus emission in the worker flame region.

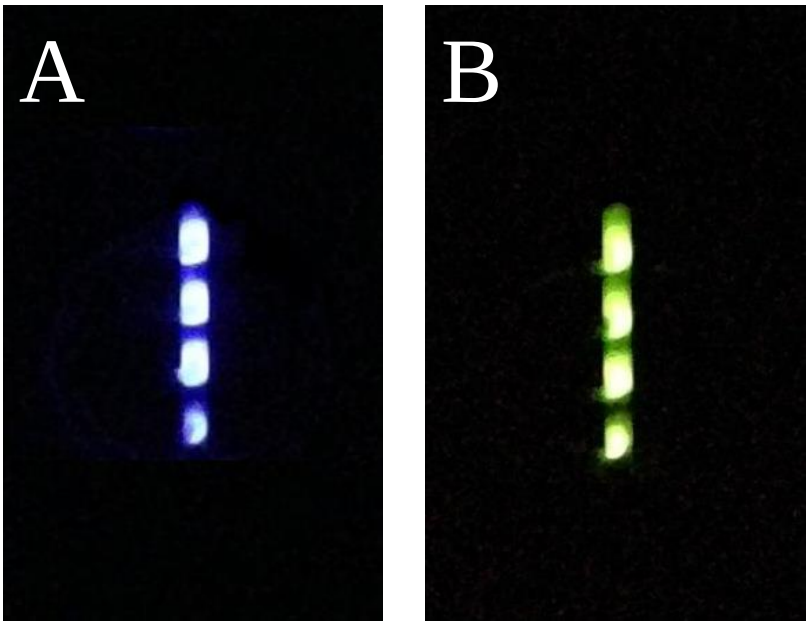

Figure 5-7: Images of the SS mFPD (2 mm wide central channel) during operation with sulfur emission (A) and phosphorus emission (B) present.

Since the background emission of these worker flames was also low in the SS mFPD, as demonstrated in Figure 5-4, it presented an interesting and unique opportunity to probe analyte response in them directly for the first time. Of note, this task was impossible with the quartz tube mFPD due to its enormous background level at this same position. Further, to the best of our knowledge, monitoring the collective chemiluminescence of multiple flames simultaneously has not been previously demonstrated in an FPD. Therefore since this could be readily attempted in the SS mFPD, the response characteristics of the worker flames were also preliminarily examined here.

To investigate this, analyte emission in three different modes (S_2*, HSO*, and HPO*) was monitored through the worker flame viewport using a large quartz light guide (150 mm × 18 mm O.D.) leading to the PMT. As well, the central channel of the SS mFPD was entirely extended to 2 mm wide to further facilitate analyte chemiluminescence, as mentioned earlier. Optimized worker flame gas flows for sulfur emission (S_2* and HSO*) used 20 mL/min oxygen and 100 mL/min hydrogen, while phosphorus emission used 20 mL/min oxygen and 120 mL/min hydrogen. Under their respective optimum conditions, analytes were then measured in the analytical flame and worker flame monitoring modes and the results were directly compared.

Overall, the worker flames provided better signal characteristics in each mode. Table 5-1 shows a comparison of some signal-to-noise ratios in the analytical flame and worker flames in the SS mFPD using the three different modes of detection. For example, S_2* emission produced S/N values that were as much as 10 times greater in the worker flames than in the analytical flame. Interestingly, however, S_2* emission in the worker flames was also found to be consistently quadratic, as opposed to the shifting

response slope observed for the analytical flame (as seen in Figure 5-5). Figure 5-8 further illustrates this comparison with a calibration plot for tetrahydrothiophene response as a function of analyte quantity in both S_2* operating modes. As shown in this figure, the S/N enhancement reduced to a factor near 3 at lower concentrations and the MDL was little changed.

Table 5-1: A comparison of signal-to-noise ratios in the analytical flame and worker flames of the SS mFPD using three different modes of detection.

Mode	Compound	Injected Amount (ng)	Analytical Flame S/N Ratio	Worker Flames S/N Ratio	Factor Increase
S_2*	tetrahydrothiophene	105.0	35174	390767	11.1
		10.5	762	7532	9.9
		0.5	13	34	2.6
HSO*	tetrahydrothiophene	105.0	242	986	4.1
		10.5	22	99	4.5
HPO*	trimethyl phosphite	108.0	4873	94511	19.4
		10.8	461	8694	18.9

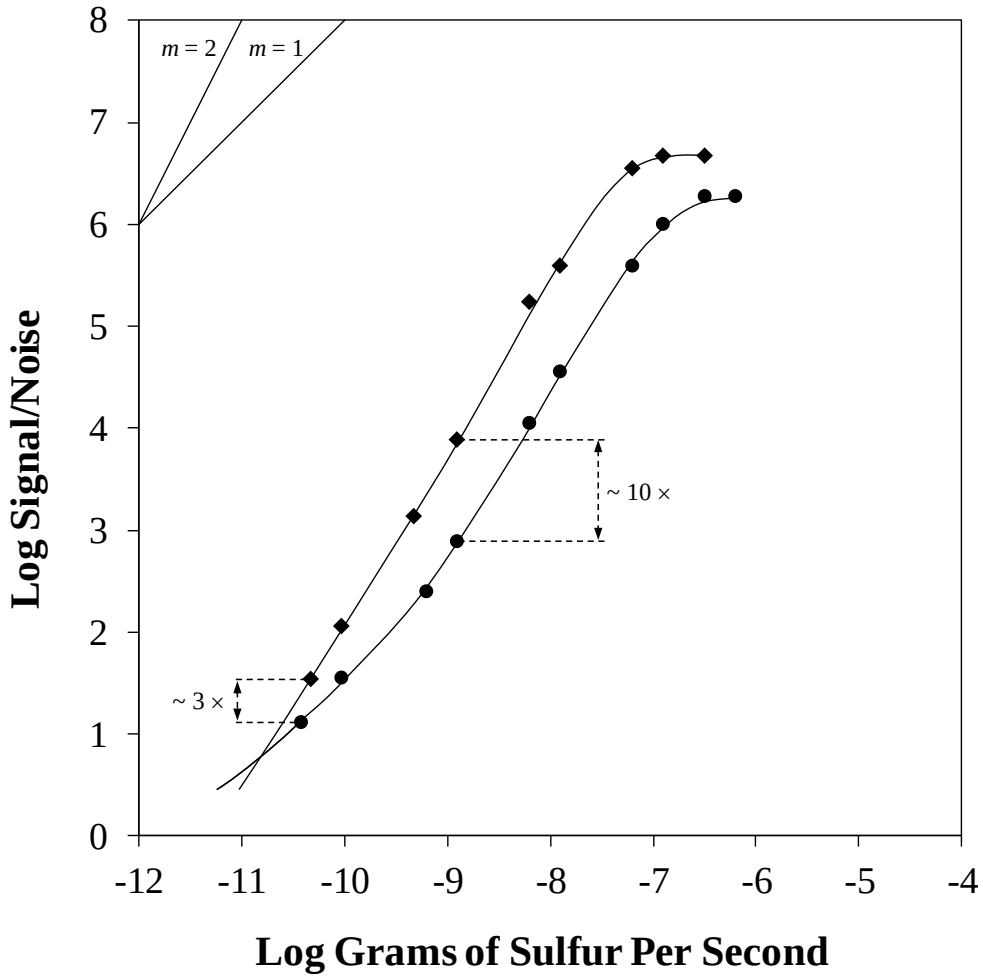

Figure 5-8: Plot showing sulfur response as a function of analyte amount for tetrahydrothiophene in the SS mFPD while monitoring the worker flames (♦) and the analytical flame (●) under optimized S_2* conditions. As well, lines depicting a purely quadratic (*m* = 2) and linear (*m* = 1) trend line are shown for comparison. An oven temperature of 90 °C was used.

Since linear sulfur response has also been previously established in the mFPD[108], it was interesting to explore here as well. In particular, since the emitter (HSO*) is oxygenated it was wondered if the additional oxygen supplied to the worker flames may be able to, for example, enhance the formation of this species[88,108,130]. In fact, as shown in

Table 5-1 under optimal HSO* conditions, linear sulfur response was found to provide S/N values that were about 4 times greater in the worker flames than in the analytical flame. The calibration plots shown in Figure 5-9 further illustrate this difference. As shown, the HSO* emission demonstrates a linear response over nearly 4 orders of magnitude in each mode. However, the worker flame enhancement was consistent and yielded an MDL near 3×10^{-11} gS/s. As such, this is within about a factor of 3 to the quadratic mode of Figure 5-5, and compares well to linear sulfur modes reported in a conventional FPD[25] and pFPD[69]. Thus, this linear sulfur mode is still accessible in the SS mFPD and also displays the same positive response attributes as noted in the quartz tube mFPD.

The most striking difference arose for phosphorus response (as HPO*), which is well known in the FPD[24] and mFPD[88,130]. Under their respective optimal conditions, it was found that HPO* emission in the worker flames produced S/N values that were about 20 times greater than those observed in the analytical flame. Figure 5-10 illustrates this comparison with a calibration plot for trimethyl phosphite response as a function of analyte quantity in both HPO* operating modes. As shown, both modes indicate a linear response spanning nearly 6 orders of magnitude. However, this enhanced response in the worker flames produced an MDL near 2×10^{-13} gP/s, which is lower than that reported for the quartz tube mFPD[88] and agrees well with that of a conventional FPD[24]. Figure 5-11 demonstrates the improvement noted for 1 ng of trimethyl phosphite in each mode. As can be seen on the expanded scale shown, the S/N characteristics are much more favorable for this analyte in the optimized worker flame monitoring mode than they are in the optimized analytical flame monitoring mode.

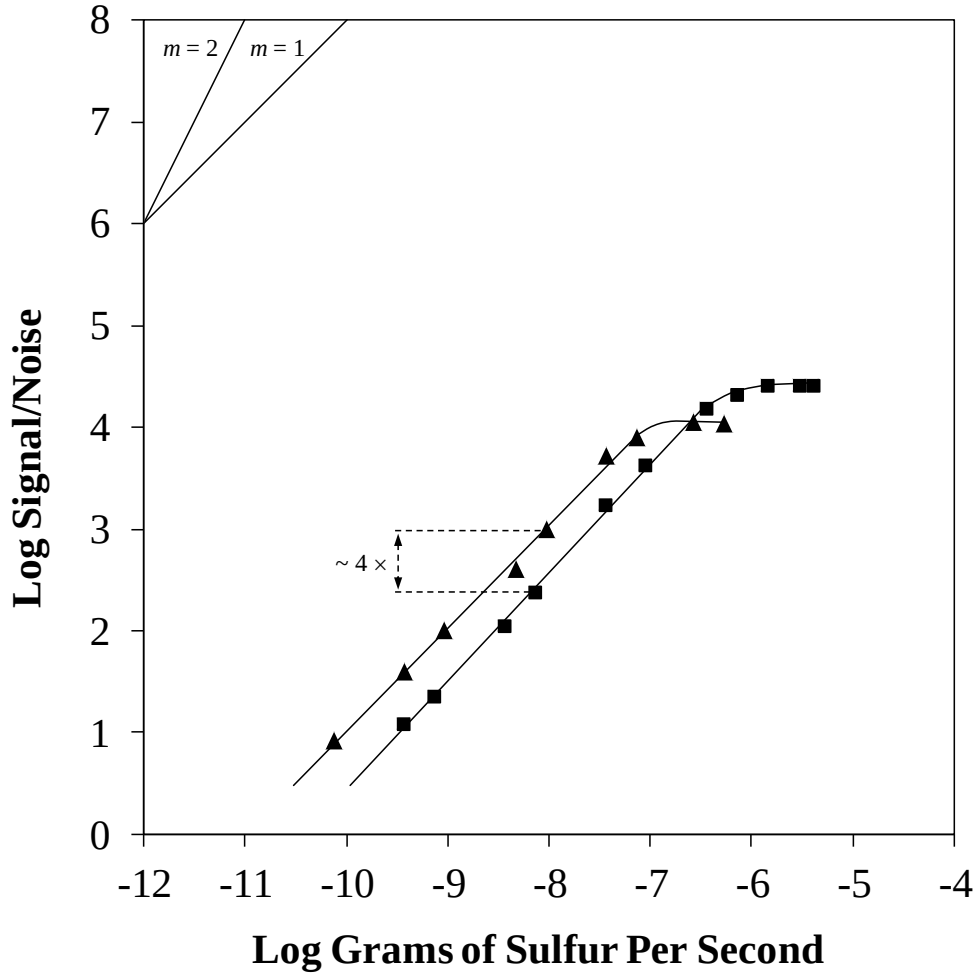

Figure 5-9: Plot showing sulfur response as a function of analyte amount for tetrahydrothiophene in the SS mFPD while monitoring the worker flames (▲) and the analytical flame (■) under optimized HSO* conditions. As well, lines depicting a purely quadratic (*m* = 2) and linear (*m* = 1) trend line are shown for comparison. An oven temperature of 90 °C was used.

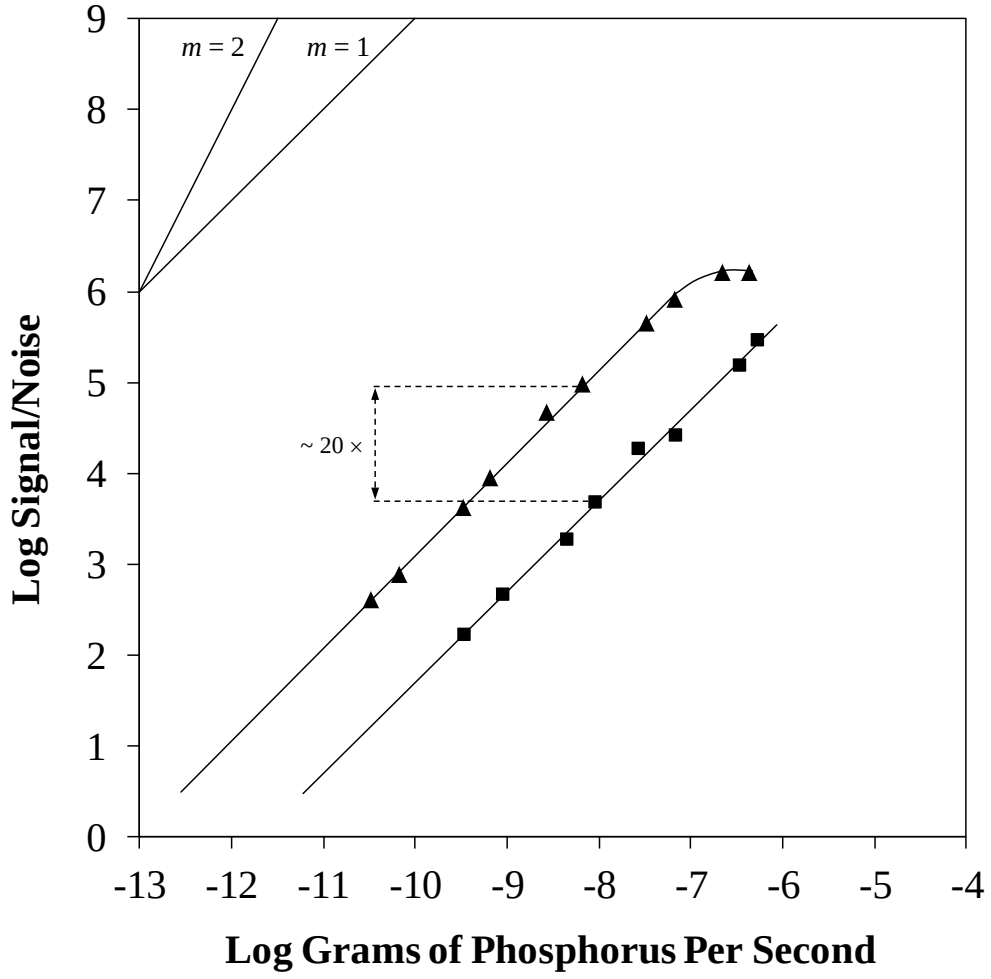

Figure 5-10: Plot showing phosphorus response as a function of analyte amount for trimethyl phosphite in the SS mFPD while monitoring the worker flames (▲) and the analytical flame (■) under optimized HPO* conditions. As well, lines depicting a purely quadratic (*m* = 2) and linear (*m* = 1) trend line are shown for comparison. An oven temperature of 90 °C was used.

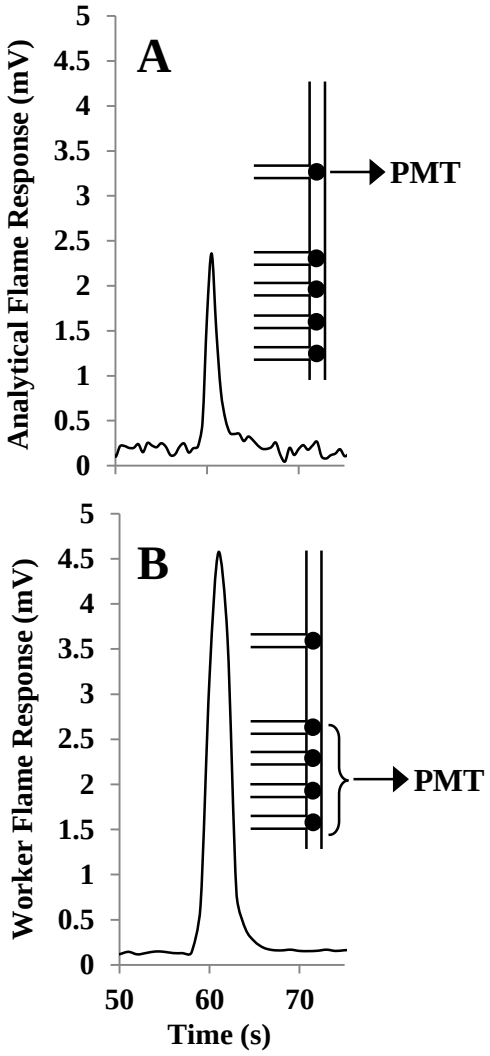

Figure 5-11: Chromatograms showing the typical SS mFPD HPO* response obtained from 1 ng of trimethyl phosphite in the analytical flame (A) and the worker flames (B) under optimized conditions. The arrangement of each monitoring mode is illustrated. An oven temperature of 90 °C was used.

Overall, this improved performance of the worker flames generally arose from both an increase in analyte signal and a decrease in baseline noise. The former is likely due to greater chemiluminescence being generated in this battery of flames, possibly from more efficient excitation of the emitting species. Conversely, noise decreased in each case except for S_2* emission, which oddly showed little change between flame modes. This indicates a possible difference between the background flame emission profiles of the worker flames and the analytical flame, but needs further examination to establish.

Further, the gas flows through the central channel provide a peak residence time in the space between the worker and analytical flame of only about 10 ms (and 19 ms through the entire detector). Thus, peak dispersion along the channel path cannot account for the difference noted between these flame monitoring modes either. Therefore, the preliminary data here demonstrate that improved response characteristics are attainable in this novel multiple flame monitoring mode of the SS mFPD. Thus, its further development could be potentially beneficial.

5.7 Conclusions

An improved mFPD for GC has been developed based on a novel detector design of interconnecting fluidic channels milled into the face of a planar SS plate. Advantages of this new SS mFPD include significantly lower background flame emission and noise, an orthogonal analytical flame position, easier operation, and better signal collection properties. As a result, the SS mFPD provides improved sensitivity and further resistance to hydrocarbon response quenching than the previous quartz tube mFPD prototype.

Additionally, due to the favorably low background properties of the SS mFPD, a new operating mode was introduced which monitored the collective emission of all worker flames for the first time. The preliminary results indicate that this battery of flames can generally provide significantly greater analyte response and reduced background noise relative to the analytical flame position. As such, further development of this unique multiple flame monitoring mode of the SS mFPD could be potentially beneficial.

CHAPTER SIX: SUMMARY AND FUTURE WORK

6.1 Summary

This thesis describes an advancement of a multiple flame photometric detector for gas chromatography. The design and flame arrangements characterized in this study have shown great improvements over the initial prototype of this detector. Additionally, the mFPD device developed here has demonstrated similar (and enhanced) performance attributes relative to other selective GC detectors. Therefore, these results indicate that this device could potentially serve as a beneficial alternative method of detection for sulfur and phosphorus monitoring applications.

In order to facilitate calibrations and positively impact response reproducibility in the mFPD, the preliminary objective of this research was aimed at developing and characterizing a linear sulfur response in the device. Optimal conditions were found through monitoring HSO* emission in the red spectral region at 750 nm using select gas flow rates to the mFPD's analytical and worker flames. By employing these parameters, a linear response was obtained for a variety of sulfur compounds that demonstrated good sensitivity, selectivity, and response dynamics. Notably, however, this mode provided enhanced response uniformity and reproducibility, as well as significant resistance toward interference from hydrocarbon quenching. These results suggest that this new linear mFPD response mode could be a very useful for the analysis of sulfur-containing compounds in conventional or fast GC applications.

Next, to fully characterize this device, emission spectra of the mFPD were acquired and examined for the first time. Through monitoring a broad spectral range from

250 to 850 nm, it was found that the mFPD produces sulfur emission as S_2*, but HSO* can also be isolated in the red spectral region. Further, phosphorus emission in the mFPD was found to stem from HPO*, while carbon emission was attributed to CH* and C_2*. As such, the device does not appear to qualitatively differ from a conventional single-flame FPD with respect to the species responsible for emission. However, quantitatively, it was found that the mFPD consistently produced greater emission intensity for typical sulfur and phosphorus analytes but notably lower intensity for hydrocarbon species. Consequently, the findings have indicated that a relative reduction of C_2 radical and an increase of oxidized carbon in the analytical flame of the mFPD could play a central role in the observed quenching-resistant behavior of this detector.

Finally, an improved multiple flame photometric detector was introduced based upon interconnecting fluidic channels within a planar stainless steel plate. Relative to the quartz tube mFPD prototype, the SS mFPD provided a 50% reduction in background emission levels, an orthogonal analytical flame, easier operation, and better signal collection properties. As a result, the sulfur response in the device yielded improved detection limits that correspond well to those reported in modern day commercial FPDs. However, unlike conventional FPDs, the SS mFPD additionally provides exceptionally large resistance to hydrocarbon response quenching even more so than the quartz tube mFPD prototype. Furthermore, this SS mFPD design uniquely allows analyte emission monitoring collectively in the multiple worker flames for the first time. The findings suggest that this mode can potentially further improve upon the analytical flame response of sulfur (both linear -HSO, and quadratic -S_2) and also phosphorus. In all, the new mFPD that has been constructed and characterized in this study, shows significant

advantages over previous approaches, and establishes a foundation from which future work by others may evolve.

6.2 Future Work

6.2.1 mFPD Applications

As discussed throughout this thesis, the mFPD has demonstrated some promising attributes with respect to quenching-resistant applications. However, most of the applications that were shown involved only petroleum-based samples. For instance, although during the mFPD work a few petroleum applications were shown, other extensive real-world samples were not yet tested with this device. Therefore, it would be beneficial to actually show how the detector can perform when faced with analyzing sulfur and phosphorus amongst some other challenging types of matrices. For instance, GC-FPD has become a popular detection method for profiling organic sulfur compounds in beer and wine aroma[132-134]. However, it has been reported that the sensitivity of the FPD toward sulfur-containing compounds in these beverages can be affected when matrix compounds containing considerable amounts of carbon are also present[135-137]. Therefore, such applications that would typically quench sulfur and phosphorus emissions in an FPD may prove more successful in the mFPD. Similarly, the determination of volatile sulfur and/or phosphorus compounds in natural gas[60], chemical warfare agents[138], and pesticide residues[139] are additional areas of concern where the mFPD could also be beneficial.

6.2.2 Multiple Flame Arrangements in an mFPD

As demonstrated in Chapter Five, collective monitoring of analyte chemiluminescence in multiple flames can be accomplished in the SS mFPD for the first time. This task was impossible with the quartz tube mFPD due to its enormous background level at this same position. Since the background emissions of all the flames were low in the SS mFPD, it presented an interesting and unique opportunity to probe analyte response in them directly. To the best of our knowledge, monitoring the collective chemiluminescence of multiple flames simultaneously has not been previously demonstrated in an FPD. Nonetheless, the preliminary optimization done in this study was only directed to the typical 4 worker flame arrangement found in the SS mFPD.

However, to fully realize the benefits of monitoring multiple flames, more flame arrangements and different burner configurations in this SS mFPD device may ultimately improve analyte response. For instance, since analyte degradation and excitation is occurring within each flame, monitoring more orthogonal flames in series (i.e. more than the 4-flame arrangement shown in this study) may further provide an increase in analyte response. Consequently, improvements in the optical light throughput to the PMT may also be required. For example, instead of an increasingly wider quartz light guide, a plano-convex or bi-convex lens may be employed to efficiently converge collimated light of multiple flames to a single spot on the PMT. Such FPD optical modifications have been proposed in the past[140] and have shown to be beneficial when incorporated into certain commercial FPD models[107]. However, until now, this has not been used to address the collection of analyte chemiluminescent

emission from multiple flames. Therefore, given the relatively low background emission provided in the SS mFPD, more flame arrangements with enhanced optical throughput may collectively provide significant improvements for analyte response in this device.

6.2.3 New Elemental Response Modes in the mFPD

All things considered, design improvements and technical advancements should not be the only focus for future mFPD research. For instance, while the conventional FPD is known for the sensitive and selective detection of phosphorus and sulfur containing compounds, many other elements have also generated a response in the detector[18,25,141]. Specifically, a variety of volatile organometallic compounds containing elements such as germanium, tin, ruthenium, chromium, nickel, lead, and manganese have all demonstrated a selective response in both the FPD and pFPD[18,70,142]. However, none of these elements have been selectively examined, nor even attempted in the mFPD. Given both the similarities and dissimilarities that exist between the mFPD and the FPD, it would thus be useful to examine whether the mFPD is indeed capable of measuring other elements; particularly, for example, organotin compounds that have been observed to respond strongly in the FPD[142,143]. In this regard, the mFPD has demonstrated the ability to process and convert more analytes into the necessary emitting species prior to entering the analytical flame for measurement. This, in turn, may promote better sensitivity in the mFPD for other elements than in a conventional single-flame FPD, which must first decompose analytes into the same emitting species and then promote excitation/emission all within a single flame region. Therefore, it may be worthwhile to characterize, optimize, define, and obtain useful spectral information of responses (such as organotin

compounds) in greater detail. In this way, the mFPD may become analytically valuable not only for sulfur and phosphorus compounds but also a useful detection tool for volatile compounds of other elements.

REFERENCES

1. Poole, C. F. *The Essence of Chromatography*; Elsevier Science: Amsterdam, The Netherlands, 2003, pp 225-266.

2. Klee, M. S. In *Gas Chromatography*; Elsevier: Oxford, England, 2012, pp 307-347.

3. Tuan, H. P.; Janssen, H.-G. M.; Cramers, C. A.; Kuiper-van Loo, E. M.; Vlap, H. *J. High Resolut. Chromatogr.* **1995**, *18*, 333-342.

4. Robards, K.; Haddad, P. R.; Jackson, P. E. *Principles and Practice of Modern Chromatographic Methods*; Academic Press: Boston, USA, 2004, pp 458-462.

5. Andersson, J. T. In *Practical Gas Chromatography: A Comprehensive Reference*; Springer Berlin Heidelberg: Berlin, Germany, 2014, pp 205-248.

6. Ardrey, R. E. In *Liquid Chromatography – Mass Spectrometry: An Introduction*; John Wiley & Sons, Ltd.: West Sussex, England, 2003, p 135.

7. Miller, J. M. *Chromatography: Concepts and Contrasts*; John Wiley & Sons, Inc.: Hoboken, USA, 2005, p 285.

8. Hill, H. H.; McMinn, D. G. *Detectors for Capillary Chromatography*; John Wiley & Sons, Inc.: New York, USA, 1992, pp 1-5.

9. Selucky, M. L. *Chromatographia* **1971**, *4*, 425-434.

10. Kok, W. T. In *Handbook of HPLC*; Marcel Dekker, Inc.: New York, USA, 1998, pp 145-147.

11. LoBrutto, R.; Tarun, P. In *HPLC for Pharmaceutical Scientists*; John Wiley & Sons, Inc.: Hoboken, USA, 2007, pp 455-499.

12. Stout, T. H.; Dorsey, J. G. In *Handbook of Pharmaceutical Analysis*; Marcel Dekker, Inc.: New York, USA, 2002, pp 116-117.

13. Foley, J. P.; Dorsey, J. G. *Chromatographia* **1984**, *18*, 503-511.

14. McNair, H. M.; Miller, J. M. *Basic Gas Chromatography*; John Wiley & Sons, Inc.: New York, USA, 1998, pp 101-125.

15. Farwell, S. O. In *Analytical Instrumentation Handbook, 2nd ed.*; Marcel Dekker, Inc.: New York, USA, 1997, pp 1257-1258.

16. Colón, L. A.; Baird, L. J. In *Modern Practice of Gas Chromatography, 4th ed.*; John Wiley & Sons, Inc.: Hoboken, USA, 2004, pp 277-337.

17. McNair, H. M.; Miller, J. M. *Basic Gas Chromatography*, 2nd ed.; John Wiley & Sons, Inc.: Hoboken, USA, 2009, pp 104-128.

18. Sun, X.-Y.; Millier, B.; Aue, W. A. *Can. J. Chem.* **1992**, *70*, 1129-1142.

19. Analytical Methods Committee. *Analyst* **1987**, *112*, 199-204.

20. Currie, L. A. *Pure Appl. Chem.* **1995**, *67*, 1699-1723.

21. Harris, D. C. *Quantitative Chemical Analysis, 8th ed.*; W. H. Freeman and Company: New York, USA, 2010.

22. Bernal, E. In *Advances in Gas Chromatography*, InTech, Ed.; InTech: Rijeka, Croatia, 2014, pp 57-81.

23. Currie, L. A. *Anal. Chim. Acta* **1999**, *391*, 105-126.

24. Dressler, M. *Selective Gas Chromatographic Detectors*; In: Journal of Chromatography Library, 36, Elsevier Science Publishers: Amsterdam, The Netherlands, 1986.

25. Aue, W. A.; Sun, X.-Y. *J. Chromatogr.* **1993**, *633*, 151-162.

26. Ševčík, J.; Nguyen thi Phuong, T. *Chromatographia* **1975**, *8*, 559-562.

27. Scott, R. P. W. *Introduction to Analytical Gas Chromatography, 2nd ed.*; Marcel Dekker, Inc.: New York, USA, 1997.

28. Farwell, S. O.; Barinaga, C. J. *J. Chromatogr. Sci.* **1986**, *24*, 483-494.

29. Burnett, C. H.; Adams, D. F.; Farwell, S. O. *J. Chromatogr. Sci.* **1978**, *16*, 68-73.

30. Guiochon, G.; Guillemin, C. L. In *Quantitative Gas Chromatography*; Journal of Chromatography Library, 42, Elsevier Science Publishers: Amsterdam, The Netherlands, 1988, pp 393-480.

31. McWilliam, I. G.; Dewar, R. A. *Nature* **1958**, *181*, 760-760.

32. Harley, J.; Nel, W.; Pretorius, V. *Nature* **1958**, *181*, 177-178.

33. Marriott, P. J. In *Chromatography 6th ed.*, Heftmann, E., Ed.; Elsevier: Amsterdam, The Netherlands, 2004, pp 319-368.

34. Hill, H. H.; Baim, M. A. *Trends Anal. Chem.* **1982**, *1*, 206-210.

35. Holm, T. *J. Chromatogr. A* **1999**, *842*, 221-227.

36. Smith, R. M. *J. Chromatogr. A* **1999**, *856*, 83-115.

37. Brody, S. S.; Chaney, J. E. *J. Gas Chromatogr.* **1966**, *4*, 42-46.

38. Gui-Bin, J.; Qun-Fang, Z.; Bin, H. *Environ. Sci. Technol.* **2000**, *34*, 2697-2702.

39. Marriott, P. J.; Mitrevski, B.; Amer, M. W.; Chaffee, A. L. *Anal. Chim. Acta* **2013**, *803*, 174-180.

40. Poole, C. F.; Schuette, S. A. In *Contemporary Practice of Chromatography*; Elsevier: Amsterdam, The Netherlands, 1984, pp 145-212.

41. Schofield, K. *Combust. Flame* **2001**, *124*, 137-155.

42. Sugiyama, T.; Suzuki, Y.; Takeuchi, T. *J. Chromatogr. A* **1973**, *77*, 309-316.

43. Syty, A.; Dean, J. A. *Appl. Opt.* **1968**, *7*, 1331-1336.

44. Olesik, S. V.; Pekay, L. A.; Paliwoda, E. A. *Anal. Chem.* **1989**, *61*, 58-65.

45. Sugden, T. M.; Demerdache, A. *Nature* **1962**, *195*, 596-596.

46. Aue, W. A.; Thurbide, K. B. *Spectrochim. Acta, Part B* **2002**, *57*, 843-852.

47. Gaydon, A. G.; Whittingham, G. *Proc. R. Soc. London, A* **1947**, *189*, 313-325.

48. Gilbert, P. T. In *Analytical Flame Spectroscopy*, Mavrodineanu, R., Ed.; Springer-Verlag: New York, USA, 1970, pp 181-377.

49. Poole, C. F.; Poole, S. K. In *Chromatography Today*; Elsevier: Amsterdam, The Netherlands, 1991, pp 231-309.

50. Patterson, P. L.; Howe, R. L.; Abu-Shumays, A. *Anal. Chem.* **1978**, *50*, 339-344.

51. Sugimaya, T.; Suzuki, Y.; Takeuchi, T. *J. Chromatogr. A* **1973**, *80*, 61-67.

52. Poole, C. F. In *Encyclopedia of Analytical Science, 2nd ed.*; Elsevier: Oxford, England, 2005, pp 95-105.

53. Aue, W. A.; Sun, X.-Y. *J. Chromatogr.* **1993**, *641*, 291-299.

54. Kalontarov, L.; Jing, H.; Amirav, A.; Cheskis, S. *J. Chromatogr. A* **1995**, *696*, 245-256.

55. Liu, G. H.; Fu, P. R. *Chromatographia* **1989**, *27*, 159-163.

56. Chin, S.-T.; Wu, Z.-Y.; Morrison, P. D.; Marriott, P. J. *Anal. Methods* **2010**, *2*, 243-253.

57. Wardencki, W. In *Sulfur Compounds: Gas Chromatography, Reference Module in Chemistry, Molecular Sciences and Chemical Engineering*; Elsevier Inc.: Gdańsk, Poland, 2014, pp 1-23.

58. Rupprecht, W. E.; Phillips, T. R. *Anal. Chim. Acta* **1969**, *47*, 439-449.

59. Patterson, P. L. *Anal. Chem.* **1978**, *50*, 345-348.

60. Janssen, H.-G.; Tuan, H. P.; Cramers, C. A.; Smit, A. L. C.; van Loo, E. M. *J. High Resolut. Chromatogr.* **1994**, *17*, 373-389.

61. Adlard, E. R. In *Encyclopedia of Separation Science*, Wilson, I. D., Ed.; Academic Press: Oxford, England, 2000, pp 456-464.

62. Dyson, M. *Anal. Proc. (London)* **1993**, *30*, 79-88.

63. Chester, T. L. *Anal. Chem.* **1980**, *52*, 1621-1624.

64. Holdway, D. A.; Nriagu, J. O. *Int. J. Environ. Anal. Chem.* **1988**, *32*, 177-186.

65. Lee, M. L.; Markides, K. E.; Lee, E. D.; Bolick, R. *Anal. Chem.* **1986**, *58*, 740-743.

66. Ferguson, D. A.; Luke, L. A. *Chromatographia* **1979**, *12*, 197-203.

67. Baig, A. R.; Cowper, C. J.; Gibbons, P. A. *Chromatographia* **1982**, *16*, 297-300.

68. Amirav, A.; Atar, E.; Cheskis, S. *Anal. Chem.* **1991**, *63*, 2061-2064.

69. Cheskis, S.; Atar, E.; Amirav, A. *Anal. Chem.* **1993**, *65*, 539-555.

70. Amirav, A.; Jing, H. *J. Chromatogr. A* **1998**, *805*, 177-215.

71. Catalan, L. J. J.; Liang, V.; Jia, C. Q. *J. Chromatogr. A* **2006**, *1136*, 89-98.

72. Schulz, H.; Böhringer, W.; Ousmanov, F.; Waller, P. *Fuel Process. Technol.* **1999**, *61*, 5-41.

73. Chambers, L.; Duffy, M. L. *J. Chromatogr. Sci.* **2003**, *41*, 528-534.

74. Hawthorne, S. B.; Eckert-Tilotta, S. E.; Miller, D. J. *J. Chromatogr.* **1992**, *591*, 313-323.

75. Link, D. D.; Baltrus, J. P.; Rothenberger, K. S.; Zandhuis, P.; Minus, D.; Striebich, R. C. *J. Chromatogr. Sci.* **2002**, *40*, 500-504.

76. Benner, R. L.; Stedman, D. H. *Anal. Chem.* **1989**, *61*, 1268-1271.

77. Shearer, R. L. *Anal. Chem.* **1992**, *64*, 2192-2196.

78. Glinski, R. J.; Martin, H. R. *Appl. Spectrosc.* **1992**, *46*, 948-952.

79. Yan, X. *J. Sep. Sci.* **2006**, *29*, 1931-1945.

80. Benner, R. L.; Stedman, D. H. *Appl. Spectrosc.* **1994**, *48*, 848-851.

81. Wardencki, W.; Zygmunt, B. *Anal. Chim. Acta* **1991**, *255*, 1-13.

82. Wardencki, W. *J. Chromatogr. A* **1998**, *793*, 1-19.

83. Navas, M. J.; Jiménez, A. M. *Crit. Rev. Anal. Chem.* **2000**, *30*, 153-162.

84. Cooke, M.; Leathard, D. A.; Webster, C.; Rogerson, V. *J. High Resolut. Chromatogr.* **1993**, *16*, 660-662.

85. Quimby, B. D.; Grudoski, D. A.; Giarrocco, V. *J. Chromatogr. Sci.* **1998**, *36*, 435-443.

86. Kim, K.-H.; Pandey, S. K. *Environ. Sci. Technol.* **2009**, *43*, 3020-3029.

87. Chawla, B. In *Analytical Advances for Hydrocarbon Research*, Hsu, C., Ed.; Springer: New York, USA, 2003, pp 57-72.

88. Hayward, T. C.; Thurbide, K. B. *Anal. Chem.* **2009**, *81*, 8858-8867.

89. Gaydon, A. G.; Wolfhard, H. G. *Flames: Their Structure, Radiation, and Temperature, 3rd Rev.*; Chapman and Hall Ltd.: London, England, 1970, pp 85-174.

90. Tsuji, H. *Prog. Energy Combust. Sci.* **1982**, *8*, 93-119.

91. Thurbide, K. B.; Anderson, C. D. *Analyst* **2003**, *128*, 616-622.

92. Thurbide, K. B.; Cooke, B. W.; Aue, W. A. *J. Chromatogr. A* **2004**, *1029*, 193-203.

93. Thurbide, K. B.; Hayward, T. C. *Anal. Chim. Acta* **2004**, *519*, 121-128.

94. Hayward, T. C.; Thurbide, K. B. *J. Chromatogr. A* **2006**, *1105*, 66-70.

95. Thurbide, K. B.; Hayward, T. C. *Talanta* **2007**, *73*, 583-588.

96. Kendler, S.; Reidy, S. M.; Lambertus, G. R.; Sacks, R. D. *Anal. Chem.* **2006**, *78*, 6765-6773.

97. Aue, W. A.; Flinn, C. G. *J. Chromatogr. A* **1978**, *158*, 161-170.

98. Sun, X.-Y.; Aue, W. A. *J. Chromatogr. A* **1994**, *667*, 191-203.

99. Thurbide, K. B.; Aue, W. A. *J. Chromatogr. A* **1994**, *684*, 259-268.

100. Sevcik, J. *Int. J. Environ. Anal. Chem.* **1983**, *13*, 115-128.

101. Schurath, U.; Weber, M.; Becker, K. H. *J. Chem. Phys.* **1977**, *67*, 110-119.

102. Engewald, W. In *Quantification in LC and GC*, Kuss, H.-J.; Kromidas, S., Eds.; Wiley-VCH: Weinheim, Germany, 2009, pp 222-223.

103. Matisová, E.; Dömötörová, M. *J. Chromatogr. A* **2003**, *1000*, 199-221.

104. Korytár, P.; Janssen, H. G.; Matisová, E.; Brinkman, U. A. T. *Trends Anal. Chem.* **2002**, *21*, 558-572.

105. Hinshaw, J. V. *LC GC Europe* **2002**, *15*, 152-155.

106. Agilent Technologies. In *Technical Note 5991-1436EN, Agilent 7890B Network Gas Chromatograph Data Sheet*: Wilmington, USA, 2013.

107. Shimadzu Corporation. In *Specification Sheet C184-E014G, Shimadzu Capillary and Packed Gas Chromatograph GC- 2014 Product Guide*: Kyoto, Japan, 2013.

108. Clark, A. G.; Thurbide, K. B. *J. Chromatogr. A* **2014**, *1326*, 103-109.

109. Singh, H.; Eisener, C. G.; Aue, W. A. *J. Chromatogr. A* **1996**, *734*, 405-409.

110. Gaydon, A. G.; Pearse, R. W. B. *The Identification of Molecular Spectra, 4th ed.*; Chapman and Hall: London, England, 1976.

111. Aue, W. A.; Singh, H. *J. Chromatogr. A* **1996**, *746*, 43-51.

112. Cheskis, S. *Combust. Flame* **1995**, *100*, 550-558.

113. Gaydon, A. G.; Charton, M. *Proc. R. Soc. London, A* **1958**, *245*, 84-92.

114. Smith, G. P.; Luque, J.; Park, C.; Jeffries, J. B.; Crosley, D. R. *Combust. Flame* **2002**, *131*, 59-69.

115. Davis, M. G.; McGregor, W. K.; Mason, A. A. *J. Chem. Phys.* **1974**, *61*, 1352-1356.

116. Kathrotia, T.; Fikri, M.; Bozkurt, M.; Hartmann, M.; Riedel, U.; Schulz, C. *Combust. Flame* **2010**, *157*, 1261-1273.

117. Kathrotia, T.; Riedel, U.; Seipel, A.; Moshammer, K.; Brockhinke, A. *Appl. Phys. B: Lasers Opt.* **2012**, *107*, 571-584.

118. Thurbide, K. B.; Aue, W. A. *J. Chromatogr. A* **1995**, *694*, 433-440.

119. Selim, H.; Al Shoaibi, A.; Gupta, A. K. *Applied Energy* **2011**, *88*, 2601-2611.

120. Mossholder, N. V.; Fassel, V. A.; Kniseley, R. N. *Anal. Chem.* **1973**, *45*, 1614-1626.

121. Lakowicz, J. R. *Principles of Fluorescence Spectroscopy, 3rd ed.*; Springer Science: New York, USA, 2006, pp 27-62.

122. Singh, H.; Millier, B.; Aue, W. A. *J. Chromatogr. A* **1996**, *724*, 255-264.

123. Wolfhard, H. G.; Gaydon, A. G. *Flames: Their Structure, Radiation, and Temperature, 4th ed.*; Chapman and Hall: London, England, 1979, pp 241-254.

124. ASTM International. In *ASTM E840-95: Standard practice for using flame photometric detectors in gas chromatography*: West Conshohocken, USA, 2013.

125. Thurbide, K. B.; Anderson, C. D.; Gilbert, S.; Aue, W. A. *Anal. Chim. Acta* **2003**, *477*, 269-277.

126. Peeters, J.; Lambert, J. F.; Hertoghe, P.; van Tiggelen, A. *Symposium (International) on Combustion* **1971**, *13*, 321-332.

127. Cheng, W. K.; Summers, T.; Collings, N. *Prog. Energy Combust. Sci.* **1998**, *24*, 89-124.

128. Kállai, M.; Veres, Z.; Balla, J. *Chromatographia* **2001**, *54*, 511-517.

129. Thurbide, K. B.; Hayward, T. C. *Can. J. Anal. Sci. Spectrosc.* **2004**, *49*, 302-308.

130. Clark, A. G.; Thurbide, K. B. *Can. J. Chem.* **2014**, *92*, 629-634.

131. Pandey, S. K.; Kim, K.-H. *Anal. Chim. Acta* **2008**, *615*, 165-173.

132. Moreira, N.; Guedes de Pinho, P.; Santos, C.; Vasconcelos, I. *Food Chem.* **2010**, *123*, 1198-1203.

133. Xiao, Q.; Yu, C.; Xing, J.; Hu, B. *J. Chromatogr. A* **2006**, *1125*, 133-137.

134. Marriott, P. J.; Chin, S.-T.; Eyres, G. T. *J. Chromatogr. A* **2011**, *1218*, 7487-7498.

135. Ferreira, V.; Franco-Luesma, E. *J. Chromatogr. A* **2014**, *1359*, 8-15.

136. Hill, P. G.; Smith, R. M. *J. Chromatogr. A* **2000**, *872*, 203-213.

137. Guasch, J.; Mestres, M.; Busto, O. *J. Chromatogr. A* **2000**, *881*, 569-581.

138. Seto, Y.; Kanamori-Kataoka, M.; Tsuge, K.; Ohsawa, I.; Maruko, H.; Sekiguchi, H.; Sano, Y.; Yamashiro, S.; Matsushita, K.; Sekiguchi, H.; Itoi, T.; Iura, K. *Toxin Rev.* **2007**, *26*, 299-312.

139. Liu, X.; Mitrevski, B.; Li, D.; Li, J.; Marriott, P. J. *Microchem. J.* **2013**, *111*, 25-31.

140. Aue, W. A.; Eisener, C. G.; Gebhardt, J. A.; Lowery, N. B. *J. Chromatogr. A* **1994**, *688*, 153-159.

141. Aue, W. A.; Singh, H. *Spectrochim. Acta, Part B* **2001**, *56*, 517-525.

142. Aue, W. A.; Sun, X.-Y.; Millier, B. *J. Chromatogr. A* **1992**, *606*, 73-86.

143. Aue, W. A.; Flinn, C. G. *J. Chromatogr. A* **1977**, *142*, 145-154.

APPENDIX A: COPYRIGHT PERMISSION FOR USE OF PUBLISHED WORK

Adrian Clark

From: pubs@nrcresearchpress.com
Sent: Wednesday, April 15, 2015 9:16 AM
To: Adrian Clark
Subject: RE: Permission to re-use published content

Dear Adrian,

Yes, indeed.
Please review: http://www.nrcresearchpress.com/page/authors/information/rights

As one of the authors of this paper, you may reuse your published material.
Permission is granted.
Thank you for checking.

Best regards,

Eileen

Canadian Science Publishing

Eileen Evans-Nantais
Client Service Representative
Canadian Science Publishing

Adrian Clark

From: Permissions Helpdesk <permissionshelpdesk@elsevier.com>
Sent: Friday, April 17, 2015 10:56 AM
To: Adrian Clark
Subject: RE: Permission to re-use published content

Dear Adrian,

Thank you for your e-mail.

Permission is covered by the rights you retain as an Elsevier journal author as outlined at http://www.elsevier.com/about/policies/author-agreement/lightbox_scholarly-purposes which include *inclusion in a thesis or dissertation*, provided that proper acknowledgement is given to the original source of publication. Should you require any further clarification, please let me know.

Best of luck with your thesis.

Laura

Laura Stingelin
Permissions Helpdesk Associate
Elsevier